Development of a Tm^{3+}-doped Fluoride Glass Optical Fibre Laser for Gas Sensing

By

Fergal J. McAleavey   B.Sc. (Hons)

A thesis presented
to
Dublin City University

For the degree of Master of Science

September 1995

School of Physical Sciences
Dublin City University
Ireland

Declaration

I hereby certify that this material, which I now submit for assessment on the programme of study leading to the award of M.Sc. is entirely my own work and has not been taken from the work of others, save and to the extent that such work has been cited and acknowledged within the text of my work.

Signed : _Fergal Mc Heavey_   Date : _21 − 9 −'95_

Dedication

This thesis is dedicated to Kay, for her love and friendship.

Acknowledgments

A large number of people contributed in many ways to this thesis. I would like to thank a number of them, including:

'The intellect of man is forced to choose
Perfection of the life, or of the work...'

'The Choice',   William Butler Yeats (1865 - 1939)

Abstract

The development of a fluoride fibre laser for hydrocarbon gas sensing is discussed. The use of a fibre laser as a source for optical sensing has many advantages including small size and ease of adaptability into industrial systems. The fibre laser constructed in this work has an operating wavelength of $\lambda = 2.3$ µm, which corresponds to an absorption band of many hydrocarbon gases.

The thulium-doped fibre has been fully characterised in terms of absorption, fluorescence and fluorescence lifetimes. These data were then used to choose a pump laser diode and appropriate laser mirrors.

The operational fibre laser was fully characterised in terms of output power and slope efficiency. Two fibre laser configurations were demonstrated. The first fibre laser exhibited a dual laser emission simultaneously at 1.92 µm and 2.31µm, with output powers of 7 mW and 1.2 mW, respectively. A second fibre laser was also demonstrated; this device was optically pumped with a low power laser diode. The output from the fibre laser pumped by the low power laser diode was utilised as a unique source for detection of methane. A detection limit of 1000 ppm metres was routinely demonstrated with this unoptimised system.

Table of Contents

Chapter 1

Introduction

1.1 Introduction

One of the most exciting recent developments in the field of optics has been the emergence of the fibre laser (**L**ight **A**mplification by **S**timulated **E**mission of Radiation). According to France [1] *'it is probably the most significant development since the monomode optical fibre'*. The basic concept of rare-earth doped fibres is simple. By incorporating an optically active ion into the core of an optical fibre, one obtains a unique medium that exhibits both a low propagation loss and interesting laser properties. The claims made on behalf of doped fibres are that they will provide low cost, easily produced sources and amplifiers at wavelengths that are important for both current and projected future requirements, in fields such as telecommunications, medicine, sensing and spectroscopy.

This chapter describes the main types of laser systems including fibre lasers which are currently available. The suitability of a fibre laser for use as a source for optical gas sensing is proposed, and the objectives of this project are outlined.

1.2 Amplifiers and oscillators

The most obvious application for the amplifying mechanism of a laser medium is as a signal amplifier for optical systems. A sample of laser material can be pumped by an external power source to build up a population inversion in the sample. When a signal beam is passed through the sample it will emerge with a larger amplitude but with the same frequency.

Mirrors may be placed at each end of the sample so that the emerging radiation is reflected back into the sample. When mirrors are placed at both ends and are suitably aligned to form a resonant cavity, radiation may be reflected back and forth along the axis of the sample, with a gain in intensity on each pass.

Eventually, equilibrium is reached with a high intensity of highly monochromatic coherent radiation cycling in the cavity. If the mirrors are designed to transmit a small percentage of radiation, then this percentage of the beam intensity will emerge from the cavity as a highly collimated beam of monochromatic radiation.

1.3 Three and four level systems

For a laser system to work, a population inversion must be achieved between two energy levels in the medium, whose energy difference will correspond to the energy of photons of the lasing wavelength. The two main categories of laser systems are three-level lasers and four-level lasers. Other lasers systems exist and three- and four-level systems do not provide a complete classification for all lasers.
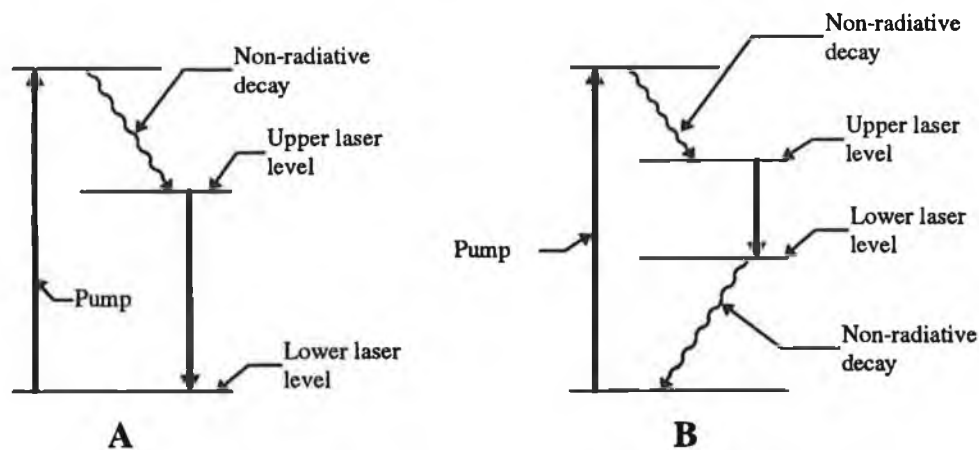
FIGURE 1.1 THREE- AND FOUR-LEVEL LASER SYSTEMS

A three-level laser system is displayed in figure 1.1A. Population inversion is achieved by a pumping mechanism which excites atoms from the ground state to an excited state, from which they decay non-radiatively to the upper lasing level. From this level, the atoms undergo transitions to the ground state, from where they are available for re-excitation. In a three-level laser, the majority of the population initially lies in the ground state, so that more than half the population must be excited to the upper level to achieve a population inversion and obtain laser action. Three-level lasers have the advantage however, that there is only one transition which does not contribute to the laser output, with the result that they are potentially more efficient.

The system is described as a four-level laser (Fig. 1.1B), if the lower lasing level lies above the ground state. After undergoing laser action the atoms decay

non-radiatively to the ground state, from which they may be re-excited. A four-level laser usually has the lower laser level almost empty, and so any population which reaches the upper level will easily achieve population inversion. The disadvantage is that the two transitions not contributing to laser action both emit energy from the system which is not in a useful form. As a result four-level systems are generally less efficient than three-level systems.

1.4 Laser systems

Laser systems may be divided into three categories, based on the physical state of the laser medium, i.e. those based on gases, liquids and solids. There are numerous subdivisions of these general groupings. In particular, solid state lasers may be divided into those based on bulk material, and those where the active medium is in the form of a waveguide or optical fibre.

1.4.1 Gas lasers

A large group of gas lasers operate across the spectrum from the UV to the far IR (150 nm to 1 mm). The best known of these are helium-neon (He-Ne), argon and krypton, as well as several molecular gas systems such as carbon dioxide, hydrogen fluoride and molecular nitrogen (N_2). The He-Ne laser is currently the most popular laser, usually providing a few milliwatts of continuous wave (CW) power in the visible at 632.8 nm. Argon lases mainly in the green, blue-green (514.4 nm and 488 nm), and such lasers are used in either pulsed or continuous operation. All of the noble gases (He, Ne, Ar, Kr, Xe) have been made to lase individually. The CO_2 laser, which lases at 10.6 μm, offers high CW powers ($\cong$ 10 kWatts). This type of laser is often used in industry for cutting or welding because of its intense heating properties. Gas lasers are usually excited by electrical means, i.e. pumping is achieved by passing a sufficiently large current (d.c. or pulsed) through the gas.

1.4.2 Dye lasers

In dye lasers the active medium is a constantly moving jet of liquid dye. This is usually a complex organic dye, dissolved in a suitable solvent (such as ethyl alcohol, methyl alcohol, or water). A wide variety of dyes is available with differing absorption and emission wavelengths. These dyes usually belong to one of the following classes, whose emission bands are shown in parentheses : (i) polymethine dyes (0.7 - 1.0 μm), (ii) xanthene dyes (0.5 - 0.7 μm), (iii) coumarin dyes (0.4 -0.5

μm), (iv) scintillator dyes ($\lambda < 0.4$ μm). Dye lasers are generally pumped optically by another laser operating at a shorter wavelength and they are useful for providing a wide range of output wavelengths which may not easily be produced by other laser sources. These dyes, exhibit an intense broadband fluorescence spectrum, and consequently, dye lasers have been demonstrated over wide tuning ranges.

1.4.3 Solid state lasers

Solid state lasers are usually based on a host crystal or glass doped with active laser ions. The first report of an operational laser was made by Maiman in 1961[§]. This was a ruby laser, in which chromium ions were used to emit a high intensity pulse of red light when excited by a Xenon flashlamp. Many different host crystals and glasses are now available with a wide range of dopants, covering a multitude of pump and signal wavelengths.

Another important solid state laser is the semiconductor diode laser. This is based on a slab of semiconductor material producing light as an electric current is passed through. The same mechanism is used in a light emitting diode (LED) which is an almost identical device. Electrons crossing the band gap release their surplus energy as photons following the electron-hole recombination. In a laser diode, the end faces of the semiconductor are usually polished and used as reflectors to produce a cavity inside the semiconductor. The light is amplified and emerges as a monochromatic, but usually quite divergent beam. Laser diodes can be made quite powerful and stacked together in groups to produce tens of watts or they can be microscopic in size. They are highly efficient and have opened up new laser applications such as communications, sensing, optical data storage, optical computing and data transmission.

1.4.4 Waveguide lasers

Recently there have been developments in incorporating dopant ions into host materials to form a solid state laser in the form of an optical fibre or waveguide. This has given rise to very efficient small scale amplifiers and lasers which guide radiation within the cavity producing good confinement and high intensities at low power levels. This has allowed very low thresholds to be achieved from amplifiers and lasers and has provoked much interest. These systems are also suitable for

---

[§] His initial paper, which would have made his findings known in a more traditional fashion, was rejected for publication by the editors of *Physical Review Letters*.

optical pumping by laser diodes which are also small and efficient, producing a compact electrically powered laser system for use in long-haul communications, integrated fibre systems and sensors.

1.5 Glass fibre lasers

The incorporation of rare-earth ions into glass fibres to form fibre lasers and amplifiers is not a recent development. The first glass laser demonstrated [2] was flash-pumped in the form of an optical fibre, a configuration that was used to overcome the difficulties in obtaining high-quality glass in bulk form. Apart from a report [3] in 1974 of laser operation in an Nd^{3+}-doped silica multimode fibre, the idea of guided-wave glass lasers attracted little attention for the next 24 years. The potential of single-mode rare-earth doped fibres was widely recognised for the first time in 1985, following the demonstration of a very low threshold fibre laser by Mears *et al.* [4] at the University of Southampton. This result was achieved because both optical fibre [5] and laser diode technologies had advanced to a stage where low-loss, rare-earth-doped, single-mode fibres could be made and high-power semiconductor sources were available to pump them. The device reported by the University of Southampton was a laser made of a 2 metre length of neodymium-doped silica fibre fabricated by an extension of the well known Modified Chemical Vapour Deposition (MCVD) process. This 1088 nm fibre laser was optically pumped with a GaAlAs diode laser and required only 600 μW of absorbed power to reach threshold. This pioneering work demonstrated that the well-established fibre technology could be used in a straightforward manner to generate a new and versatile laser medium. From that moment, extensive worldwide activity has brought numerous new fibre laser and amplifier developments. After a time-lag of only five years after the first research announcement, commercial fibre amplifier products were on the market.

Fibre lasers offer certain advantages over bulk lasers. The waveguide properties of the fibre allow much higher intensities to be achieved within the fibre core, and maintained throughout the length of the fibre giving an extended active region. A long length of fibre can give efficient absorption of pump radiation even in the case of weak absorptions. In crystals the interaction length is limited to the length of the focus of the radiation. The confinement properties of fibre geometry allows laser systems to have thresholds lower than equivalent bulk glasses and although fibre lasers are generally low power, this is not always the case [6,7].

The laser material of interest in this work is thulium-doped fluoride glass. The first Tm^{3+}-doped fluoride fibre laser was reported by Esterowitz *et al.* [8] in 1988. Since that fibre laser was reported, a wide variety of devices and configurations based on the thulium ion have been published. Each of the Tm-fluorescence bands in the near-IR have been shown to be compatible with laser action [9,10,11]. A number of groups have demonstrated tunability of the thulium laser emission in the near-IR [12,13]. Visible laser emission at 480 nm (blue) has been reported by Grubb *et al.* [14] by using a process called *upconversion*[§], in Tm^{3+}-doped fluoride fibre.

1.6 Optical fibre sensing

The development of low-loss optical fibres and the introduction of a wide range of optoelectronic emitters and detectors has helped in the development of a wide range of optical sensors. An optical fibre sensor may be defined as a device in which a guided optical signal is modulated in response to a measurand. The information from the measurand may then be recovered from the transmitted signal in the fibre.

There are two basic classes of optical fibre sensors, as shown in figure 1.2 [15]. The first is called an extrinsic sensor, where the optical fibre functions only as a signal carrier. An example of this type of sensor is a sensor based on spectroscopic absorption by an analyte. In this type of sensor the fibre acts as a light guide which couples light to the analyte volume, where it is modified spectrally by the optical characteristics of the analyte, and returns the light from the sample to the detector. A range of species-specific [16,17] sensors based on spectroscopic absorption by an analyte have been demonstrated.

The second type, an intrinsic sensor, is one in which the light is modulated within the fibre by the parameter to be measured. An example of an intrinsic sensor is the distributed temperature sensor [18,19]. This sensor operates by measuring changes in Raman scattering within the fibre due to changes in temperature. Other intrinsic sensors include high current sensors using Faraday rotation [20] and evanescent wave sensors [21].

[§] The upconversion process is explained by the absorption of pump energy by an already excited electron to a higher level, thereby giving the electron a higher energy than the pump source. When the electron relaxes to the ground state the photon it emits has a shorter wavelength than the pump source. Grubb's paper reported a CW room-temperature blue (480 nm) fibre laser when pumped by Nd:YAG laser operating at 1120 nm.
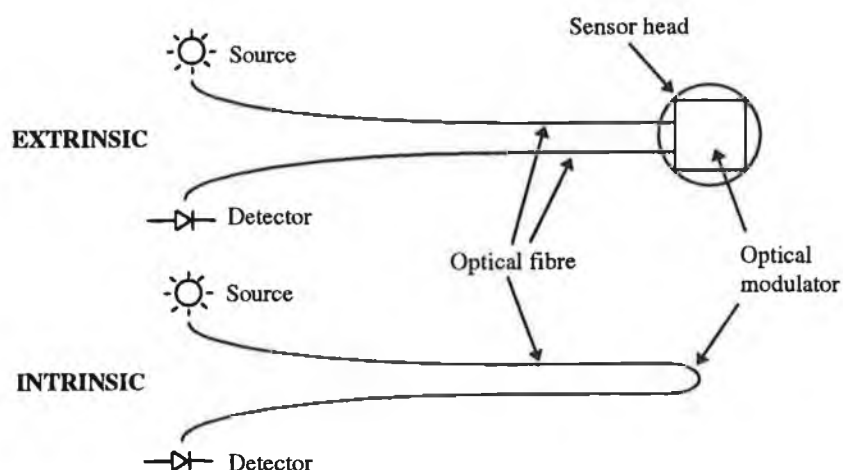
FIGURE 1.2 EXTRINSIC AND INTRINSIC OPTICAL FIBRE SENSORS

Most gas sensors are based on the detected change in signal due to absorption by the gas present. This method relies on conventional spectroscopic techniques, in conjunction with a coupled optical fibre. Some gas sensors use an indicator which is used to transduce the gas concentration into a measurable optical parameter. This approach is applied when the gas has no useful intrinsic optical property. Typical examples of indicator-mediated optrodes include those for oxygen and carbon dioxide [22,23]. Typical examples of simple optical fibre sensors based on the absorption of the gas, include those for chlorine, methane, carbon monoxide, and nitrogen oxides.

1.6.1 Hydrocarbon gas sensing

The detection of hydrocarbon gases, in particular methane, in collieries, offshore installations and various mines is an important quantity. Methane is highly explosive when present in air at levels above 5 %. Methane is also a major constituent in city gas. Fibre optic gas sensors are inherently safe and therefore can serve to detect gas leaks. Detection of methane using direct fibre absorptiometry is the most common method of detection.

A number of fibre optic methane sensors have been demonstrated based on absorption lines of methane at 1.33 μm [24] and at 1.66 μm [25,26]. Most optical sensors to date use either a LED operating at one of these wavelengths or an incandescent source in conjunction with narrow bandpass filters. However, both of these sources have disadvantages. LED's operating at these wavelengths are an emerging technology, and consequently are not reliable as sources. Incandescent

sources have a limited lifetime and the transmission wavelength of the filters is temperature dependent.

1.7 Thesis overview and objectives

The aim of this work was to construct and characterise an optical fibre laser using thulium-doped fluoride glass fibre and to use this novel laser source in a remote hydrocarbon gas sensing system based on infra-red absorption.

The strong fundamental absorptions of most gases of industrial interest and environmental interest are found in the mid-IR spectral region beyond 2 μm where standard telecommunication (silica) optical fibres have prohibitively high attenuation. Fluoride glass fibres, however, are suitable for this region as they exhibit useful transmission out to 5 μm. The major problem in applying this technology is the lack of suitable sources for this region. As yet there are no convenient solid-state sources available and broadband incandescent sources have many disadvantages (limited lifetime, fragile, heat generation) which render them unsuitable in many situations. This deficiency of sources was the underlying motivation for this project. The possibility of using a fibre laser as a narrowband source with potential tunability was very attractive. Active fibre devices such as this can combine the excellent properties of standard laser materials with the high energy confinement available in optical fibres. They often exhibit high energy conversion efficiencies and are obviously compatible with optical fibres. This is particularly important in terms of coupling the output into optical fibre systems.

Before the fibre laser cavity was constructed, a number of characterisations were carried out. The doped fibre was characterised in terms of maximum absorption, and these data were used to select a pump laser diode. The characteristics of the input and output laser mirrors were considered, before deciding on their transmission characteristics. The optical launch lens system was modelled, in order to select lenses to achieve the maximum possible launch efficiency. Once the fibre laser was fully operational the laser was characterised in terms of laser threshold, output power and conversion efficiency.

A demonstration sensor rig was developed to illustrate the sensing of low concentrations of hydrocarbon (methane) gas, with the fibre laser source.

The possibility of utilising the fluorescence bands of Tm^{3+} as a source for optical sensing was investigated. This approach offers the advantages of a stable output spectrum, reasonable output power and an intrinsic reference signal. Two optical fibre water sensor configurations are presented. The first demonstrates the viability of detection of water content, while, the second demonstrates the viability of a distributed or remote water content sensor.

References :

1. France P.W. : **'Optical Fibre Lasers & Amplifiers'**, CRC Press, Boca Raton, FL, 1991

2. Snitzer E. : **'Optical maser action of Nd^{3+} in a barium crown glass'**, Phys. Rev. Lett., 1961, Vol. 7, No. 12, pp. 444-446

3. Stone J., Burrus C.A. : **'Neodymium-doped fiber lasers : room temperature CW operation with an injection pump laser'**, Applied Optics, 1974, Vol. 13, pp. 1256

4. Mears R.J., Reekie L., Poole S.B., Payne D.N. : **'Neodymium-doped silica single-mode fibre lasers'**, Electronics Letters, 1985, Vol. 21, No. 17, pp. 738-740

5. Poole S.B., Payne D.N., Fermann M.E. : **'Fabrication of low-loss optical fibres containing rare-earth ions'**, Electronics Letters, 1985, Vol. 21, No. 17, pp. 737-738

6. Miyajima Y., Komukai T., Sugawa T. : **'1-W CW Tm-doped fluoride fibre laser at 1.47 µm'**, Electronics Letters, 1993, Vol. 29, No. 8, pp. 660-661

7. Dennis M.L., Dixon J.W., Aggarwal I. : **'High power upconversion lasing at 810 nm in Tm:ZBLAN fibre'**, Electronics Letters, 1994, Vol. 30, No. 2, pp. 136-137

8. Esterowitz L., Allen R., Aggarwal I. : **'Pulsed laser emission at 2.3 µm in a thulium-doped fluorozirconate fibre'**, Electronics Letters, 1988, Vol. 24, No. 17, p. 1104

9. Hanna D.C., Jauncey I.M., Percival R.M., Perry I.R., Smart R.G., Suni P.J., Townsend J.E., Tropper A.C. : **'Continuous-wave oscillation of a monomode thulium-doped fibre laser'**, Electronics Letters, 1988, Vol. 24, No. 19, pp. 1222-1223

10. Percival R.M., Carter S.F., Szebesta D., Davey S.T., Stallard W.A. : **'Thulium-doped monomode fluoride fibre laser broadly tunable from 2.25 to 2.5 µm'**, Electronics Letters, 1991, Vol. 27, No. 21, pp. 1912-1913

11.   Percival R.M., Szebesta D., Davey S.T. : **'Highly efficient CW cascade operation of 1.47 and 1.82 μm transitions in Tm-doped fluoride fibre laser'**, Electronics Letters, 1992, Vol. 28, No. 20, pp. 1866-1868

12.   Barnes W.L., Townsend J.E. : **'Highly tunable and efficient diode pumped operation of Tm3+ doped fibre lasers'**, Electronics Letters, 1990, Vol. 26, No. 11, pp. 746-747

13.   Allain J.Y., Monerie M., Poignant H. : **'Tunable CW lasing around 0.82, 1.48, 1.88 and 2.35 μm in thulium-doped fluorozirconate fibre'**, Electronics Letters, 1989, Vol. 25, No. 24, pp. 1660-1662

14.   Grubb S.G., Bennett K.W., Cannon R.S., Humer W.F. : **'CW room-temperature blue upconversion fibre laser'**, Electronics Letters, 1992, Vol. 28, No. 13, pp. 1243-1244

15.   Culshaw B., : **'Optical fibre sensing and signal processing'**, IEE, 1984

16.   Thompson R.B., Lakowicz J.R., : **'Fiber optic pH sensor based on phase fluorescence lifetimes'**, Analytical Chemistry, 1993, Vol. 65, pp. 853-856

17.   Wolfbeis O.S. (ed.) : **' Fibre optic chemical sensors and biosensors'**, CRC Press, Boca Raton, FL, 1991, Vol. 2, Chapter 10

18.   Wakami T., Tanaka S. : **'1.55 μm long span fiber-optic distributed temperature sensor'**, Culshaw B., Jones J.D.C. (eds.), 10th Optical Fibre Sensors Conference, 1994, SPIE Vol. 2360, pp. 134-137

19.   Dakin J.P., Pratt D.J., Bibby G.W., Ross J.N. : **'Distributed optical fibre Raman temperature sensor using a semiconductor light source and detector'**, Electronic Letters, 1985, Vol. 21, No. 13, pp. 569-570

20.   Dandridge A., Tveten A.B., Sigei G.H., West E.J., Giallorenzi T.G. : **'Optical fibre magnetic field sensor'**, Electronics Letters, 1980, Vol. 16, pp. 408-409

21.   McCabe S., MacCraith B.D. : **'Novel mid-infrared LED as a source for optical fibre gas sensing'**, Electronics Letters, 1993, Vol. 29, No. 19, pp. 1719-1721

22. MacCraith B.D., O'Keeffe G., McDonagh C., McEvoy A.K. : **'LED-based fibre optic oxygen sensor using sol-gel coating'**, Electronics Letters, 1994, Vol. 30, No. 11, pp. 888-889

23. Orellana G., Moreno-Bondi M.C., Segovia E., Marazuela M.D. : **'Fiber-optic sensing of carbon dioxide based on excited-state proton transfer to a luminescent ruthenium (II) complex'**, Analytical Chemistry, 1992, Vol. 64, No. 19, pp. 2210-2215

24. Alarcon M.C., Ito H., Inaba H. : **'All-optical remote sensing of city gas through CH$_4$ gas absorption employing a low-loss optical fibre link and an InGaAsP light-emitting diode in the near-infrared region'**, Applied Physics B, 1987, Vol. 43, pp. 79-83

25. Sweeney J. : **'Development of a fibre optic sensor for methane gas'**, M.Sc. Thesis, Dublin City University, 1994

26. Chan K., Ito H., Inaba H. : **'Remote sensing system for a near-infrared differential absorption of CH$_4$ gas using low-loss optical fibre link'**, Applied Optics, 1984, Vol. 23, No. 19, pp. 3415-3420

Chapter 2

Structure and Spectroscopy of rare-earth doped fibres

2.1 Introduction to rare-earth doped fibres

The rare-earths are divided into two groups each containing 14 elements. The lanthanides are characterised by the filling of the $4f$ electron shell, Cerium (Ce) being the first with an atomic number Z of 58 and ending with Lutetium (Lu, Z=71). The actinides begin with Thorium (Th, Z=90) which starts filling the $5f$ electron shell and end with Lawrencium (Lr, Z=103). Both groups have similar optical and electronic properties. However, the actinides have no isotopes stable enough to be useful in optical devices and are therefore ignored. Only the lanthanides have received attention as they are easily incorporated into many laser and amplifier materials, Nd^{3+} in a YAG host being the most widely known. In condensed matter the trivalent level of ionization is the most stable for lanthanide ions with the exception of Eu and Yb, and therefore most optical devices use trivalent ions.

Nearly all the lanthanide rare-earth ions have been incorporated into optical fibres to form fibre lasers or amplifiers except three, Promethium (Pm^{3+}), Gadolinium (Gd^{3+}) & Lutetium (Lu^{3+}). The first glass fibre laser was demonstrated in 1961 by Snitzer [1] and contained Neodymium (Nd^{3+}) in the fibre core. Currently the rare earth ion attracting most research attention is Erbium (Er^{3+}). Erbium-doped silica fibre lasers and amplifiers have been studied at length in the past number of years for their potential as sources for telecommunication systems operating within the third window at 1.55 μm. The first Thulium (Tm^{3+}) doped fibre laser was reported in 1967 by Gandy *et al.* [2] and only a moderate level of research had been maintained until the recent upsurge of interest in fibre lasers since 1985. Much of the interest in Tm^{3+} stems from its emission that occurs in the spectral gaps between Nd^{3+} and Er^{3+}.

Rare earths have many important characteristics that distinguish them from other optically active ions: they emit and absorb over narrow wavelength ranges, the wavelengths of the emission and absorption transitions are relatively insensitive to the host material, the intensities of these transitions are weak, the lifetimes of the metastable states are long and the quantum efficiencies tend to be high. Many of the absorption bands of rare earth ions lie in the near-IR. This region is well covered by commercially available semiconductor laser diodes which can serve as pump sources.

The remainder of this chapter deals with the absorption and fluorescence of rare earth ions in a fluoride based glass.

2.2 Electron energy levels

The electron energy levels of lanthanides are labelled according to Russell-Saunders or L-S coupling. This labeling system is based on the quantum numbers L, S and J which are governed by the outer electron shell structure. The outer electron shell configuration is determined by the number of electrons present in the atom and the order in which they are filled. The diagram shown below in figure 2.1 displays the order in which the electron shells are filled.

$$
\begin{array}{ccccc}
\ell = & 0 & 1 & 2 & 3 \\
& 1s^2 & & & \\
& 2s^2 & 2p^6 & & \\
& 3s^2 & 3p^6 & 3d^{10} & \\
& 4s^2 & 4p^6 & 4d^{10} & 4f^{14} \\
& 5s^2 & 5p^6 & 5d^{10} & 5f^{14} \\
& 6s^2 & 6p^6 & 6d^{10} & \\
& 7s^2 & 7p^6 & & \\
& 8s^2 & & &
\end{array}
$$
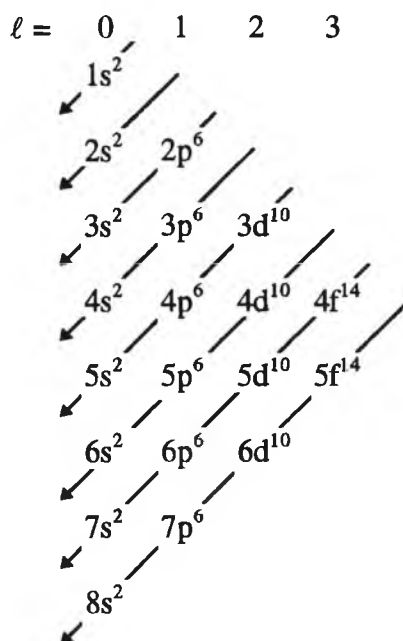
FIGURE 2.1 FILLING OF ELECTRON SHELLS

The lanthanide series begin with Cerium having Z=58 number of electrons. As shown in figure 2.1, these electrons fill in the following order :

$$Xe : \quad 1s^2\, 2s^2\, 2p^6\, 3s^2\, 3p^6\, 4s^2\, 3d^{10}\, 4p^6\, 5s^2\, 4d^{10}\, 5p^6$$

$$Ce : \quad [Xe]\, 6s^2\, 4f\, 5d$$
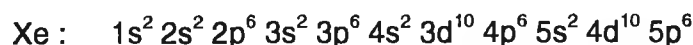
The filling of the $4f$ subshell is irregular and complicated with competition taking place between the $4f$ and $5d$ levels. The lanthanide series continue to fill the $4f$ shell with the exception of Gd and Lu which have a $5d$ subshell. For example, neutral Erbium has the following electron configuration :

$$Er : \quad [Xe]\, 6s^2\, 4f^{12}$$

In the case of triply ionised lanthanides the $6s$ shell empties before the $4f$ shell, so that, Er^{3+} for example, has the following electron configuration :

$$Er^{3+} : \quad [Xe]\, 4f^{11}$$

where one electron is removed from the $4f$ shell and two from the $6s$ shell.

The *term* for a particular electronic configuration is obtained using L-S coupling notation :

$$^{2S+1}L_J$$

where J is the total angular momentum quantum number, L is the total orbital angular momentum quantum number and S the total spin quantum number. If an atom contains just one electron, the orbital angular momentum is given by the value of ℓ, and just as the orbital nomenclature uses the identification $\ell = 0, 1, 2, 3, ... \leftrightarrow$ s, p, d, f, g, ..., the term symbols use S, P, D, F, G, ... Where there is more than one electron, the total orbital angular momentum is obtained by combining the orbital angular momenta of the individual electrons by using the Clebsch - Gordan series. Thus if one electron has ℓ_1 and the second has ℓ_2 their combined orbital angular momentum has possible values of L given by :

$$L = \ell_1 + \ell_2, \; \ell_1 + \ell_2 - 1, \; \ell_1 + \ell_2 - 2, \; ... \; |\ell_1 - \ell_2|$$

In the case where there are three electrons, the third electron is coupled with the possible values of L obtained from the first two electrons and so on for more electrons. For atoms with more than one electron in its valence band there are many possible values for L, the total orbital angular momentum. The total spin

quantum number, S, is determined by the number of unpaired electrons. The total spin is represented by the operator :

$$S = S_1 + S_2 + S_3 + ... + S_n$$

where S_1, S_2, S_3, ...,S_n all equal ½. For example, a $4f$ shell with 10 electrons will have 4 unpaired electrons, as shown below

↓↑	↓↑	↓↑	↓	↓	↓	↓
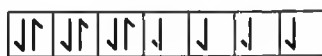
as an f shell may contain 14 electrons. (An electron may have two possible spin orientations ,spin up or spin down.) This yields a corresponding total spin quantum number, S, of 4 x ½ = 2. The permitted values of J, the total angular momentum quantum number are given by :

$$J = L+S, L+S-1, L+S-2, ..., |L-S|$$

The L - S coupling *term* is obtained from

$$^{2S+1}L_J$$

where the 2S + 1 represents the multiplicity of the *term* , i.e. the number of possible orientations of the total spin of the atom.

In the case of the previous example, triply ionised Erbium (Er^{3+}), the last unfilled shell was $4f^{11}$. This shell will have 3 unpaired electrons, as shown below,

↓↑	↓↑	↓↑	↓↑	↓	↓	↓
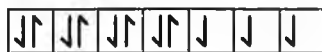
giving a total spin quantum number, S, of 3 x ½ = $^3/_2$. The left superscript in the *term* symbol has a value of $(2 \times {}^3/_2) + 1 = 4$. There are three values of orbital angular momentum ℓ_1, ℓ_2 and ℓ_3. By combining $\ell_1 = 3$ and $\ell_2 = 3$ to obtain L' using the Clebsch - Gordan series, this will yield L' values of 6, 5, 4, 3, 2, 1 and 0. The next step is to couple $\ell_3 = 3$ with L', which yields 28 possible values for L. By combining the 28 possible values of L with S = $^3/_2$ to obtain a value for the total angular momentum quantum number, J, this gives 364 possible combinations. The correct *term* for the ground state of an atom is extremely complicated and may only be inferred from absorption and emission spectra used in conjunction with the possible L, S and J terms.

Figure 2.2 displays the electronic energy levels of triply ionised rare earth ions [3]. This demonstrates all available pump and emission levels from the visible region to the near-IR.

FIGURE 2.2 THE ELECTRONIC ENERGY LEVELS OF TRIVALENT RARE EARTH IONS
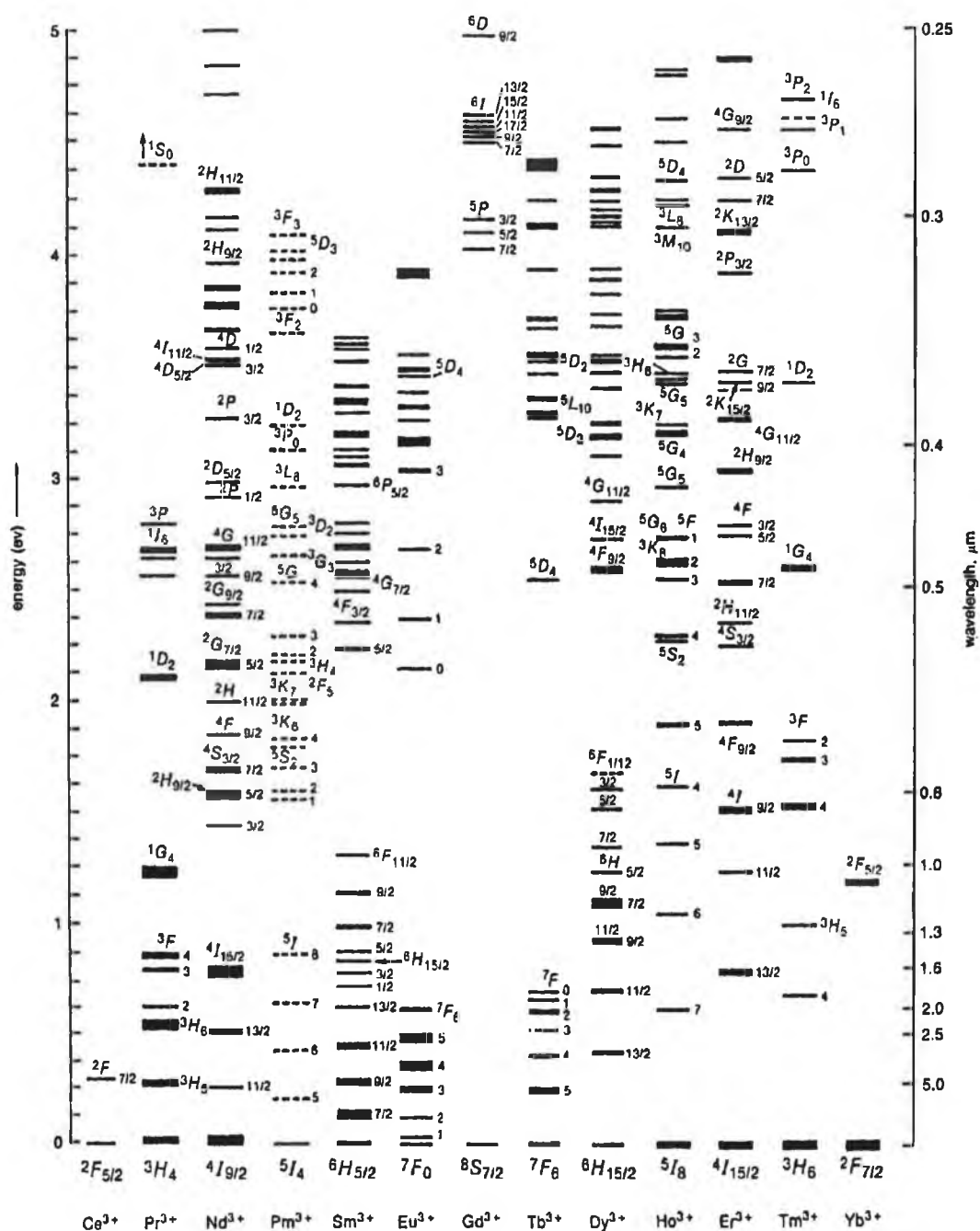
2.3 Spectroscopy

Isaac Newton was the first to resolve white light into separate colours by dispersion with a prism in 1666, but it was not until 1752 that Melvill first showed that light from an incandescent gas was composed of a large number of discrete frequencies called emission lines. Subsequently, it was discovered that atoms exposed to white light can only absorb certain discrete frequencies called absorption lines. In 1859, G.R. Kirchhoff was the first to show that only certain definite frequencies can be absorbed or radiated by a given element and that the emission frequencies coincide with the absorption frequencies. The fact that each element has its own characteristic atomic line spectrum is the foundation of atomic spectroscopy.

There are a wealth of absorption bands in the visible and near-IR, where many suitable sources are available for optically exciting a particular atom. An abundance of emission bands occurs in the near and mid-IR with overlaps corresponding to absorption bands of many species of interest in the area of optical sensing. The absorption and emission bands of most trivalent rare earth ions are examined in the next two sections.

2.3.1 Absorption

Absorption spectra are recorded by measuring the optical transmittance of a sample with a broadband light source. Light from the source is passed through a dispersing element and light exiting from the sample is recorded using a detector.

The absorption spectra of rare earth ions do not vary significantly from one glass host to another. However, small changes in absorption are likely to occur, and it is important to have a complete knowledge of the absorption levels in order to make a proper choice of pump wavelength for fluorescence/laser applications. Appendix A displays the absorption spectra for rare earth ions in a ZBLANp glass (when PbF_2 is used to increase the refractive index of the core, this glass is known as ZBLANp) [4]. Of the fourteen rare earth ions only the absorption spectra of Ce^{3+} (Cerium), Pr^{3+} (Praseodymium), Nd^{3+} (Neodymium), Sm^{3+} (Samarium), Eu^{3+} (Europium), Tb^{3+} (Terbium), Dy^{3+} (Dysprosium), Ho^{3+} (Holmium), Er^{3+} (Erbium), Tm^{3+} (Thulium) and Yb^{3+} (Ytterbium) are displayed, with Pm^{3+} (Promethium), Gd^{3+} (Gadolinium) and Lu^{3+} (Lutetium) omitted. Promethium is radioactively unstable and short-lived. The electronic structure of Gadolinium is $4f^7$, and therefore the $4f$

transitions are spin forbidden. Lutetium contains a full $4f^{14}$ shell and no transitions are observed.

2.3.2 Fluorescence

Fluorescence describes the emission which follows the absorption of photons which excite the electrons into higher energy levels. The electrons then relax to a lower energy level. In general, initial relaxation is by nonradiative decay (i.e., by lattice phonons) and thereafter, the electrons decay by the emission of a photon (fluorescence). The resulting fluorescence from the sample is collected usually at right angles to the direction of pump propagation and analysed using a monochromator in conjunction with a suitable detector. Once the fluorescence spectra have been determined in bulk glasses, this information can be subsequently used to determine fluorescence/laser behavior in fibres.

As in the case for absorption, the host material does not significantly alter the emission properties of the rare earth element under investigation. However, in a silica glass host , transitions with energies less than 5000 cm^{-1} (i.e. $\lambda > 2$ μm) lose energy nonradiatively, compared with a value of 2000 cm^{-1} ($\lambda > 5$ μm) in heavy metal fluoride fibres. In fluoride-based fibres the multi-phonon absorption edge is shifted to longer wavelengths and therefore the fibre transmits further into the IR.

The following fluorescence spectra [4] of rare earth ions in a ZBLANp host, shown in figures 2.3 (a)-(i), were obtained by exciting the various rare earths with an argon ion laser which had emission lines at 0.4579, 0.4658, 0.4727, 0.4765, 0.4880, 0.4965, 0.5017 and 0.5145 μm. Promethium, Gadolinium and Lutetium exhibit no fluorescence emission for reasons explained in section 2.3.1. Cerium (Ce^{3+}) and Ytterbium (Yb^{3+}) are excluded as Ce^{3+} emission occurs in the mid-IR and is absorbed by the lattice in the form of phonon absorption and Yb^{3+} exhibits only one emission band at 1μm.

In addition to changing their electronic state through interaction with the electromagnetic field (i.e. the absorption and emission of photons), rare earth ions in solids can undergo transitions as a result of their interaction with vibrations of the host material in the form of phonon absorption and emission. Other loss mechanisms include up-conversion, cross-relaxation and line broadening due to the glass host.
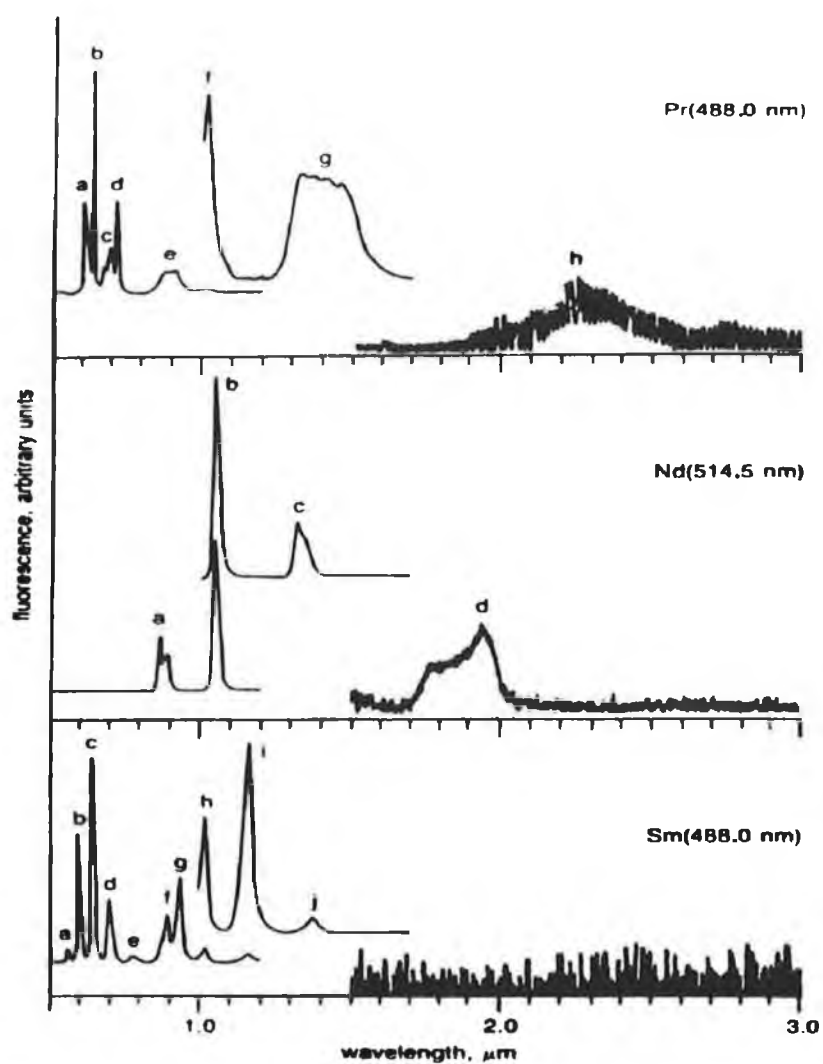
Peak	Praseodymium		Neodymium		Samarium	
	Transition	**λ (μm)**	**Transition**	**λ (μm)**	**Transition**	**λ (μm)**
a	$^3P_0 \to {}^3H_6$	0.603	$^4F_{3/2} \to {}^4I_{9/2}$	0.867	$^4G_{5/2} \to {}^6H_{5/2}$	0.560
b	$^3P_0 \to {}^3F_2$	0.635	$^4F_{3/2} \to {}^4I_{11/2}$	1.048	$^4G_{5/2} \to {}^6H_{7/2}$	0.595
c	$^1D_2 \to {}^3H_5$	0.695	$^4F_{3/2} \to {}^4I_{13/2}$	1.318	$^4G_{5/2} \to {}^6H_{9/2}$	0.641
d	$^3P_0 \to {}^3F_4$	0.717	$^4F_{3/2} \to {}^4I_{15/2}$	1.945	$^4G_{5/2} \to {}^6H_{11/2}$	0.704
e	$^3P_0 \to {}^1G_4$	0.908			$^4G_{5/2} \to {}^6H_{13/2}$	0.782
f	$^1D_2 \to {}^3F_4$	1.014			$^4G_{5/2} \to {}^6H_{15/2}$	0.896
g	$^1G_4 \to {}^3H_5$ $^1D_2 \to {}^1G_4$	1.326			$^4G_{5/2} \to {}^6F_{5/2}$	0.936
h	$^1G_4 \to {}^3F_2$ $^3H_6 \to {}^3H_4$	2.300			$^4G_{5/2} \to {}^6F_{7/2}$	1.022
i					$^4G_{5/2} \to {}^6F_{9/2}$	1.162
j					$^4G_{5/2} \to {}^6F_{11/2}$	1.376

FIGURE 2.3 (a-c) THE FLUORESCENCE SPECTRA OF THE TRIVALENT RARE EARTH IONS Pr, Nd AND Sm IN A ZBLANp GLASS. THE WAVELENGTH USED TO EXCITE THE ION IS GIVEN IN BRACKETS.

Eu(457.9 nm)

Tb(488.0 nm)

Dy(457.9 nm)

fluorescence, arbitrary units

1.0 2.0 3.0

wavelength, μm
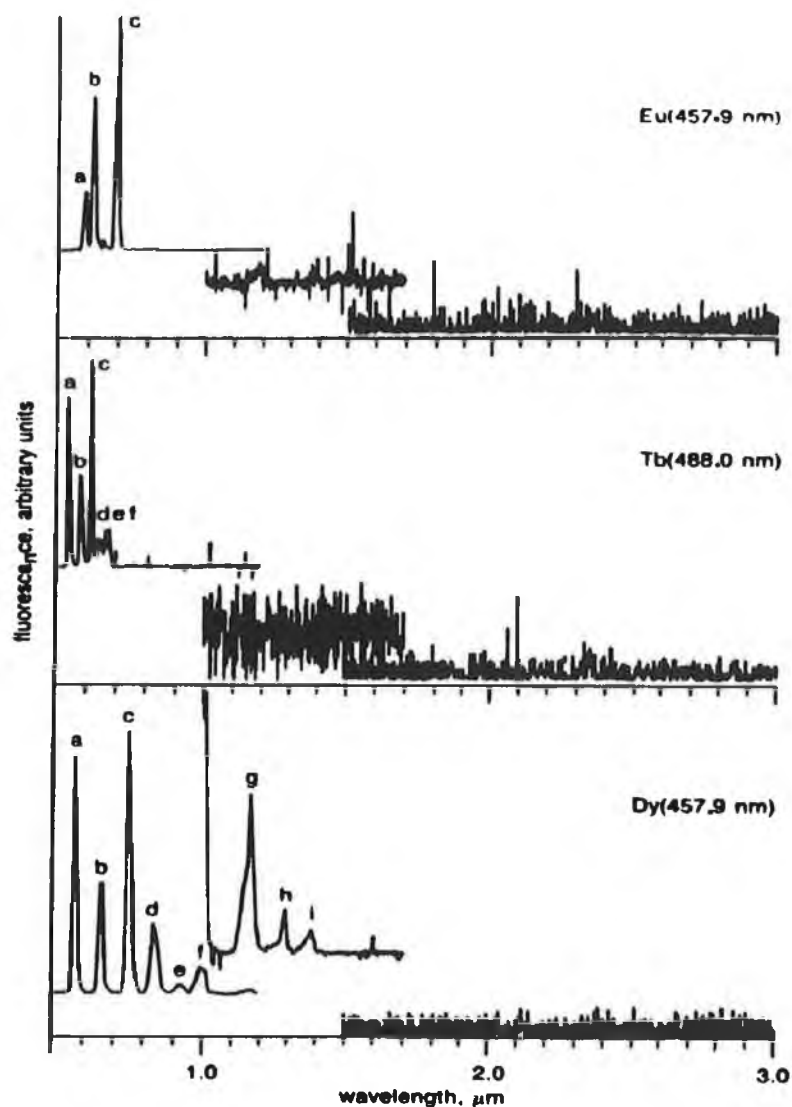
Peak	Europium		Terbium		Dysprosium	
	Transition	λ (μm)	Transition	λ (μm)	Transition	λ (μm)
a	$^5D_0 \to\ ^7F_1$	0.591	$^5D_4 \to\ ^7F_5$	0.543	$^4F_{9/2} \to\ ^6H_{13/2}$	0.575
b	$^5D_0 \to\ ^7F_2$	0.615	$^5D_4 \to\ ^7F_4$	0.585	$^4F_{9/2} \to\ ^6H_{11/2}$	0.661
c	$^5D_0 \to\ ^7F_4$	0.698	$^5D_4 \to\ ^7F_3$	0.621	$^4F_{9/2} \to\ ^6H_{9/2}$ $^4F_{9/2} \to\ ^6F_{11/2}$	0.750
d			$^5D_4 \to\ ^7F_2$	0.649	$^4F_{9/2} \to\ ^6H_{7/2}$ $^4F_{9/2} \to\ ^6F_{9/2}$	0.834
e			$^5D_4 \to\ ^7F_1$	0.668	$^4F_{9/2} \to\ ^6H_{5/2}$	0.924
f			$^5D_4 \to\ ^7F_0$	0.681	$^4F_{9/2} \to\ ^6F_{7/2}$	1.000
g					$^4F_{9/2} \to\ ^6F_{5/2}$	1.170
h					$^4F_{9/2} \to\ ^6F_{3/2}$	1.294
i					$^4F_{9/2} \to\ ^6F_{1/2}$	1.384

FIGURE 2.3 (d-f) THE FLUORESCENCE SPECTRA OF THE TRIVALENT RARE EARTH IONS Eu, Tb AND Dy IN A ZBLANp GLASS. THE WAVELENGTH USED TO EXCITE THE ION IS GIVEN IN BRACKETS.

Peak	Holmium		Erbium		Thulium	
	Transition	**λ (μm)**	**Transition**	**λ (μm)**	**Transition**	**λ (μm)**
a	$^5S_2 \rightarrow {}^5I_8$	0.543	$^4S_{3/2} \rightarrow {}^4I_{15/2}$	0.543	$^1G_4 \rightarrow {}^3F_4$	0.649
b	$^5S_2 \rightarrow {}^5I_7$	0.750	$^4F_{9/2} \rightarrow {}^4I_{15/2}$	0.655	$^1G_4 \rightarrow {}^3H_5$ $^3H_4 \rightarrow {}^3H_6$	0.799
c	$^5S_2 \rightarrow {}^5I_6$	1.015	$^4S_{3/2} \rightarrow {}^4I_{13/2}$	0.847	$^1G_4 \rightarrow {}^3H_4$ $^3F_3 \rightarrow {}^3F_4$ $^3H_5 \rightarrow {}^3H_6$	1.184
d	$^5I_6 \rightarrow {}^5I_8$	1.154	$^4I_{11/2} \rightarrow {}^4I_{15/2}$	0.977	$^1G_4 \rightarrow {}^3F_3$ $^3H_4 \rightarrow {}^3F_4$	1.464
e	$^5I_6 \rightarrow {}^5I_8$	1.191	$^4S_{3/2} \rightarrow {}^4I_{11/2}$	1.219	$^3F_4 \rightarrow {}^3H_6$	1.847
f	$^5S_2 \rightarrow {}^5I_5$	1.381	$^4I_{13/2} \rightarrow {}^4I_{15/2}$	1.538	$^3H_4 \rightarrow {}^3H_5$	2.307
g	$^5S_2 \rightarrow {}^5I_4$	1.953	$^4I_{11/2} \rightarrow {}^4I_{13/2}$	2.719		
h	$^5I_7 \rightarrow {}^5I_8$	2.039				
i	$^5I_6 \rightarrow {}^5I_7$	2.848				

FIGURE 2.3 (g-i) THE FLUORESCENCE SPECTRA OF THE TRIVALENT RARE EARTH IONS Ho, Er AND Tm IN A ZBLANp GLASS. THE WAVELENGTH USED TO EXCITE THE ION IS GIVEN IN BRACKETS.

2.3.3 Fluorescence Lifetimes

The fluorescence lifetime represents the average amount of time the electron remains in the excited state prior to its return to the ground state. There are two widely used methods for the measurement of fluorescence lifetimes. These are the pulse method and harmonic or phase-modulation method. In the pulse method the sample is excited with a short pulse of light and the time-dependent decay of fluorescence intensity is measured. In the harmonic method the sample is excited with sinusoidally modulated light. The phase shift and demodulation of the emission, relative to the incident light, is used to calculate the lifetime. Each method possesses its own advantages and disadvantages, but as the pulse method is used in this work, it will be discussed in more detail.

Consider the excitation of a fluorophore with an infinitely short pulse of light, resulting in an initial population (N_o) of fluorophores in the excited state. The rate of decay of the initially excited population is

$$\frac{dN(t)}{dt} = -(\gamma + k)N(t) \qquad \qquad \textit{Eqn. 2. 1}$$

where *N(t)* is the number of excited electrons at a time *t* following excitation, γ is the radiative decay rate, and *k* is the rate of nonradiative decay. Where *N(t)* = N_o at *t* = 0, integration of equation 2.1 yields

$$N(t) = N_o \, e^{-t/\tau} \qquad \qquad \textit{Eqn. 2. 2}$$

where $\tau = (\gamma + k)^{-1}$ is the lifetime of the excited state. Hence, the fluorescence intensity *F(t)*, which is proportional to the excited state population (*F(t)* = $\gamma N(t)$), will decay exponentially as shown in figure 2.4. The fluorescence lifetime is generally equated with the time required for the intensity to decay to 1/e of its initial value, which is $(\gamma + k)^{-1}$. With t = τ, this yields

$$N(t) = N_o \, e^{-1} \qquad \qquad \textit{Eqn. 2. 3}$$

$$\frac{N(t)}{N_o} = 0.3679 \qquad \qquad \textit{Eqn. 2. 4}$$

The fluorescence lifetime of the fluorophore can be determined from the fluorescence decay curve, using equation 2.4, as the time taken for the excited

electrons to decay to 1/e or 36.79 % of the total number of excited electrons. Alternatively, the lifetime may be determined from the slope of a plot of the log *F(t)* versus *t*.
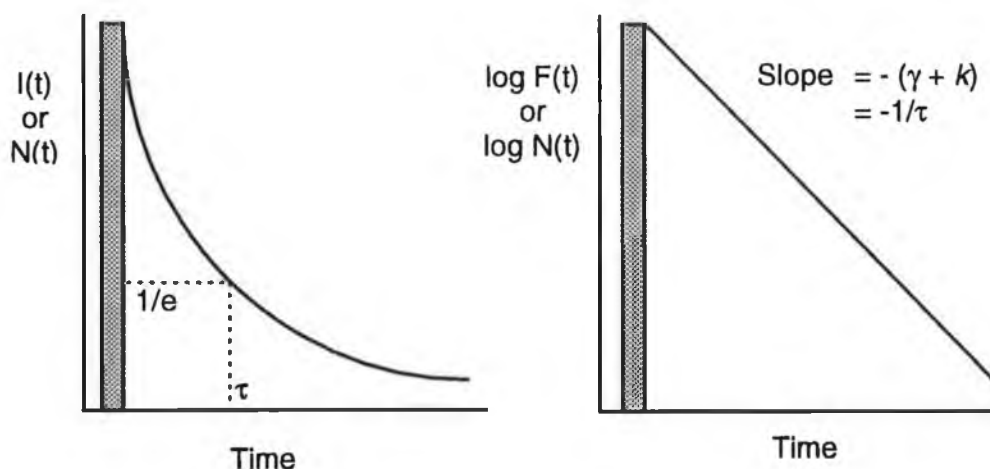
FIGURE 2.4 SCHEMATIC DESCRIPTION OF THE PULSE LIFETIME MEASUREMENTS

2.4 Summary

This chapter introduced the labeling scheme used for labeling the atomic elements and the difficulties involved in correctly labeling these electron energy levels. The spectroscopy of rare-earth ions was introduced, with particular reference to absorption, fluorescence and fluorescence lifetimes of the ions. A full range of absorption and fluorescence spectra of all the possible rare-earth ions was included. This was included in order facilitate the quick evaluation of possible pump bands in the visible to near-IR and many emission bands in the near-IR for use as sources for optical sensing. The experimental techniques used to record the absorption and fluorescence spectra will be further discussed in chapter 3.

References :

1.   Snitzer E. : **'Optical maser action of Nd^{3+} in a barium crown glass'**, Phys. Rev. Lett., 1961, Vol. 7, No. 12, pp. 444-446

2.   Gandy H.W., Ginther R.J., Weller J.F. : **'Stimulated emission of Tm^{3+} radiation in silicate glass'**, Journal of Applied Physics, 1967, No. 38, pp. 3030-3031

3.   Dieke G.H, Crosswhite H.M. : **'The doubly and triply ionized rare earths'**, Applied Optics, 1963, Vol. 2, pp. 675

4.   Davey S.T., France P.W. : **'Rare earth doped fluorozirconate glasses for fibre devices'**, Br. Telecom Technol. J., 1989, Vol. 7, No. 1, pp. 58-68

Chapter 3

Spectroscopic Characterisation of Tm^{3+} in a fluoride host

3.1 Introduction to Tm^{3+} in a fluoride host

This work is concerned with the optical properties of Tm^{3+} in a zirconium fluoride fibre host material. As was indicated in chapter 2, Tm^{3+} offers a number of fluorescence emission bands in the near-IR at approximately 1.2, 1.45, 1.9 and 2.3 μm, when optically pumped around 800 nm. This chapter deals in detail with the energy levels, absorption and fluorescence emission spectra as well as the lifetimes of Tm^{3+} in a zirconium fluoride host. In addition the characteristics of zirconium fluoride as a glass host are compared with those silica.

3.2 Zirconium fluoride glass

The discovery of the first heavy-metal fluoride glass in 1974 in the University of Rennes, France [1] occurred by accident. Professor Jacques Lucas and his research group were trying to prepare a single-crystal NaF - BaF$_2$ - 2ZrF$_4$ doped with Nd^{3+} for fluorescence experiments, but X-ray analysis of the product revealed that it was predominantly amorphous. The first product was relatively unstable, but more stable compositions were developed after some further work. The glass was found to be transmissive from approximately 0.2 μm in the UV to 7 μm in the IR. The most commonly used and most stable heavy-metal fluoride glass is ZBLAN, made from the fluorides of zirconium, barium, lanthanum, aluminum and sodium (**Zr, Ba, La, Al, Na**) in the stoichiometry 53:20:4:3:20 mol. %. The glass used to manufacture the fibre for this work is a zirconium fluoride (ZrF$_4$) glass.

The fundamental losses in silica optical fibres are impurity material absorption and Rayleigh scattering. As the impurities in the silica glasses were reduced, operation at longer wavelengths became more attractive due to the λ^{-4} dependence of Rayleigh scattering. Today the minimum absorption in silica fibres

occurs in the spectral area known as the third window, at 1.55 µm. In silica glasses beyond 1.55 µm the fundamental infrared multi-phonon absorption of the material dominates the losses which increase rapidly with λ. In order to achieve lower losses it is necessary to operate further into the infrared where scattering losses are smaller. To do this the spectral region at which multi-phonon absorption becomes significant must be shifted to longer wavelengths. Multi-phonon absorption is caused by the coupling of electromagnetic energy to the dipoles created by the lattice vibrations of the material. The cut-off frequency of the fundamental phonon is given by

$$f_o = \frac{1}{2\pi} \left(\frac{F}{\mu} \right)^{1/2}$$

Eqn. 3. 1

where F is the force constant between the atoms of the dipole and µ is the reduced mass of the atoms. Reducing F or increasing µ will therefore move the absorption cut-off to lower frequencies i.e. further into the infrared. In a heavy-metal fluoride glass the increased value of µ shifts the multi-phonon absorption band further into the IR. Figure 3.1 displays the infrared transmission curves for several heavy-metal fluorides and silica glass [2].
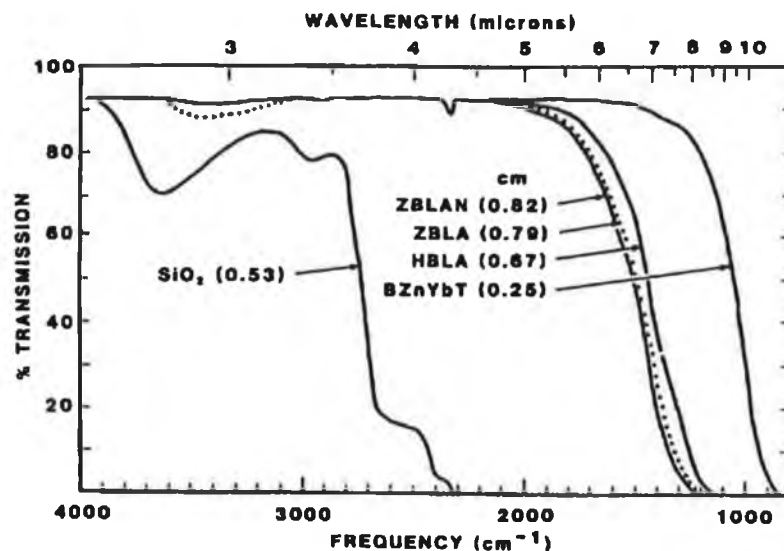
FIGURE 3.1 INFRARED TRANSMISSION CURVES. SAMPLE THICKNESS IN PARENTHESES

Other alternative compositions which offer transmission further into the IR are being investigated. These alternative compositions include chloride, bromide, iodide, chalcogenide and chalcohalide glasses whose multiphonon edges are shifted further into the IR. The next generation of optical networks is predicted to operate in the 2-3 μm region, and this will further enhance research in the area of mid-IR transmitting glass compositions.

3.3 Energy levels

As outlined in section 2.2, identification of the correct *term* for the ground state of an atom is quite complicated and may only be inferred from absorption and emission spectra used in conjunction with the possible L, S and J terms. However, the correct term may be obtained from literature, providing the outer electron shell configuration is known. Neutral Thulium has $Z = 69$ electrons. Therefore, we may represent Tm as :

$$Tm : \quad [Xe]\ 6s^2\ 4f^{13}$$

where neutral Xenon is represented by :

$$Xe : \quad 1s^2\ 2s^2\ 2p^6\ 3s^2\ 3p^6\ 4s^2\ 3d^{10}\ 4p^6\ 5s^2\ 4d^{10}\ 5p^6$$
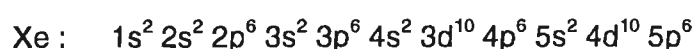
As is the case for triply ionised lanthanides, the $6s$ shell empties before the $4f$ shell, and hence, Tm^{3+} has the following electronic configuration :

$$Tm^{3+} : \quad [Xe]\ 4f^{12}$$
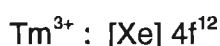
The term for a $4f$ shell with 12 electrons is $^3H_6$, corresponding to the ground state term for triply ionised Thulium. The Russell - Saunders labeling scheme of the excited levels above the ground state is extremely involved and is generally inferred from absorption and fluorescence data. In the literature, there exists much confusion with regard to the labeling of the $^3H_4$ and $^3F_4$ levels in Tm^{3+}. This is due to the labeling of levels by some authors using the dominant L-S contribution while others use the L-S term it would have if the spin-orbit interaction were negligible. More recent theoretical work [3] has shown that the correct labeling is to assign $^3H_4$ to the higher energy level at approximately 12,000 cm^{-1}. This is now generally accepted in the literature as the correct labelling scheme and is shown in figure 3.2.
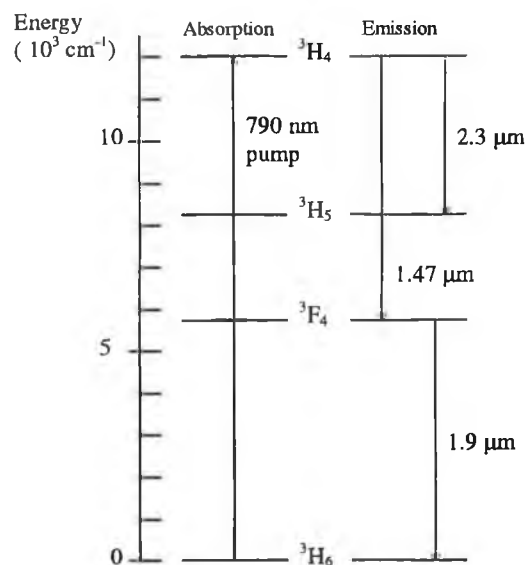
FIGURE 3.2 ENERGY LEVELS FOR Tm^{3+} IN A ZIRCONIUM FLUORIDE HOST

3.4 Absorption

As explained in section 2.3.1 it is important to have a complete knowledge of the absorption spectrum of the material under investigation for laser development. This spectrum also facilitates the selection of the optimum source for optical pumping. Figure 3.3 displays the experimental setup used to acquire the absorption spectrum of doped fibre samples.
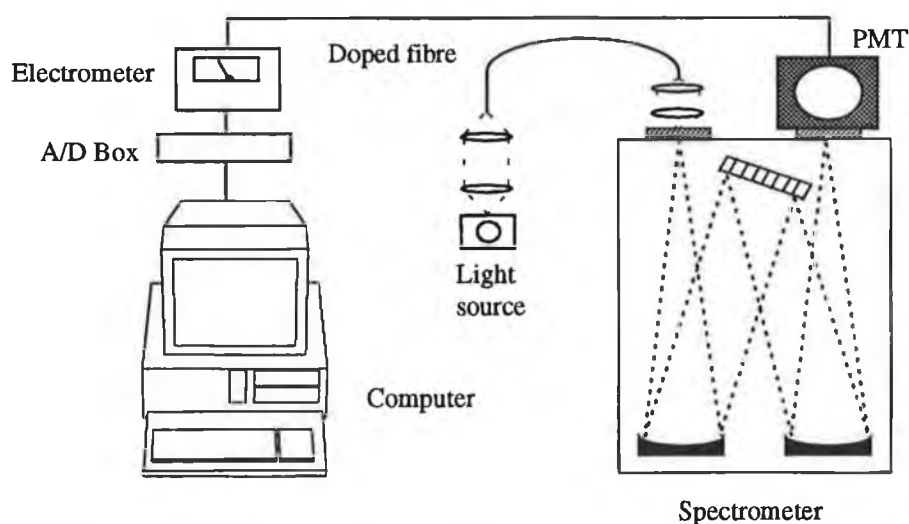
FIGURE 3.3 EXPERIMENTAL SETUP FOR ABSORPTION SPECTRUM MEASUREMENT

White light from a 50 W tungsten source was collimated and launched into a short length of Tm^{3+}-doped zirconium fluoride fibre. The absorption spectrum was recorded on a 1 metre Jobin-Yvon spectrometer (Model THR 1000) in a Czerny-Turner configuration with a Hamamatsu photomultiplier (Model R928). A computer was used to control the spectrometer and record the spectral data.

A reference spectrum of the tungsten source was first obtained. From the reference spectrum, the tungsten source was seen to have a uniform intensity in the 760 - 810 nm region. Due to the uniformity of the reference spectrum, the absorption spectrum was not divided into the reference spectrum. For this reason, the absorption spectrum is displayed in terms of intensity and not absorbance. A short length of doped fibre was used due to the strong absorption of the Tm^{3+} in the fibre.
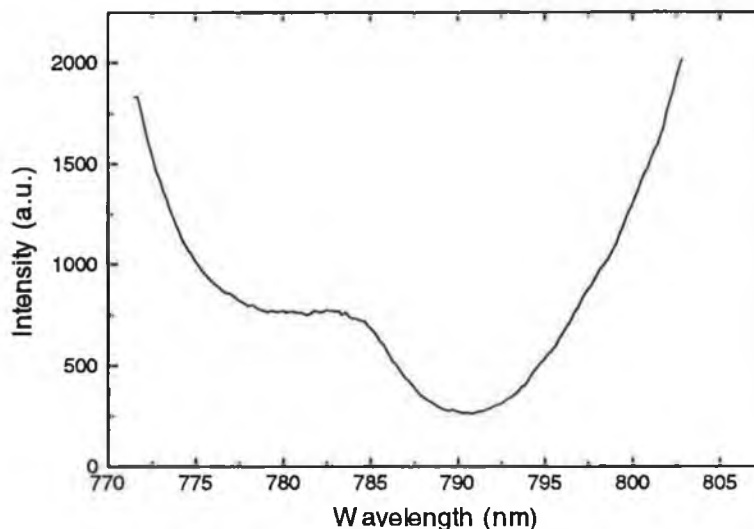
FIGURE 3.4 Tm^{3+}-DOPED ZIRCONIUM FLUORIDE FIBRE

Figure 3.4 displays the recorded absorption spectrum of zirconium fluoride fibre with a Tm^{3+} dopant concentration of 1000 ppm. The maximum absorption in the 800 nm region occurs at 791 nm (12642 cm^{-1}). Other absorption regions (see Appendix A) were not investigated as suitable high power pump sources are not readily available.

3.5 Fluorescence

The fluorescence spectrum was recorded in a manner similar to the absorption spectrum. The previous section (3.4) established the wavelength of

maximum absorption. A laser diode with a room temperature emission wavelength of 790 nm was used as a pump for fluorescence measurements. The apparatus used in obtaining the fluorescence spectrum is shown in figure 3.5.
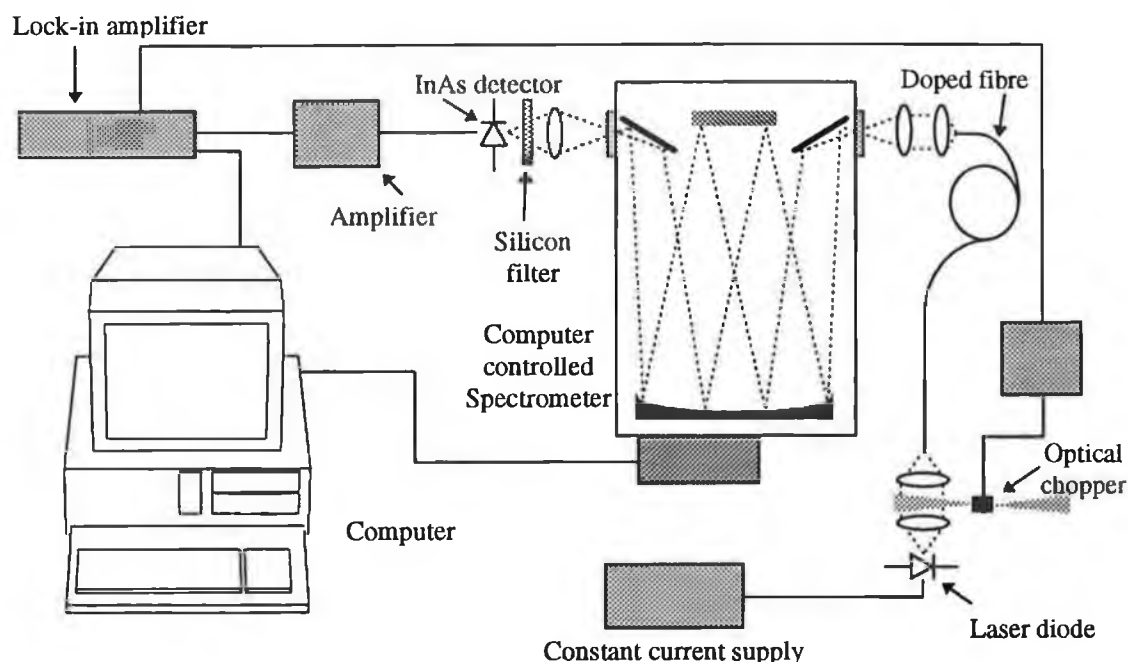
FIGURE 3.5 EXPERIMENTAL APPARATUS FOR FLUORESCENCE SPECTRUM COLLECTION

Due to the low levels of fluorescence, lock - in detection techniques were employed. The light from the laser diode was launched using two specifically selected lenses (discussed in detail in section 4.3.3). Fluorescence from the fibre was collected by a computer-controlled 10 cm compact spectrometer (Optometrics Minichrom Model No. AMC1-M351) in a Fastie-Ebert configuration in conjunction with a thermo - electrically cooled InAs detector. The spectral data was digitised with an A/D card (Bytronics) and passed to a computer for storage and display. The monochromator has a spectral resolution of 5 nm with the entrance and exit slits used (150 μm). A piece of silicon was used as a blocking filter for the pump laser line at 790 nm, as silicon absorbs strongly below 900 nm. Figure 3.6 displays the recorded fluorescence spectrum of the Tm^{3+}-doped zirconium fluoride fibre, which is in agreement with reported spectra in the literature.
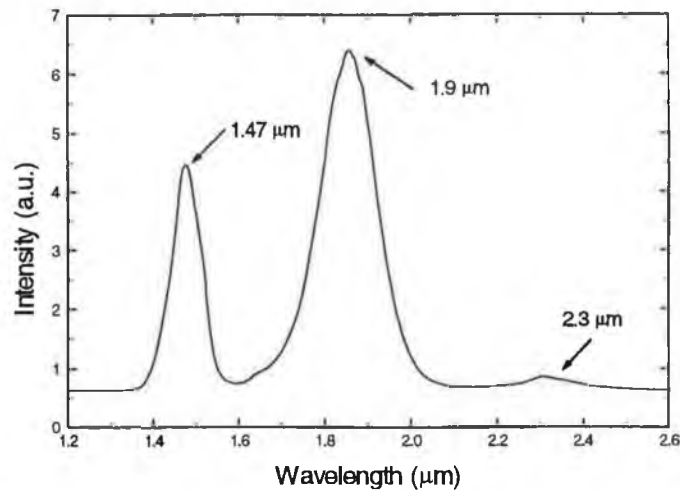
FIGURE 3.6 FLUORESCENCE SPECTRUM OF Tm^{3+}-DOPED FIBRE

As seen in figure 3.6 the fluorescence peaks at 1.47 μm (^{3}H$_4$ → ^{3}F$_4$) and 1.9 μm (^{3}F$_4$ → ^{3}H$_6$) are wide and featureless providing a potentially broad tuning range for lasers. The low level of fluorescence at 2.3 μm (^{3}H$_4$ → ^{3}H$_5$) is due to the low branching ratio between these levels. The branching ratio $\beta_{a,b}$, for the transition a → b is the fraction of all spontaneous decay processes that occur through that channel. The following table lists the branching ratios for a number of relevant Tm^{3+} transitions [4].

Transition	Wavelength (nm)	Branching Ratio β
^{3}H$_4$ → ^{3}H$_6$	790	0.893
^{3}H$_4$ → ^{3}F$_4$	1470	0.083
^{3}H$_4$ → ^{3}H$_5$	2300	0.024
^{3}F$_4$ → ^{3}H$_6$	1900	1.000

TABLE 3.1 RELEVANT BRANCHING RATIOS FOR Tm^{3+} IN A FLUORIDE GLASS

3.6 Fluorescence Lifetimes

The concept of fluorescence lifetimes was introduced in section 2.3.3. This section describes the experimental apparatus used to obtain the lifetime data and the curve fitting technique used to calculate the radiative lifetime. The pulse method

is used as the experimental method to determine the fluorescence lifetime. Figure 3.7 displays the experimental apparatus used to collect the lifetime data.
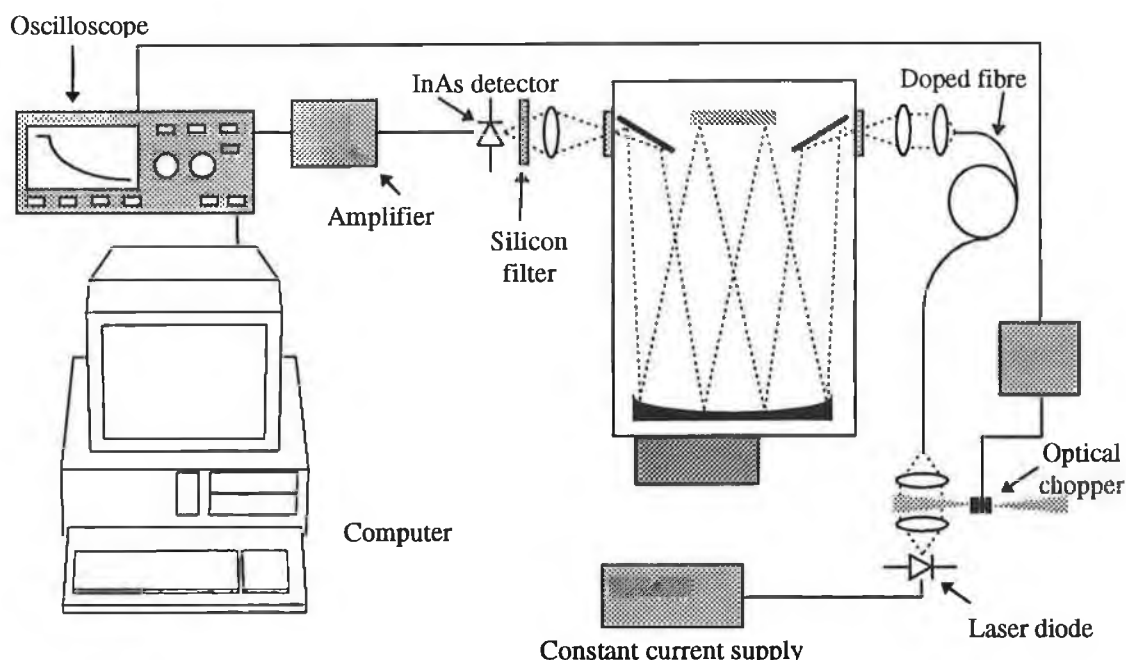
FIGURE 3.7 EXPERIMENTAL APPARATUS FOR FLUORESCENCE LIFETIME COLLECTION

The output of the pump laser diode was mechanically chopped before launch into the doped fibre. The monochromator (with entrance and exit slits removed to decrease the spectral resolution) was utilised as a broad filter to select the required fluorescence peak. After the signal amplification, the signal is displayed on the oscilloscope which is triggered by the optical chopper. Computer software is used to download the data to the serial port of the computer. 2000 data points were downloaded from the oscilloscope from each fluorescence decay curve and 25 fluorescence decay curves were collected for each fluorescence peak. Lifetime data were collected from two energy levels, $^3H_4$ and $^3F_4$. The following figures (3.8 and 3.9) display the fluorescence decay curves for $^3H_4$ and $^3F_4$.
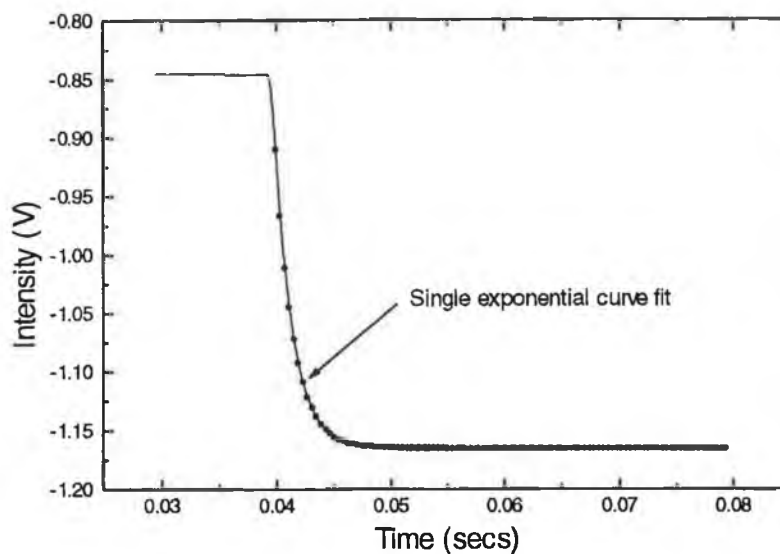
FIGURE 3.8 FLUORESCENCE DECAY FROM THE $^3H_4$ LEVEL
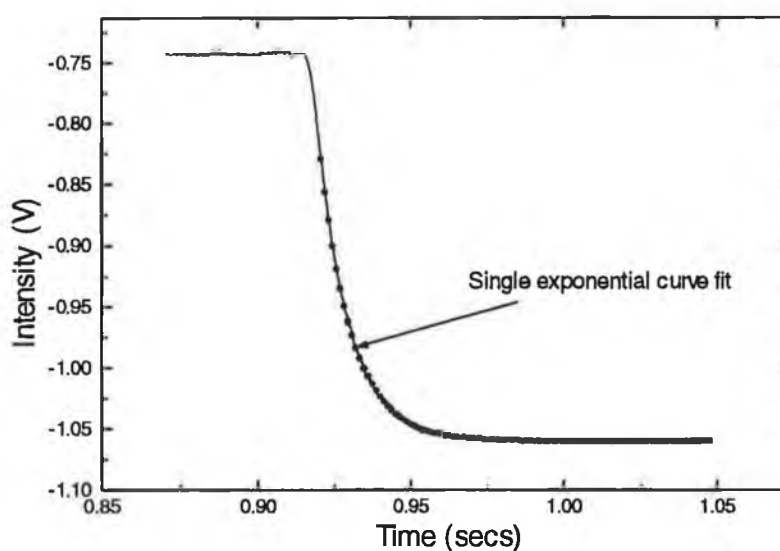
FIGURE 3.9 FLUORESCENCE DECAY FROM $^3F_4$ LEVEL

The decay curves were imported into a graphics package (Origin - Technical Graphics and Data Analysis in Windows) and were fitted to single exponential decay curves. This single exponential function fits a curve to the data set using equation 3.2. The graphing software uses the Marquardt-Levenberg non-linear least-squares curve fitting algorithm. The fit curve is created by successively modifying the

parameters in the selected fitting equation. This is an iterative process, in which the software draws a curve, checks to see how closely the curve matches the data, modifies the parameters and draws a new curve, until a best fit is achieved. The equation used to fit the data is shown below

$$y = y_0 + Ae^{\left(\frac{-(x-x_0)}{t}\right)}$$

<div align="right">*Eqn. 3. 2*</div>

where x_0 is the X axis offset, y_0 is the Y axis offset, A is the amplitude and t is the decay constant. Using equation 3.2 each of the 25 lifetime curves for both $^3H_4$ and $^3F_4$ energy levels were fitted to the experimental data. A decay constant was extracted for each lifetime curve, and an average fluorescence lifetime was obtained for $^3H_4$ and $^3F_4$ energy levels. The measured lifetime for the $^3H_4$ energy level is 1.56 +/- 0.05 msecs, based on 25 values and 10.65 +/- 0.1 msecs for the $^3F_4$ energy level. The values cited in literature for the $^3H_4$ (1.50 ms) [4] and $^3F_4$ (12 ms) [5] energy levels are in close agreement with the experimentally determined values for Tm^{3+} in a similar glass host. Values for radiative fluorescence lifetimes vary in literature, but this is probably due to the differing compositions of the glass hosts. The nonradiative level $^3H_5$ has a lifetime typically less than 10 µs.

A knowledge of the lifetimes of the various excited states allows one to predict which transitions may lase. By pumping at 790 nm there are four possible radiative transitions $^3H_4 \rightarrow {}^3H_6$ (800 nm), $^3H_4 \rightarrow {}^3F_4$ (1470 nm), $^3H_4 \rightarrow {}^3H_5$ (2300 nm) and $^3F_4 \rightarrow {}^3H_6$ (1900 nm). A prerequisite for population inversion in lasers requires that the upper laser level have a longer lifetime than the lower laser level.

Energy Level	Lifetime (ms)
$^3H_4$	1.56 +/- 0.05
$^3H_5$	0.01
$^3F_4$	10.65 +/- 0.1
$^3H_6$	—

TABLE 3.2 FLUORESCENCE LIFETIMES FOR SELECTED TRANSITIONS

Using the data in table 3.2, the following transitions $^3H_4 \rightarrow {}^3H_6$, $^3H_4 \rightarrow {}^3H_5$ and $^3F_4 \rightarrow {}^3H_6$ satisfy the prerequisite for population inversion and can be configured for laser operation. However, the transition $^3H_4 \rightarrow {}^3F_4$ has been configured as a laser even though its upper laser level has a shorter lifetime than the lower laser level and it should be self-terminating. Allain *et al.* [6] have reported laser oscillation at 1.48 μm. This laser had a low conversion efficiency of pump photons into laser photons and required high pump powers. The lifetime of the $^3F_4$ level can be artificially decreased by forcing simultaneously laser action at 1.48 and 1.9 μm by proper choice of mirrors. This *'trick'* increases laser efficiency by the quick depopulation of $^3F_4$ due to laser action at 1.9 μm.

3.7 Summary

This chapter has discussed the *correct* energy level labeling scheme for Tm^{3+} in a fluoride glass host. Absorption, fluorescence and fluorescence lifetimes were experimentally determined for Tm^{3+} in a zirconium fluoride glass host. The absorption data allowed the optimal choice of pump laser and the fluorescence data will be subsequently used in the selection of the characteristics of the input and output laser mirrors. Fluorescence lifetime data identified possible laser transitions. Other results will be extracted from these data in subsequent chapters.

References :

1. Poulain M., Lucas J., Brun P. : **'Verres fluorés au tetrafluorure de zirconum : Propriétés optiques d'un verre dopé au Nd^{3+}'**, Materials Research Bulletin, 1975, Vol. 10, No. 4, pp. 243-246

2. Digonnet M.J. (ed.) : **'Rare earth doped fiber lasers and amplifiers'**, Marcel Dekker, New York, 1993, Chapter 10

3. Aggarwal I.D. : Private Communication with Esterowitz L., Naval Research Laboratory, Washington, D.C.

4. Guery C., Adam J.L., Lucas J. : **'Optical properties of Tm^{3+} ions in indium-based fluoride glasses'**, Journal of Luminescence, 1988, Vol. 42, pp. 181-189

5. Esterowitz L., Allen R., Kintz G., Aggarwal I., Ginther R.J. : **'Laser emission in Tm^{3+} and Er^{3+} -doped fluorozirconate glass at 2.25, 1.88 and 2.70 μm'**, Technical Digest, Conference on Lasers and Electro-Optics, Optical Society of America, Anaheim, CA, 1988, paper THH1

6. Allain J.Y., Monerie M., Poignant H. : **'Tunable CW lasing around 0.82, 1.48, 1.88 and 2.35 μm in thulium-doped fluorozirconate fibre'**, Electronics Letters, 1989, Vol. 25, No. 24, pp. 1660-1662

Chapter 4

Experimental Fibre Laser Components

4.1 Introduction

The basic elements of a fibre laser, which include the doped fibre, the pump laser source and the laser mirrors, are represented in figure 4.1.
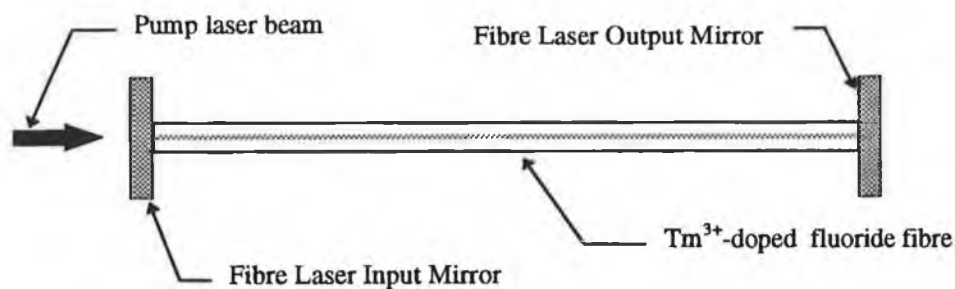
FIGURE 4.1 BASIC STRUCTURE OF A FIBRE LASER

In this chapter, the characteristics of the doped fibre, the pump laser source and the laser mirrors for the fibre laser cavity are discussed. Due to the difficulties involved with launching light from a high power laser diode source into a singlemode fibre, an optical lens design software package was employed to model the problem. The simulated model of the laser diode and launch lens system is discussed in detail, and this software model was used to select lenses for the launch optics. Finally, the monochromator and detector are described together with the software for data acquisition.

4.2 Properties of the doped fibre

The fibre used in this work was of Zirconium Fluoride (ZrF_4) composition, and was supplied under contract from *'Le Verre Fluoré'*, Brittany, France. The rare-earth

ion thulium, was doped in the fibre core and had a dopant concentration of 2000 ppm mole (specified by the manufacturer), i.e. 2000 μmoles of Tm^{3+} per 1 mole of ZrF_4. The number of Tm^{3+} ions per m^3 was calculated as follows :

2000 ppm mole = Tm^{3+} conc. in the ZrF_4 fibre

2000 ppm mole = 2000 μM / 1 M (ZrF_4)

= 2 mM (Tm^{3+}) / 1 M (ZrF_4)

= 0.002 M (Tm^{3+}) / 1 M (ZrF_4)

Molecular weight of ZrF_4 = 167.21 g

$\therefore$ 0.002 M (Tm^{3+}) / 167.21 g (ZrF_4)

$\therefore$ (0.002/167.21)*1000 M (Tm^{3+}) / 1 kg (ZrF_4)

= 0.01196 M (Tm^{3+}) / 1 kg (ZrF_4)

$\Rightarrow$ No. of Tm^{3+} ions = 0.01196 * Avogadro's Number = 7.2035 * 10^{21} ions / kg

Density (ρ) of Zirconium Fluoride = 4430 kg / m^3

$\Rightarrow$ 3.19116 * 10^{25} Tm^{3+} ions / m^3 in the fibre core

The density of Tm^{3+} ions in the fibre core, was used in further calculations in chapter 6. The fibre used here had a core and cladding diameter of 11 μm and 125 μm, respectively. The refractive indices of the core and cladding were 1.5165 and 1.5085, respectively, yielding a numerical aperture (NA) of 0.156. The LP_{11} mode cutoff wavelength was specified by the manufacture to be 2.1 μm; therefore, the fibre is in the singlemode regime for all wavelengths above 2.1 μm. For the pump laser at 790 nm, however, the fibre is multimode. The modal overlap, or the efficiency with which the pump beam couples power into the fibre laser beam will be further discussed in chapter 6. The fibre was covered in a protective coating of UV-cured polyacrylate, due to the hydrophobic nature of the fibre. The attenuation curve of the fibre glass material was supplied by *'Le Verre Fluoré'* and is displayed in figure 4.2.
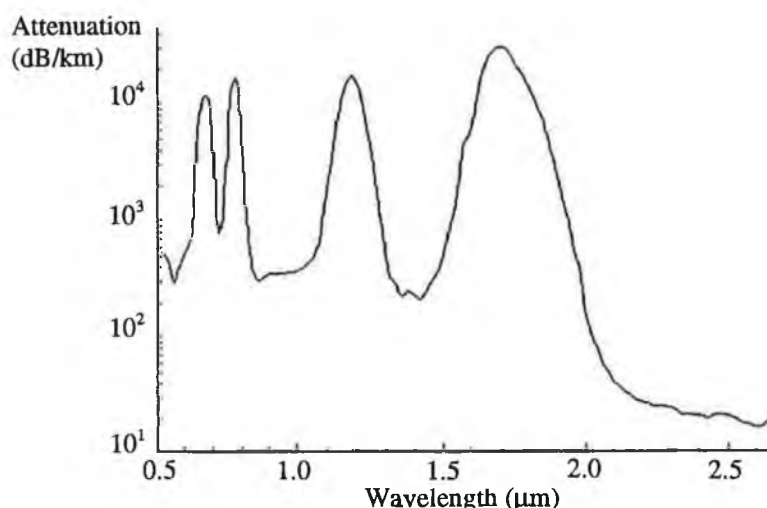
FIGURE 4.2 ATTENUATION CURVE OF GLASS MATERIAL USED IN THE FIBRE

4.3 High power pump source

The following sections detail the characteristics of the high power laser pump source and the electronic circuitry used to supply current to the device. The experimental determination of the optimum wavelength (791 nm) for optical pumping of the doped fibre was reported in chapter 3. The problem of coupling power from the high power source is modelled and discussed in detail at the end of this section.

4.3.1 High power source and drive electronics

A high power SONY laser diode (SLD 323 XT-1) with an integral cooler was selected as the pump laser source. This device, which is a GaAlAs double-heterostructure, had a high optical density, emitting 1 Watt of CW optical power from an aperture of 100 μm by 1 μm. An output wavelength of 794.7 nm was emitted by the device at room temperature (25°C). Fine tuning of the wavelength was possible by controlling the laser chip temperature. The laser chip was mounted on a thermo-electric (TE) cooler with a thermistor for temperature monitoring. The complete specifications for the laser diode are detailed in Appendix B.1.

A laser diode driver must be capable of supplying high current levels at a low voltage with high accuracy, low noise and long term stability. The driver must have several safety features, including full transient protection and full diode status monitoring. Full temperature control over the laser diode chip must be maintained at

all times. These requirements must be fulfilled in order to ensure trouble free operation of the laser diode.

Due to these strict requirements, a commercial laser driver was purchased from IE Optomech, England. The complete specifications of the *'AK series combination high power laser diode driver and laser controller'* can be found in Appendix C.

This computer-controlled laser driver afforded the user full control over the diode laser drive current and laser chip temperature. Three modes of operation were available, all with full servo-controlled feedback: current mode allows control of laser diode current, power mode controls the laser diode power to ensure noise free operation and external control mode allows the output of the laser diode to be controlled by an external analogue voltage input. A temperature control feedback circuit in the laser driver controller was used to continuously adjust the current delivered to the TE cooler on which the laser chip is mounted.

The light-current characteristics of the device were investigated. Figure 4.3 displays the output power versus the drive current. The output power was measured with a calibrated OPHIR (Model PD2-A) {Jerusalem, Israel} laser power meter. The collimated output power of the laser diode was reduced by the collimation optics, because the beam was clipped by one of the collimation lenses (discussed in section 4.3.3). A maximum collimated output power of 650 mW was achieved instead of 1000 mW which was emitted by the laser diode.
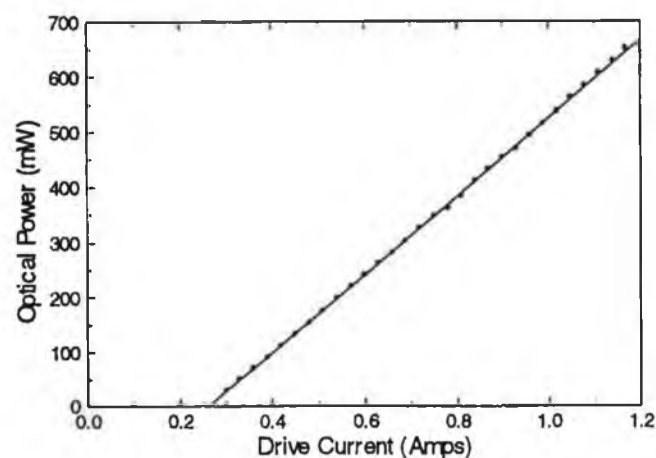
FIGURE 4.3 LIGHT-CURRENT CHARACTERISTICS OF THE SONY LASER DIODE

4.3.2 High power source emission properties

The basic structure of a broad area laser diode, similar to the SONY device that was used in this work, is shown in figure 4.4.
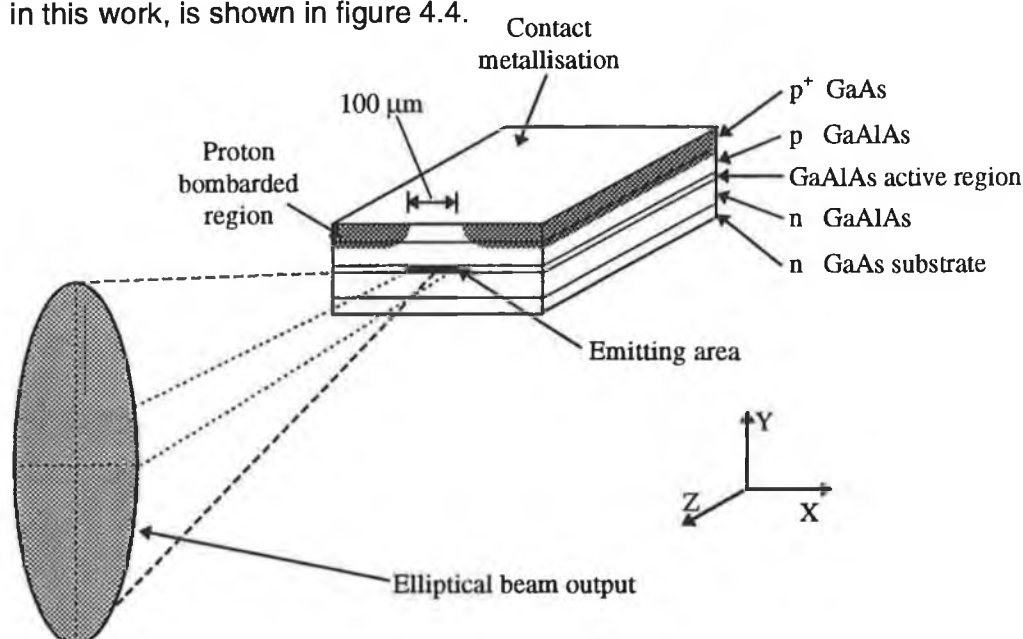
FIGURE 4.4 SCHEMATIC OF BROAD AREA LASER DIODE

The divergence of a laser diode output beam is represented by two angles of divergence. These angles are measured at the laser beam's full width, half-maximum intensity points (FWHM), measured both parallel ($\theta_\parallel$) and perpendicular ($\theta_\perp$) to the junction plane. SONY quoted values of 9.6° for $\theta_\parallel$ and 32.5° for $\theta_\perp$. These values were not checked in this work, as SONY tests each individual device before shipment (see Appendix B.2).

The other important factor with respect to source emission properties is the size of the emitting aperture of the device. This device had an emitting aperture of 100 μm parallel to the junction plane and 1 μm perpendicular to the junction plane.

4.3.3 Launch efficiency and optics

Coupling of light from a laser diode into a singlemode fibre with a high degree of efficiency is not easily achieved. There are two main difficulties involved : firstly there is a substantial area mismatch between the large rectangular area of the laser diode facet and the small circular area of the core of the singlemode fibre.

Secondly, there are differing divergences between the highly divergent laser diode and the small numerical aperture (NA) of singlemode fibres. These problems are summarised in table 4.1, shown below.

	LASER DIODE PROPERTIES	DOPED-FIBRE PROPERTIES
DIMENSIONS	100 µm X 1 µm	11 µm
DIVERGENCES	9.6° & 32.5°	8.97°

TABLE 4.1 SUMMARY OF COUPLING EFFICIENCY DIFFICULTIES

This problem has been investigated in detail by different research groups employing a variety of schemes. These include various lens systems [1], fibre up-tapers [2], fibres with tapered hemispherical ends [3], fibres with a high index end face [4], fibres with a wedge-shaped end [5] and fibres with beam expanding capabilities achieved by thermally diffusing the core dopant into the cladding [6].

In this body of work a number of different launching methods have been investigated. Initially, beam reshaping with a spherical lens and a cylindrical mirror was carried out, but this method only achieved a launch efficiency of < 1%. Fibre tapers and grating couplers were also investigated, but these schemes also produced a very low coupling efficiency (« 1%). An anamorphic prism pair was used in conjunction with a high NA spherical lens to reshape the laser beam. This method offered no improvement in coupling efficiency. Finally, the use of two cylindrical lenses to collimate each of the divergent laser diode planes was found to be the most efficient method.

In order to model the output beam of the laser diode and to assist in the selection of standard stock (i.e. not custom made) collimation and focusing lenses, an optical lens design software package was employed. ZEMAX-SE was chosen due to its ability to model laser diodes and its wide range of standard lens libraries from various lens suppliers.

ZEMAX models sources on the object plane as a collection of points. Each point radiates a *cone* of light which fills the entrance pupil. Therefore it may seem

impossible to model a laser diode due to the significant astigmatism it exhibits. Diodes have different divergence angles in the X and Y directions (see Fig. 4.4), and have different apparent sources of origin in the XZ and YZ planes. It is possible, however, to model a laser diode by using a point source on axis with a defined divergence, and then in one plane only, focusing the beam with a cylindrical lens, thereby creating a different divergence in one plane. A paraxial XY surface was used to act like a cylindrical lens, with the flexibility to specify different focal powers in the X and Y directions.

In the model the diode was specified to have a FWHM in the YZ plane of $\theta_\perp$, and a FWHM in the XZ plane of $\theta_\parallel$. Therefore in the laser diode model, the rays in the XZ plane will appear to come from a point a distance t behind the point at which the YZ rays appear to diverge. The *'trick'* was to re-image a point source to a virtual or dummy plane that will act like the astigmatic diode source with the defined properties.

The laser diode was modelled in ZEMAX using three surfaces; the first surface was the object surface, the second a paraxial XY surface and the third a dummy surface that acted as the front facet of the laser diode, labeled S_0, S_1 and S_2, respectively, as shown in figure 4.5.
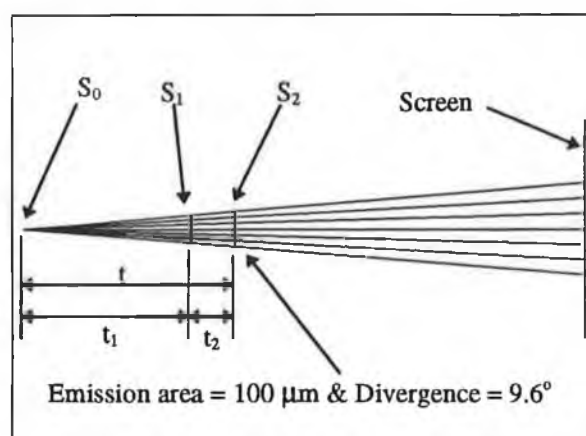
FIGURE 4.5 LASER DIODE MODEL (XZ PLANE)

Figure 4.5 displays how the laser diode was modelled in the XZ plane (i.e. parallel to the junction). S_2 was the dummy surface. The rays in the XZ plane appear to originate a distance t behind this surface coming from S_0. The first surface (S_0) was

defined as a single conventional point source, which has a numerical aperture (NA), calculated from the beam divergence in the XZ plane (NA calculated to be 0.1668). The second surface S_1, was a paraxial XY surface (this is an ideal thin lens, with the ability to specify different focal lengths in X and Y planes), which acted like a cylindrical lens. This was used to image the divergent beam emanating from the first surface onto the dummy surface (S_2). In order to describe this surface, the inverse focal lengths in the X and Y planes (φ_x and φ_y) must be calculated. These values were obtained using the following formulae:

$$t = t_1 + t_2$$

<div align="right">*Eqn. 4. 1*</div>

$$M = \frac{t_1}{t_2}$$

<div align="right">*Eqn. 4. 2*</div>

where *t* was the astigmatic distance of the laser diode and *M* was the magnification between surface S_0 and S_2.

$$M.(t - t_1) = t_1$$

<div align="right">*Eqn. 4. 3*</div>

$$M.t = t_1.(M + 1)$$

<div align="right">*Eqn. 4. 4*</div>

A value for t_1 is given by

$$t_1 = \frac{M.t}{M + 1}$$

<div align="right">*Eqn. 4. 5*</div>

Using Eqn. 4.2,

$$M.t_2 = t_1$$

<div align="right">*Eqn. 4. 6*</div>

and using Eqn. 4.1, this yields

$$t_2.(M + 1) = t$$

<div align="right">*Eqn. 4. 7*</div>

This then leads to a value for t_2

$$t_2 = \frac{t}{M + 1}$$

<div align="right">*Eqn. 4. 8*</div>

From figure 4.5, and using the standard lens equation,

$$\frac{1}{f} = \frac{1}{t_1} + \frac{1}{t_2}$$

Eqn. 4. 9

$$\varphi_y = \frac{1}{f_y} = \frac{1}{t_1} + \frac{1}{t_2} = \frac{M+1}{M.t} + \frac{M+1}{t}$$

Eqn. 4. 10

$$\varphi_y = \frac{(M+1)^2}{M.t}$$

Eqn. 4. 11

Equation 4.11 describes the inverse focal power required in the YZ plane in terms of the astigmatic distance and the magnification.

The astigmatic distance (t) of the laser diode may be obtained from the angle of deviation in the XZ plane ($\theta_\parallel$) and the length (L) of the emission facet also in the XZ plane, as displayed in figure 4.6,
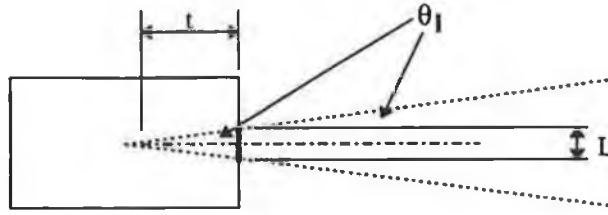
FIGURE 4.6 LASER DIODE ASTIGMATIC DISTANCE

$$\sin\theta_\parallel = \frac{\left(\frac{L}{2}\right)}{t}$$

Eqn. 4. 12

The angular magnification is given by

$$M = \frac{\tan\theta_\perp}{\tan\theta_\parallel}$$

Eqn. 4. 13

Using the values for the laser diode of interest in this work ($\theta_\parallel$ = 9.6°, $\theta_\perp$ = 32.5° and the length of the laser diode emission facet in the XZ plane of 100 µm), the following values were obtained: t = 0.2998 mm, M = 3.7666, t_1 = 0.2369 mm, t_2 =

0.629 mm, φ_y = 20.1204 mm^{-1}. Figure 4.7 displays the ZEMAX model of the laser diode in the YZ plane using the values calculated above for the paraxial XY surface, with φ_x = 0.0 mm^{-1}.
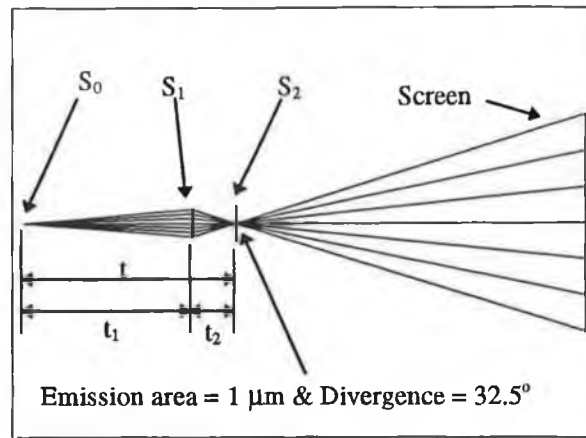
FIGURE 4.7 LASER DIODE MODEL (YZ PLANE)

Clearly, the divergent rays originating from the object surface (S_0), which strike the second surface (S_1), were focused onto the dummy surface (S_2). The emerging divergent beam had an angular divergence the same as the laser diode in the YZ plane. For reasons of clarity, the ZEMAX model of a laser diode source, viewed at an angle of 45° to the optical axis is shown in figure 4.8. From this figure the differing divergences in both the XZ and YZ planes can be clearly seen. Furthermore, the rays emanate from a line source in the XZ plane and from a point source in the YZ plane.
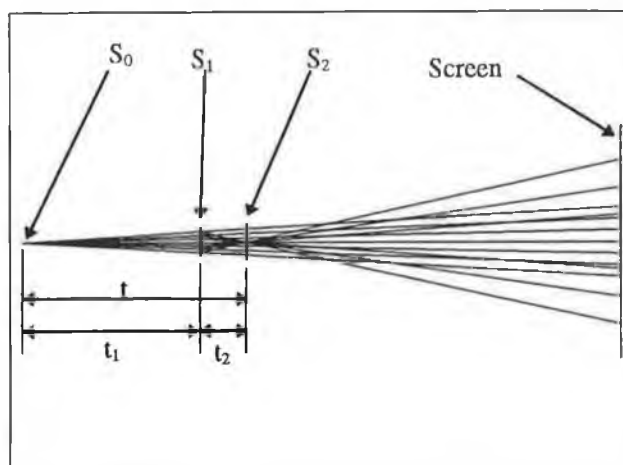
FIGURE 4.8 LASER DIODE MODEL (45^0 ROTATION)

The calculated spot diagram from ZEMAX is shown in figure 4.9. This diagram showed the expected elliptical output from the laser diode after a distance of 0.5 mm.
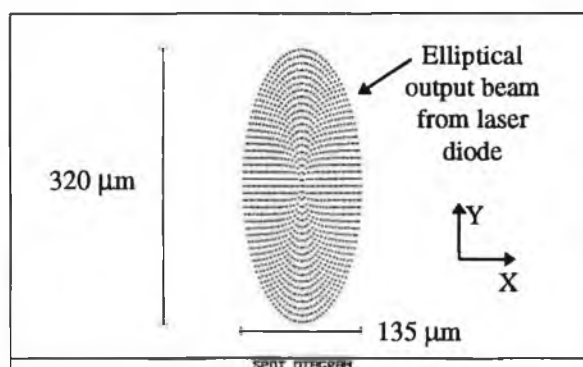
FIGURE 4.9 SPOT DIAGRAM OF LASER DIODE FROM ZEMAX

From the known emission dimensions and divergences, the expected beam sizes after a distance of 0.5 mm in the X and Y directions are 0.135 mm and 0.319 mm, respectively. The values predicted by ZEMAX are 0.135 mm and 0.320 mm, which are in close agreement, thereby validating the model.

ZEMAX was again employed in the selection of the cylindrical lenses from standard commercial lens catalogues. The final lens arrangement for the most

efficient collimation and for the launching of light into the doped fibre was arrived at after collaboration with Point Source Ltd., Winchester, England. Point Source Ltd. is a laser diode specialist company, which develop optical solutions to specific customer requirements.

In an effort to maximise the launch efficiency of the system, the collection of the highly divergent beam from the laser in the YZ plane was traded off against the de-magnification of the laser emission stripe in the XZ plane. If a short focal length cylindrical lens was used to collimate all of the divergent beam in the YZ plane then a focusing lens with a long focal length had to be used, in order to match the launch angle from the laser to the NA of the fibre. However, due to the necessity of de-magnification of the large laser diode emission facet in the XZ plane (100 µm stripe emission de-magnified onto 11 µm fibre core), the collimating cylindrical lens in the XZ plane must have a focal length much longer than the focusing lens. Furthermore, if the focal length of this cylindrical lens was too long then it would not be able to capture all of the divergent beam in the XZ plane. This problem was summarised in table 4.1, at the beginning of the section.

Figure 4.10, taken from the optical design software package ZEMAX, displays the two cylindrical lenses selected to collimate the laser beam together with the focusing lens. The diagram only displays rays in the YZ plane (plane perpendicular to the laser diode junction). The first cylindrical lens does not capture all the light emitted from the laser diode in the YZ plane for reasons stated above.
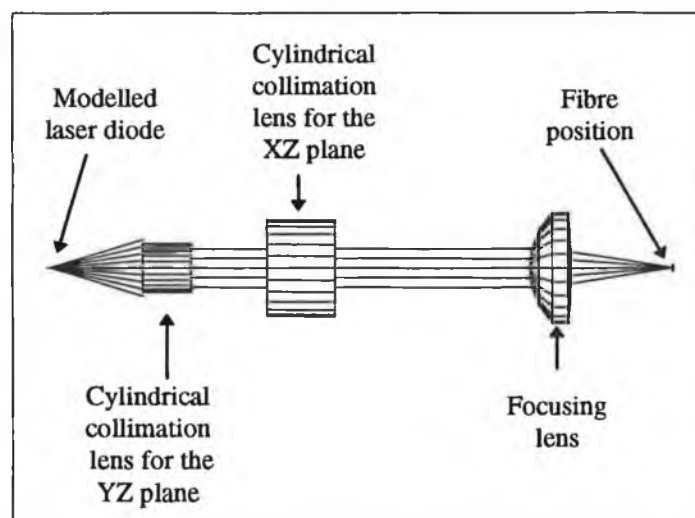
FIGURE 4.10 SCHEMATIC OF LENS ARRANGEMENT IN THE YZ PLANE

The percentage of light collimated for this configuration was calculated to be $\cong$ 72 % (a loss of 280 mW from the total output power of 1000 mW). The laser diode was driven with the maximum allowable current. The maximum output optical power was reduced (1000 mW $\rightarrow$ 650 mW) due to the clipping of the beam in the YZ plane by the cylindrical lens and by lens reflections.

The first lens had a focal length of 12.7 mm, a clear aperture of 5.08 mm, a back focal length of 9.4 mm and was manufactured from BK7 glass. Figure 4.11 displays the lens arrangement for collimation in the XZ plane.
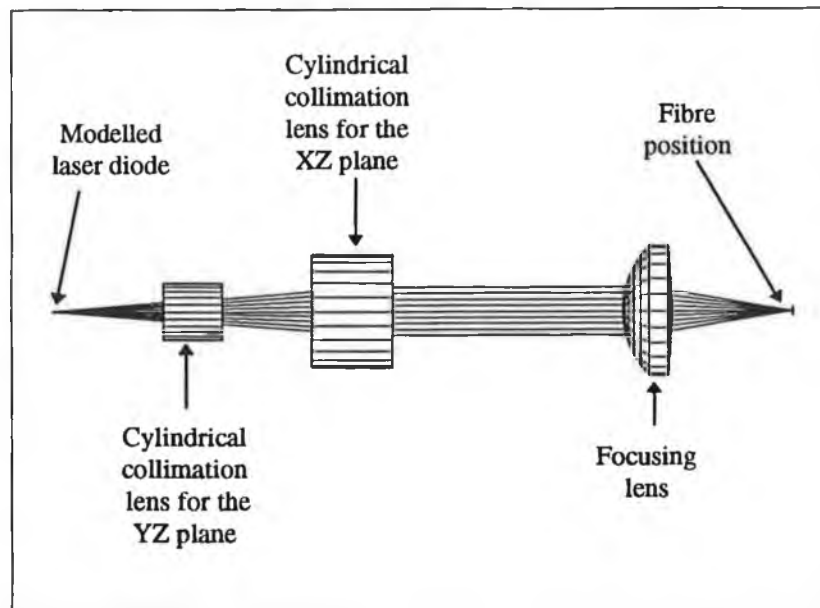
FIGURE 4.11 SCHEMATIC OF LENS ARRANGEMENT IN THE XZ PLANE

The second lens captured all the light from the laser diode in the XZ plane. This cylindrical lens had a focal length of 25.4 mm, a clear aperture of 10 mm, a back focal length of 20.8 mm and was also manufactured from BK7 glass.

With both the cylindrical lenses in the arrangement described above, the beam from the laser diode was collimated. The collimated beam was approximately square in cross-section, instead of the expected elliptical cross-section. This was due to the first lens clipping the beam in the YZ plane, and because the second cylindrical lens was further away from the laser diode, thereby producing a collimated beam with a square cross-section. Figure 4.12 displays the collimated beam spot size after the second lens. With the collimation lenses in place the

calculated spot size (5.0 mm x 4.2 mm) was found to be in close agreement with the actual spot size ($\cong$ 5 mm x 4 mm).
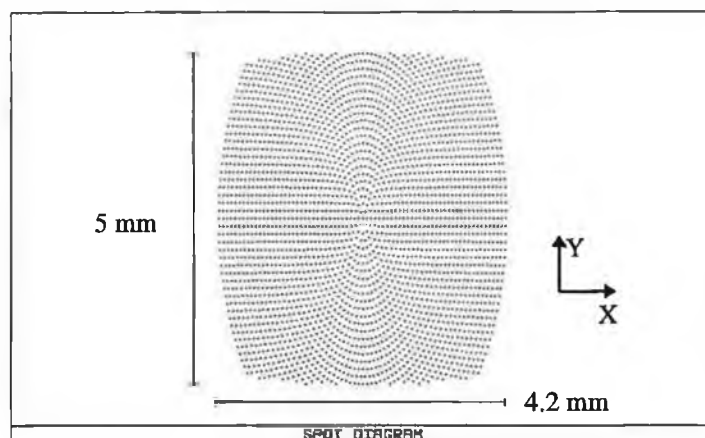
FIGURE 4.12 COLLIMATED SPOT DIAGRAM FROM ZEMAX

The focusing lens, whose characteristics were determined from ZEMAX calculations, was chosen to allow de-magnification in the YZ plane, while also matching the NA of the fibre. A Spindler & Hoyer (Part No. 063034) nonsymmetrical biconvex lens with a focal length of 12.5 mm, a clear aperture of 11.5 mm and manufactured from IRGN 6 glass was selected as the focusing lens. In the YZ plane (1 μm emission facet) this lens yielded a magnification of 0.984, where the magnification (M) was defined as f_{focus} / $f_{coll.}$. This de-magnification yielded a calculated spot size of (1 μm X 0.984) 0.984 μm. In practice this spot size was diffraction-limited to a size of 2.4 μm from Ralyeigh's criterion. In the XZ plane the magnification was calculated as defined above, giving a value of 0.492, thereby, yielding a spot size of 49.2 μm.

The focused spot size intensity pattern is demonstrated using ZEMAX, as shown in figure 4.13. Most of the light was focused to a spot size of approximately 50 μm in diameter, although edge effects from the collimating and focusing lenses cause some of the light to be dispersed as shown in the diagram. The optimum

location for the fibre was determined by ZEMAX to be 10.42 mm away from the back face of the focusing lens, thereby maximising the launch efficiency of the system.
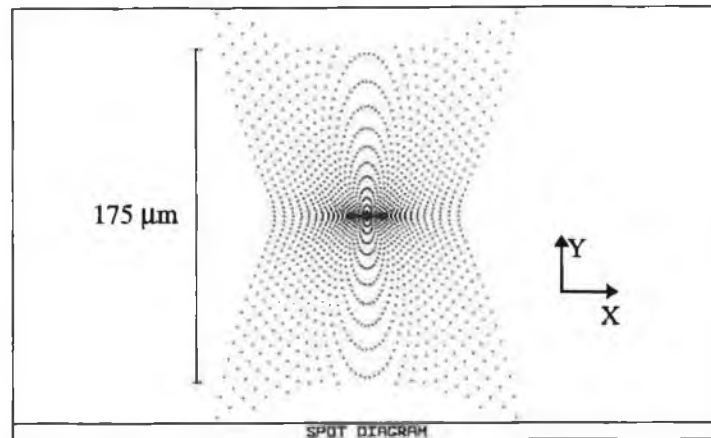
FIGURE 4.13 SPOT DIAGRAM AT FOCUS FROM ZEMAX

ZEMAX was also used to calculate the encircled energy at a particular surface (i.e. the percentage of total energy enclosed as a function of distance from the chief ray). Figure 4.14 displays the encircled energy at a distance of 10.42 mm away from the focusing lens.
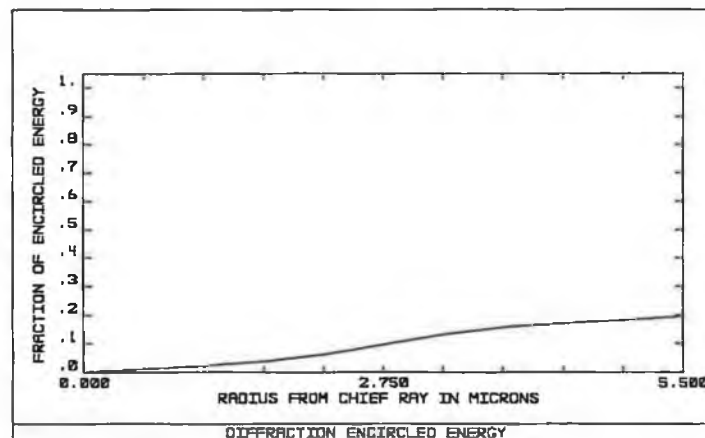
FIGURE 4.14 ENCIRCLED ENERGY DIAGRAM AT FOCUS FROM ZEMAX

The calculated fraction of energy enclosed within 5.5 μm (radius of the doped fibre) was found to be 19.28 %.

A value of 19.28 % was not realisable, due to the acceptance angle of the fibre. The NA of the focused beam from the focusing lens was calculated to be 0.196 (calculated from the spot diagram in figure 4.12 and the focal length of the focusing lens) and the NA of the doped fibre was 0.156. This NA mismatch caused a further loss of $\cong$ 38 %.

The predicted power losses from a collimated beam of 650 mW, for this configuration is outlined in table 4.2 shown below.

	% Loss	Power (mW)
Spot size mismatch	80.72	125.32
NA mismatch	38	77.70

TABLE 4.2 CALCULATED LOSSES ASSOCIATED WITH LAUNCH EFFICIENCY

Other losses were expected, due to the high dependency of the launch efficiency on the collimated beam (i.e. if the collimated beam was not perfectly collimated the launch efficiency decreases dramatically), misalignment of the system and lens imperfections.

Having selected the lenses for the collimating and focusing system, the predicted coupling efficiency from the software model, was compared with the experimentally measured coupling efficiency of the system. The cylindrical lenses and the focusing lens were located as shown in figures 4.10 and 4.11. A short length (0.4 metre) of *'Le Verre Fluoré'* un-doped fluoride fibre which had the same characteristics as the doped fibre, was used to measure the launch efficiency from the SONY laser diode. Figure 4.15 displays the measured launch efficiency with the lens system displayed in figures 4.10 and 4.11 from the SONY laser diode.
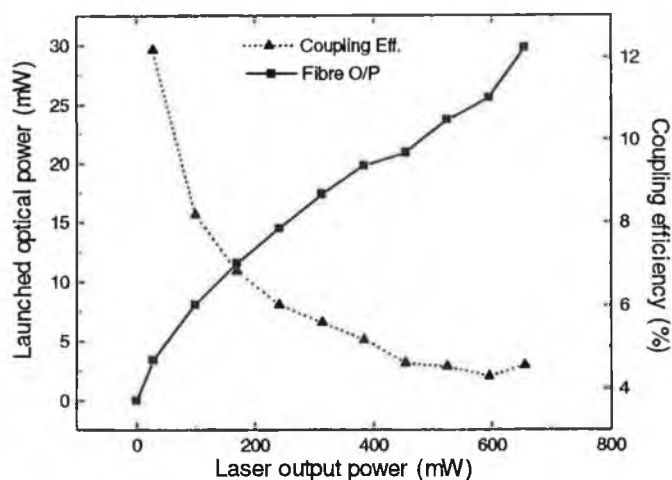
FIGURE 4.15 MEASURED LAUNCH EFFICIENCY FROM SONY LASER DIODE

The maximum power launched into the fibre core was 29 mW. The coupling efficiency was seen to decrease with an increase in optical power. This decrease in coupling efficiency may be related to a change in the modal output from the SONY laser diode as the power is increased. Nevertheless it is clear that the use of the software package helped to increase the coupling efficiency of the launch system dramatically. Further improvement in the coupling efficiency of the launch system may be achieved, by employing custom made lenses. However, this would add considerably to the cost.

4.4 Low power pump source

The following sections detail the characteristics of the low power laser pump source and the electronic circuitry used to supply current to the device. Due to the small emission area of the low power laser diode, the efficient coupling of power into the fibre was not a problem, and therefore, was not modelled using ZEMAX.

4.4.1 Low power source and drive electronics

A low power PHILIPS laser diode (CQL 7840/D) was purchased for use as a low power pump source. This device had a 40 mW CW output from a 3 μm by 1 μm emission facet. The emission wavelength of this device is 787 nm. As no thermo-electric cooler was supplied with this device it was not convenient to temperature-

tune the wavelength. The specifications of the laser diode may be found in Appendix D.

The requirements for supplying electrical power to this laser diode are not as critical as for higher power devices. However, the diode must still be protected from electrical spikes or power surges. Sharp manufacture a driver IC (IR3C02) for use with their range of laser diodes, but it can be used with any laser diode which requires a small drive current. This driver IC has an automatic power control (APC) function, where the monitor photodiode is used in a feedback loop to control the current supplied to the laser diode. The driver IC also eliminates power surges and has a *'slow-start'* function, which slowly ramps the current to the laser diode. The driver circuit for the IC and the IC are included in Appendices E.1 and E.2.

The output power versus monitor photodiode current of the laser diode is displayed in figure 4.16. As before, the optical output power was measured with a calibrated OPHIR laser power meter.
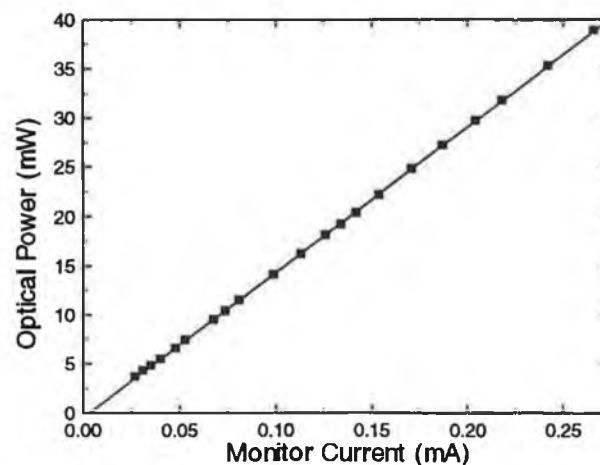
FIGURE 4.16 CALIBRATION CURVE FOR LASER DIODE

In figure 4.16, the monitor photodiode current is displayed instead of the drive current, this calibration curve was used to determine the output power from the laser diode.

4.4.2 Low power source emission properties

The PHILIPS laser diode had essentially the same structure as the SONY device displayed in figure 4.4, the major differences being the emission properties.

The PHILIPS device had a much smaller emission facet (3 μm X 1 μm) and the angle of deviation in the plane perpendicular (22°) to the laser diode junction was smaller. For these reasons, the focusing of light from this device into a fibre did not present as many problems as did the SONY device. The angle of deviation in the plane parallel to the junction was 10^0 which is similar to that of the SONY laser.

4.4.3 Launch efficiency from low power laser source

Due to the small emission area from the PHILIPS laser diode, de-magnification of the emission facet was not necessary. MELLES GRIOT provide a set of special collimating and focusing lenses, specifically for laser diode applications. These lenses have spherical aberration and coma corrected, short working distances and large numerical apertures. One of these lenses (06 GLC 002) was selected as the collimating lens for the PHILIPS laser diode. The same focusing lens was used in this setup as was used in the lens system for the SONY laser. This lens combination yielded a magnification of approximately 1.56. Therefore, the focused spot size is considerably smaller (1.56 X {3 μm X 1μm}) than the diameter of the doped fibre (11 μm). The collimating lens had an NA of 0.5 and therefore collimated at least 90.6 % of the laser beam.

The measured launch efficiency from the PHILIPS laser diode was found to be 58 %, using the lens arrangement described above in conjunction with a 0.4 metre length of un-doped fibre.

4.5 Mirrors for laser cavity

The properties of the mirrors for the laser cavity play a major role in determining the characteristics of the fibre laser. The input mirror must have dichroic properties, in that it must be highly transmissive at the pump wavelength and highly reflective at the fibre laser wavelength. The reflectivity of the output laser mirror at the lasing wavelength affects both the threshold power and the slope efficiency. This subject is addressed in chapter 6.

4.5.1 Input mirror

The input laser mirror must transmit a high percentage of the pump laser beam at 790 nm. Otherwise, the coupling efficiency is reduced and less pump power is launched into the fibre. The input mirror design specification must also take into account which fluorescence wavelengths are to be reflected and

transmitted. By using the fluorescence spectrum of the Tm^{3+}-doped fluoride fibre (chapter 3) in conjunction with the energy level diagram, one can specify which wavelengths should be reflected and which should be transmitted. As the fibre laser was designed to lase at 2.3 µm ($^3H_4 \rightarrow {}^3H_5$), the input mirror had to be highly reflective (T < 1 %) at this wavelength. Both of the fluorescence bands at 1.47 µm ($^3H_4 \rightarrow {}^3F_4$) and 1.92 µm ($^3F_4 \rightarrow {}^3H_6$) were employed to increase the efficiency of the fibre laser. By designing the input mirror to have a low reflectivity (T $\cong$ 100 %) at 1.47 µm, this allowed the fluorescence at this wavelength to exit the cavity after one pass, and therefore, it would not experience gain in the cavity. By allowing the 1.47 µm photons to exit the cavity after one pass, this released more electrons which were then free for re-absorption. By causing the fluorescence band at 1.92 µm to be reflected within the cavity, it may be used to enhance the laser emission at 2.31 µm. This occurs by helping to depopulate the lower energy levels, where a buildup of electrons would occur due to the long lifetime of the fluorescence levels which were not contributing to laser action. This process made more electrons available for excitation from the ground state. Figure 4.17 displays the transmission characteristics of both the input and output laser mirrors, which were manufactured by TecOptics, Isle of Man.
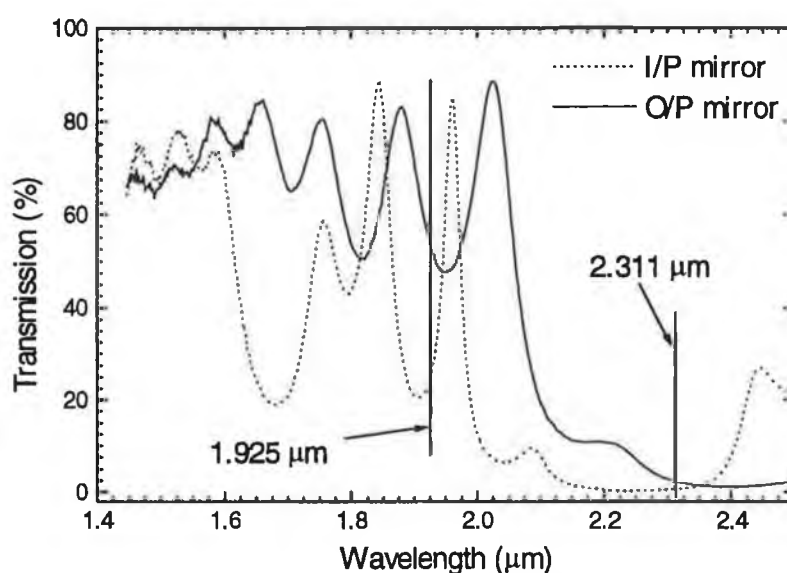
FIGURE 4.17 TRANSMISSION CURVE FOR INPUT AND OUTPUT LASER MIRRORS

The problem with obtaining mirrors with these specifications is that a high reflectivity in the 2.2 - 2.4 μm region, results in a third harmonic reflection at around 790 nm. This unwanted reflection may be suppressed by depositing layers of different coatings, which *'force'* the third harmonic reflection to higher wavelengths. However, mirrors with these specifications are very difficult to manufacture, as this type of coating is very sensitive to small deposition errors, and laying down a layer which is too thick may reduce the transmission at the pump wavelength (790 nm). Table 4.3 displays the measured transmission characteristics of the input and output mirrors at selected critical wavelengths.

	I/P MIRROR	O/P MIRROR
790 nm	92.1 %	30.1 %
1.47 μm	72.4 %	67.7 %
1.92 μm	20.1 %	55.2 %
2.31 μm	0.3 %	2.5 %

TABLE 4.3 TRANSMISSION CHARACTERISTICS FOR INPUT AND OUTPUT LASER MIRRORS

4.5.2 Output mirror

The transmission characteristics of the output mirror are dictated by the required transmission at a number of wavelengths. At 790 nm the transmission is required to be as low as possible (T < 1 %). The mirror was designed to have similar characteristics as the input mirror at 1.47 μm and 1.92 μm, for the reasons explained in the section above. The most important characteristic of the output mirror is its transmission value at the lasing wavelength (2.31 μm). The transmission of the mirror at this wavelength directly affects the threshold and the slope efficiency of the laser (see chapter 6 for equations governing threshold and slope efficiency). A transmission value of 2.5 % was determined from calculations to be the optimum transmission at the fibre laser wavelength in order to achieve lasing at a low threshold, but with a high output power.

With fibre laser mirror transmission characteristics similar to those outlined above, Percival *et al.* [7,8] have demonstrated lasing at both 2.31 μm and also at 1.92 μm in a Tm^{3+}-doped fibre.

4.6 Detector and thermo-electric cooling

Figure 4.18 displays the large range of infra-red detectors which is available together with their detectivity (D*) values. The D* of a detector [9] is defined as

$$D* = \frac{\sqrt{A.B}}{NEP}$$

<div align="right">Eqn. 4. 14</div>

where A is the active area (cm^2) of the detector, B the bandwidth of the detector (Hz), and NEP the noise equivalent power (W) of the detector. D* is a relative sensitivity parameter used to compare performance of different detector types. D* is the signal-to-noise ratio at a particular chopping frequency and in a 1 Hz bandwidth (i.e. CW) when 1 Watt of radiant power is incident on a 1 cm^2 active area detector. The higher the D* value, the better the detector.
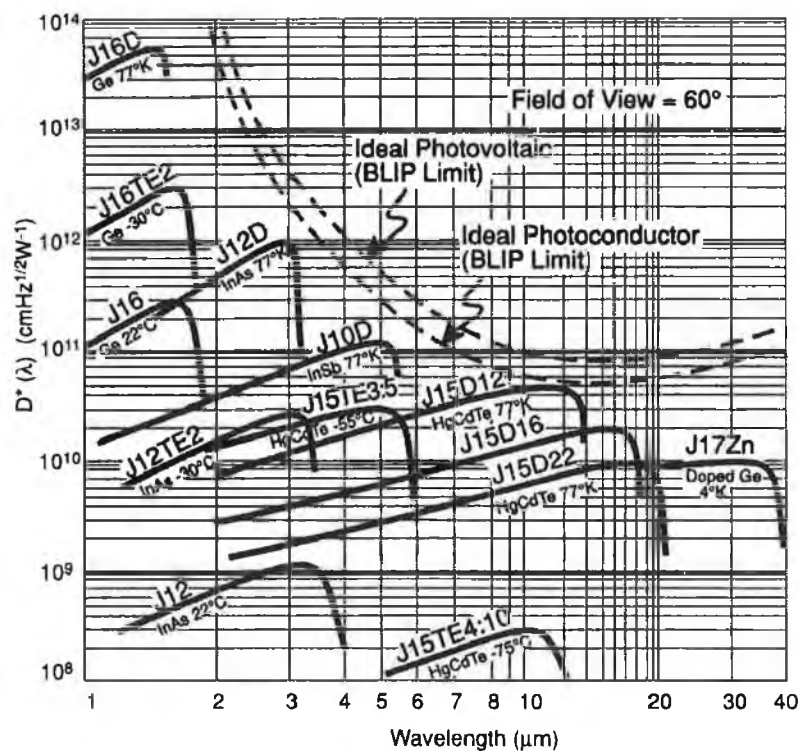
FIGURE 4.18 THE RELATIVE DETECTIVITIES D* OF VARIOUS IR DETECTOR TYPES [9]

A thermo-electrically cooled InAs (Indium Arsenide) was selected on the basis of cost and ease of use. The InAs (EG&G Judson, PA, USA - Model No. J12TE2-8B6)

detector that was used is a photovoltaic device mounted to a two-stage thermoelectric cooler which is hermetically sealed in a dry nitrogen environment. The cooler is capable of cooling the detector by approximately $50^{\circ}C$ or to approximately $-30^{\circ}C$, provided the detector is mounted on an adequate heatsink. A thermistor is provided on the detector to allow for a temperature control loop to maintain the detector at a constant temperature, by adjusting the current to the thermo-electric cooler. The circuit used to control the current to the thermo-electric cooler is displayed in Appendix F. The InAs detector has an active area of 1 mm^2 and is designed to operate in the 1 µm to 3.6 µm range. The detector has a much higher shunt resistance than room temperature detectors, resulting in higher responsivity, lower noise and better stability for DC or chopped light applications. The cooled detector has a responsivity of 0.75 A/W at 1.9 µm and 0.92 A/W at 2.3 µm.

An impedance-matched, transimpedance gain preamplifier, manufactured also by EG&G, with selectable gain from 10^3 to 10^5 V/A was used in conjunction with the detector.

4.7 Spectrometer and dedicated software

The monochromator used (Optometrics Minichrom AMC1-M351) was a Fastie-Ebert in-line monochromator with a 300 lines/mm infrared grating blazed for peak efficiency at a wavelength of 3.5 µm. The f-number of the monochromator is 3.8. The range of entrance and exit slits available yielded resolutions of between 5 nm and 10 nm. The smallest slit size was used in this work unless stated otherwise.

A stepper motor is used to rotate the grating, with a minimum step size of 1.5 nm. Control software was written in Turbo C to control the stepper motor and to collect and store data from the detector for each 1.5 nm interval. The program plotted the spectrum on-screen in real-time. A mouse pointer was incorporated into the program to allow the user to obtain an exact wavelength from the screen. A flowchart of the software is shown in figure 4.19, and the full program listing is displayed in Appendix G.

A standard AR coated silicon filter (International Research & Development Ltd., England) was used to block the pump laser at 790 nm, as silicon has very low transmission below 900 nm.
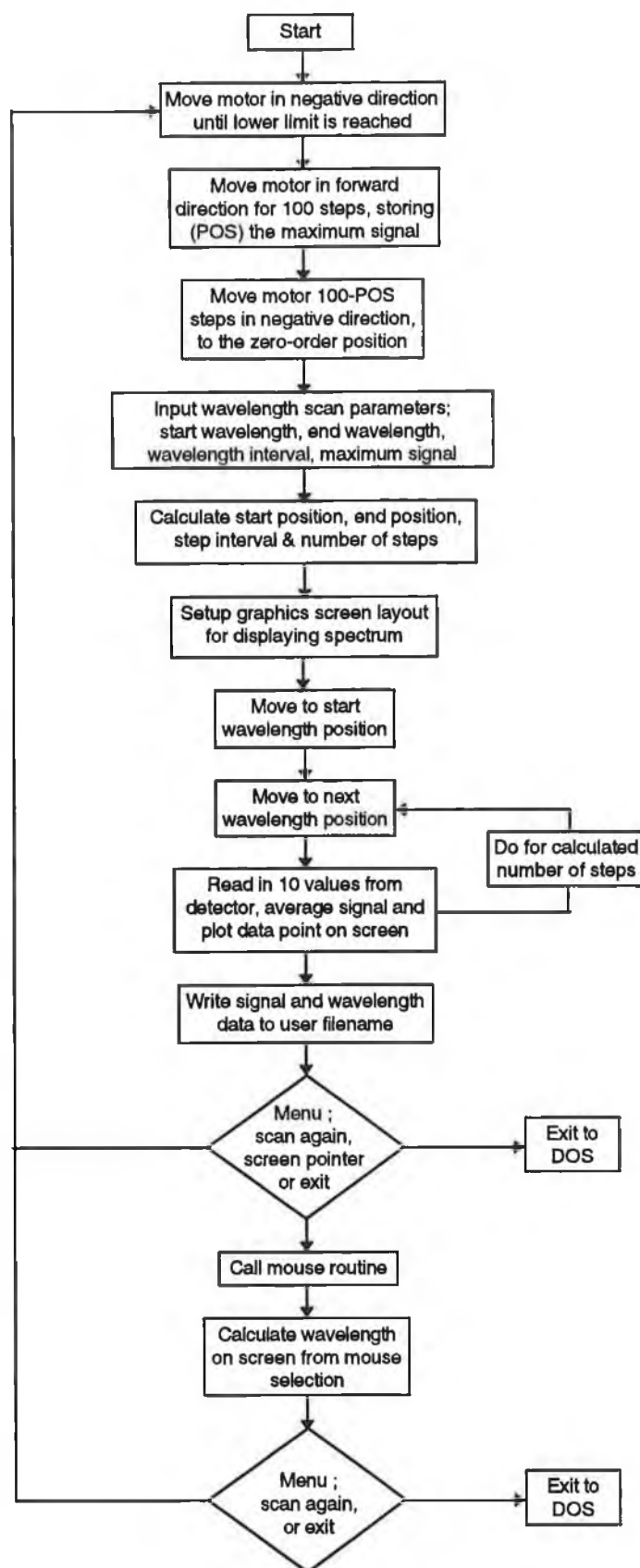
FIGURE 4.19 FLOWCHART FOR MONOCHROMATOR CONTROLLING SOFTWARE

4.8 Conclusion

In this chapter the various elements required for the construction of a fibre laser are discussed. The properties of the Tm^{3+}-doped fibre are briefly considered. The characteristics of both laser sources used for optically pumping the fibre are presented. Difficulties involved with coupling laser light from a high power laser source with a large emission area into a singlemode fibre are fully analysed. A model of the laser diode and lens system used in launching the light into the fibre was developed. This model assisted in the selection of the lenses for launching light into the doped fibre. Reasons for selection of particular characteristics, of the mirrors for the fibre laser cavity are outlined. The components used in the detection system are also discussed.

References :

1. Kawano K. : **'Coupling characteristics of lens systems for laser diode modules using single-mode fiber'**, Applied Optics, 1986, Vol. 25, No. 15, pp. 2600-2605

2. Presby H.M., Amitay N., Scotti R., Benner A.F. : **'Laser-to fiber coupling via optical fiber up-tapers'**, Journal of Lightwave Technology, 1989, Vol. 7, No. 2, pp. 274-278

3. Kuwahara H., Sasaki M., Tokoyo N. : **'Efficient coupling from semiconductor lasers into single-mode fibers with tapered hemispherical ends'**, Applied Optics, 1980, Vol. 19, No. 15, pp. 2578-2583

4. Khoe G.D., Poulissen J., deVrieze H.M. : **'Efficient coupling of laser diodes to tapered monomode fibres with high-index end'**, Electronics Letters, 1983, Vol. 19, No. 6, pp. 205-207

5. Shah V.S., Curtis L., Vodhanel R.S., Bour D.P., Young W.C. : **'Efficient power coupling from a 980-nm, broad-area laser to a single-mode fiber using a wedge-shaped fiber endface'**, Journal of Lightwave Technology, 1990, Vol. 8, No. 9, pp. 1313-1318

6. Shiraishi K., Aizawa Y., Kawakami S. : **'Beam expanding fiber using thermal diffusion of the dopant'**, Journal of Lightwave Technology, 1990, Vol. 8, No. 8, pp. 1151-1161

7. Percival R.M., Carter S.F., Szebesta D., Davey S.T., Stallard W.A. : **'Thulium-doped monomode fluoride fibre laser broadly tunable from 2.25 to 2.5 µm'**, Electronics Letters, 1991, Vol. 27, No. 21, pp. 1912-1913

8. Percival R.M., Szebesta D., Davey S.T. : **'Highly efficient and tunable operation of two-colour Tm-doped fluoride fibre laser'**, Electronics Letters, 1992, Vol. 28, No. 7, pp. 671-673

9. EG&G Judson : **'Infrared Detectors - 1992'**

Chapter 5

Doped fibres as fluorescent sources for optical sensing

5.1 Introduction

A wide range of optical sources is currently used for optical sensing based on infra-red spectroscopy. The range includes blackbody sources, incandescent sources and a variety of LED's. There are a number of disadvantages associated with these sources. Blackbody sources have low output power and are not compatible with optical fibres. Incandescent sources have a limited lifetime, are fragile, have a poor power conversion efficiency and cannot be efficiently coupled to optical fibres. They are often used in conjunction with narrow bandpass filters. The spectral transmission of these filters is temperature dependent, with the result that the output power may fluctuate. The spectral output of LED's is also temperature dependent ($\cong 0.5$ nm per C^0) and certain types of LED's such as E-LED's have significant fine structure in their output spectrum. This may cause a signal to drift when used with fine-line transmission optical filters.

The use of rare-earth doped fibres as sources for optical sensing has been proposed recently [1], such sources are attractive for several reasons : (i) they have a stable and reproducible output spectrum, where the structure may be determined by the fibre materials, (ii) they have a range of fluorescence bands covering most of the near and mid-IR regions (see chapter 2), (iii) they can be pumped by low-cost semiconductor laser diodes, and (iv) they are intrinsically compatible with mono-mode optical fibre systems.

Currently, the main application for rare-earth doped fibres as sources is as superfluorescent sources for fibre gyroscopes [2]. These sources exhibit a high power efficiency, are spatially coherent and, because the active energy levels in rare-earths belong to the $4f$ shell and are shielded by the $5s$ and $5p$ shells, they are

less sensitive to their host environment. This last issue is most important, since the mean frequency of the source determines the gyroscope scale factor [3]. Consequently, the source must have high spectral stability with respect to environmental factors such as temperature.

In this chapter, the use of Tm^{3+}-doped fluoride fibre as a fluorescent optical source for the detection of water is demonstrated. The detection and measurement of vapour-phase or liquid-phase water is important in many industrial and agricultural processes [4,5]. Water exhibits strong absorption bands compared to other substances in the near-IR (NIR) and for this reason NIR spectroscopy is especially well suited to moisture determination. A lack of suitable sources in the NIR, however, has impeded the application of optical sensors for water detection. Some LED sources for water or humidity sensing are available but often they do not provide a good spectral match to the relevant absorption bands. The fluorescent output from optically-pumped rare-earth doped fibres may overcome these problems, as they exhibit stable and reproducible output spectra, a range of possible emission bands and output power levels comparable to LED's and incandescent sources.

A Tm^{3+}-doped fluoride host exhibits relatively strong fluorescent emission bands in the NIR centered at 1.47 μm and 1.86 μm, respectively, when pumped in the 790 nm region (see chapter 3). Due to the strong overlap of the fibre fluorescence and liquid water absorption in this region, the possibility of using the doped fibre as a fluorescence source was investigated.

5.2 Liquid water measurement

The fluorescence spectrum of the doped fibre when pumped with the PHILIPS laser diode (785 nm) is shown in figure 5.1. This figure also displays the absorption spectrum of water in liquid phase. The liquid water spectrum, which was obtained with a fourier transform interferometer (FTIR) and a narrow ($\cong$ 0.4 mm) path-length cell, displays strong absorption bands at 1.92 μm and 1.47 μm. In the 1.47 μm region there exists a strong overlap between the fibre fluorescence and water absorption and this fluorescence band was investigated as an optical source for water sensing.
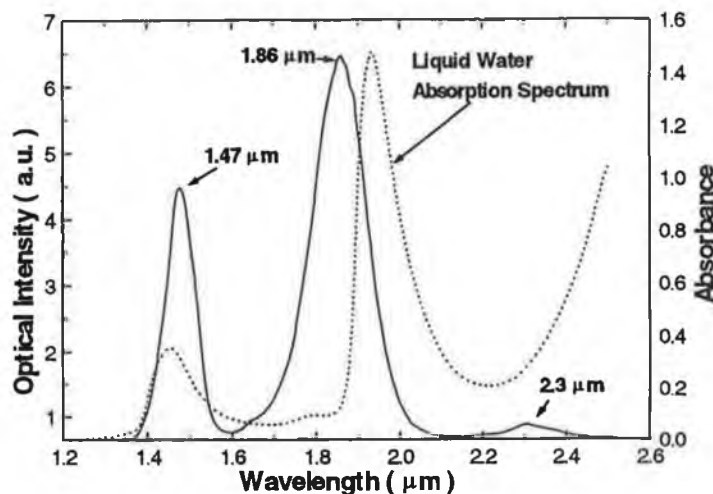
FIGURE 5.1 Tm^{3+}-DOPED FLUORIDE FIBRE FLUORESCENCE
SPECTRUM AND LIQUID WATER ABSORPTION SPECTRUM

Figure 5.2 illustrates the experimental configuration used to characterise the sensing principle. The collimated fluorescence beam, whose diameter was approximately 3 mm, is expanded in the figure for clarity. A *wedge cell* was constructed (see figure 5.3) for characterisation purposes using two glass slides held apart a one end by a spacer of known width from which the *wedge angle* (θ) could be calculated.
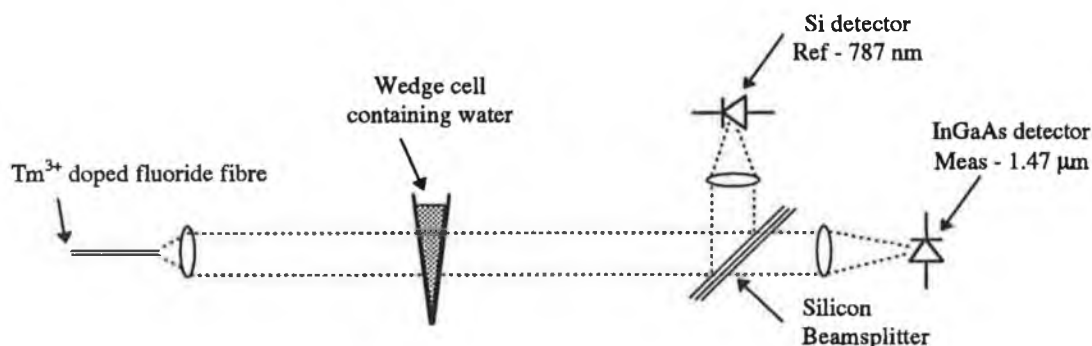
FIGURE 5.2 EXPERIMENTAL SENSING SETUP

The silicon slide displayed in figure 5.2 functions as a beamsplitter by reflecting the residual pump laser signal at 787 nm to the silicon photodiode and transmitting NIR wavelengths above 900 nm. An InGaAs detector whose response falls off rapidly above 1.7 μm detects the 1.47 μm fluorescence band, but is negligibly affected by the 1.86 μm emission. Lock-in detection techniques were

used due to the low signal levels. The signals from the LIA's were digitised with an A/D card (Bytronics) and passed to a computer for display and storage, where both signals were plotted versus time on the computer. Software was written in Turbo C to store the data and plot the data versus time. The program is listed in Appendix H.

Figure 5.3 displays the wedge cell construction.
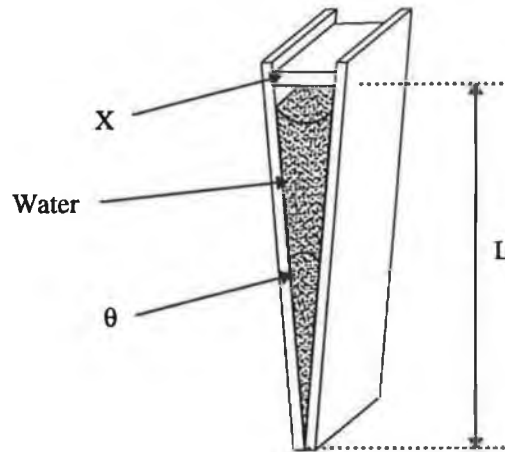
FIGURE 5.3 WEDGE CELL CONTAINING LIQUID WATER

A *wedge angle* (θ) of 0.611° was calculated from the wedge values, with L = 75 mm and X = 0.8 mm. Very small changes in transmission path-length were achieved by translating the wedge cell through the collimated beam in small increments. A nominal vertical increment of 0.5 mm corresponded to a change in path-length of approximately 5.3 µm.

Figure 5.4 displays the real-time measurement of liquid water using the system shown in figure 5.2. Each step corresponds to a change in the wedge cell pathlength of approximately 5.3 µm. Each time the pathlength was increased by 5.3 µm, the software used to record the data was paused.
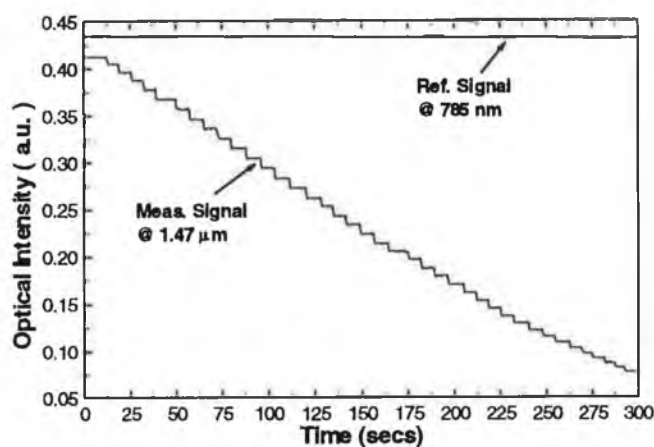
FIGURE 5.4 REAL-TIME LIQUID WATER MEASUREMENT

From figure 5.4 the reference signal (I_0) at 785 nm and the measurement signal (I) at 1.47 μm was used to calculate an effective absorbance

$$Effective\ Absorbance = \log_{10} \frac{I_0}{I}$$

Eqn. 5. 1

Figure 5.5 shows the effective absorbance plotted as a function of path-length.
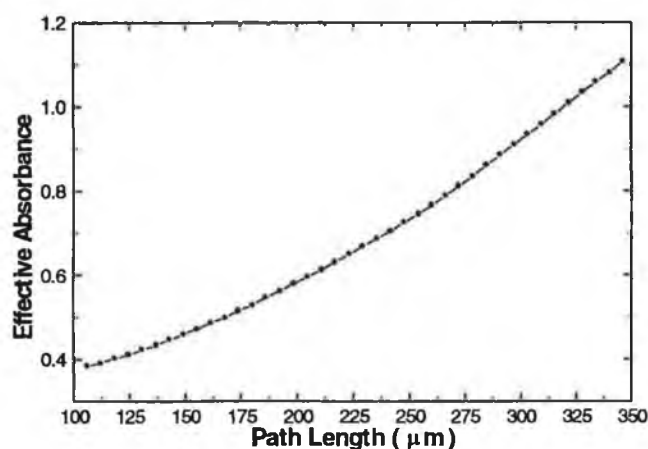
FIGURE 5.5 CALIBRATION CURVE FOR LIQUID WATER IN VARIABLE PATHLENGTH CELL

The deviation of the curve from linearity is probably due to the non-uniformity of the wedge cell construction and may also be due to the minor spectral mismatch between the fluorescent source and the water absorption band at 1.47 μm. The

noise limited minimum detectable path-length was calculated to be approximately 1 μm. This *'proof of principle'* experiment establishes the viability of measuring water over extremely short path-lengths, or, equivalently, very low concentrations of water or humidity, using a low-cost compact source.

5.3 *Detection and measurement of water in other liquids*

The detection and measurement of water concentrations in other liquids was also investigated, using the evanescent wave absorption system displayed in figure 5.6.
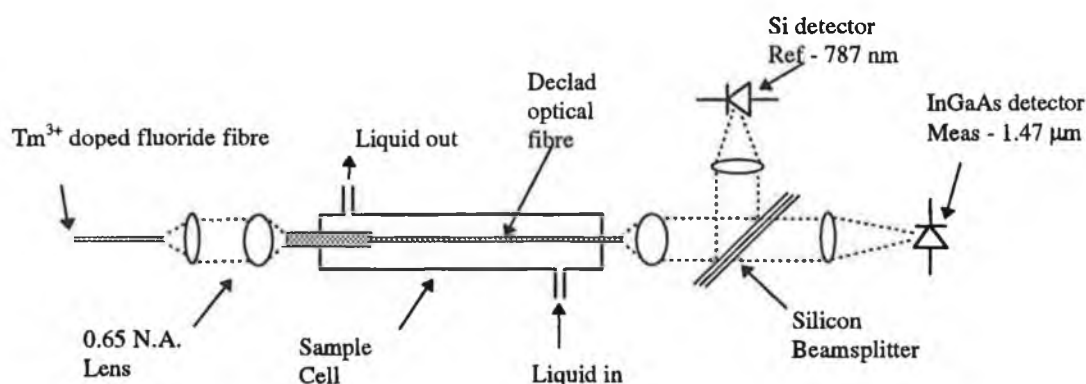
FIGURE 5.6 EXPERIMENTAL SENSING SCHEME FOR LIQUID WATER IN OTHER LIQUIDS

in this case, the collimated fluorescence beam from the doped fibre was launched into a 600 μm core declad multimode PCS fibre (0.4 NA) using a 0.6 NA lens to overfill the fibre numerical aperture. The use of this high NA lens ensured that a large penetration depth was present, and therefore, maximum evanescent wave sensing was achieved. Samples of varying water content were prepared by mixing water with methanol. Methanol was used as it is non-absorbing at both the measurement and reference wavelengths and also because the refractive index for liquid water and methanol are very similar. As before, lock-in detection techniques were used due to the low signal levels. The signals from the LIA's were digitised with an A/D card (Bytronics) and passed to a computer for storage. Figure 5.7 illustrates the real-time sensing of alternate concentrations of 100 % liquid water and 100 % methanol (i.e. 0 % liquid water).
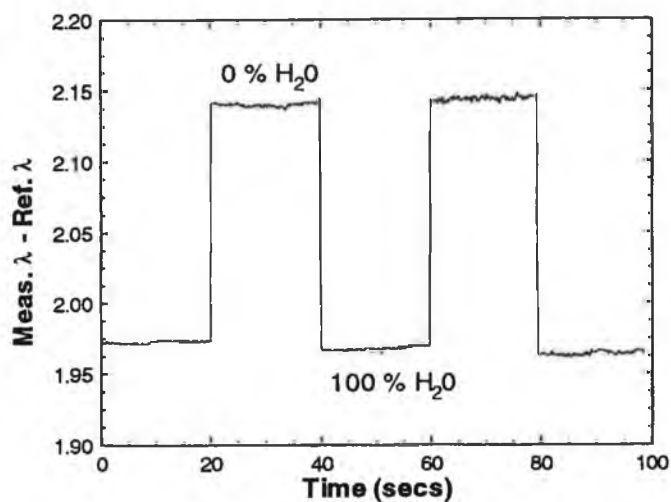
FIGURE 5.7 REAL-TIME DETECTION OF LIQUID WATER IN METHANOL

Samples containing different concentrations of water and methanol were passed through the sample cell and the measured reference (I_0) and measurement (I) signals were used to calculate an effective absorbance as defined earlier (Eqn. 5.1). Figure 5.8 displays data obtained using the system shown in figure 5.6 for water concentrations over the range 0 - 100 %. These data illustrate the potential for measuring very small changes in water concentration such as might be required in milk or alcohol analysis.
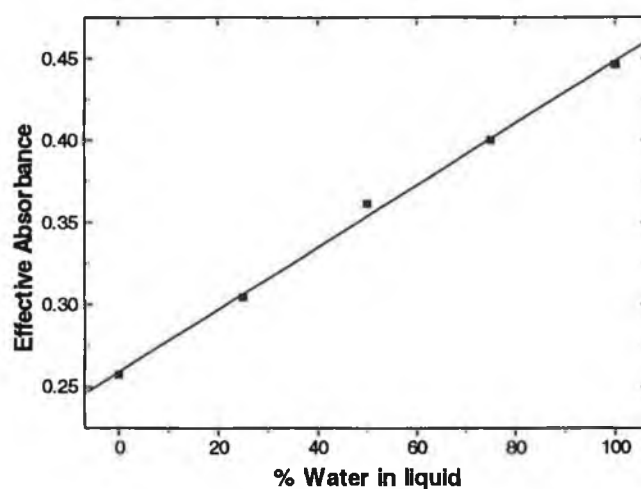
FIGURE 5.8 DETECTION OF LIQUID WATER IN METHANOL

5.4 Conclusion

The fluorescence emission from a Tm^{3+}-doped fluoride fibre pumped with a low-cost diode laser has been shown to function as a useful source for water sensing. The approach presented here offers the advantages of a stable output spectrum, reasonable output power and an intrinsic reference signal. The two configurations presented in this chapter each demonstrate potential applications of the proposed approach. The first illustrates the viability of a compact low-cost system which could be employed to monitor water content or humidity. The second demonstrates the viability of a remote or distributed probe which benefits from the fibre-compatibility of the source.

References :

1. Dong X.P., Edwards H.O., Shafir E., Dakin J.P. : **'Broadband sources for gas detection using fluorescent rare-earth-doped fibres pumped by low-cost semiconductor laser source'**, Conference proceedings OFS 9, Florence, Italy, 1993, Vol. W1.6, pp. 209-213

2. Burns W.K., Duling III I.N., Goldberg L., Moeller R.P., Villarruel C.A., Snitzer E., Po H. : **'Fiber superfluorescent sources for fiber gyro applications'**, Springer Series in Physics, Vol. 44, Optical Fiber Sensors (Arditty H.J., Dakin J.P., Kersten R.T. {eds.}), Springer-Verlag, Berlin, 1989, p. 137

3. Lefèvre H.C. : **'Fiber optic gyroscope'**, Optical Fiber Sensors : Systems and Applications, Vol. 2, (Culshaw B., Dakin J.P. {eds.}], Artech House, MA, 1989, pp. 381-429

4. Greaves P. : **'Meaningful measurement of moisture in food, pharmaceuticals and other products'**, Measurement + Control, 1992, Vol. 25, pp. 106-108

5. Hop E., Luinge H.-J, VanHemert H. : **'Quantitative analysis of water in milk by FT-IR spectrometry'**, Applied Spectroscopy, 1993, Vol. 47, No. 8, pp. 1180-1182

Chapter 6

Fibre laser modelling

6.1 Introduction

The aim of this chapter was to apply a number of equations from other published models of fibre laser operation to the system of interest in this work. These equations were used to predict the threshold, output power and slope efficiency of the fibre laser. An operational fibre laser must be an efficient source if it is to be used as a source for optical sensing. It must exhibit a low threshold, thereby reducing the power of the pump source, combined with a high conversion or slope efficiency. Model equations were used to predict the characteristics of an operational fibre laser, based on a number of different transmission values for the output fibre laser mirror.

6.2 General model for four level laser systems

Michel Digonnet [1,2,3] has developed a comprehensive model for three- and four-level fibre amplifiers and oscillators. This model was developed to quantify the pump power requirement for the different device configurations and to identify means of reducing it. The key parameter analysed was the optical gain of the fibre and its relationship to the pump power, modes and fibre parameters. The gain is the fundamental parameter of optical fibre amplifiers, but it also determines the threshold of fibre laser sources. The problem was treated by rigorous analytical models based on rate equations [4] and on the energy distributions of the pump and signal in the fibre. However, exact solutions [5] are too cumbersome and require numerical analysis. For this reason Digonnet developed closed-form approximate solutions for the more important fibre laser and amplifier parameters, such as the gain of the device, the threshold for operation, the conversion efficiency or slope efficiency from the pump beam into the signal beam, and the output power from the

device. The following equations provide a means of calculating the threshold, slope efficiency and output power from a four-level fibre laser.

According to Digonnet's model, a fast and easy means of calculating the threshold [1] for a four-level fibre laser is given by

$$P_{th} = \frac{h\nu_p A \eta_p \delta}{\sigma_e \tau_2 F_n}$$

Eqn. 6. 1

where h is Planck's constant, ν_p is the frequency of the pump laser, A is the area of the fibre core, η_p is the fraction of pump energy contained in the fibre core, δ is the round trip loss for the fibre laser cavity, σ_e is the stimulated emission by the effective cross section of the fibre, τ_2 is the spontaneous lifetime of the upper laser level and F_n is the normalised overlap integral between the pump and the signal transverse spatial distributions.

The cavity round trip loss (δ) [1] is given by

$$\delta = \delta_0 - \ln(1 - T_2)$$

Eqn. 6. 2

where δ_0 is the fibre loss, including scattering losses and coupling losses at the fibre-mirror interfaces and T_2 is the transmittance of the output mirror.

The fraction of power (η_p) in the core at the pump wavelength [6] may be obtained from equation 6.3

$$\eta_p = \frac{U_p^2}{V_p^2} \cdot \left[\frac{W_p^2}{U_p^2} + \frac{K_\ell(W_p)}{K_{\ell-1}(W_p).K_{\ell+1}(W_p)} \right]$$

Eqn. 6. 3

where $K_{\ell \pm n}$ is the modified Bessel function of the second kind and $\ell \pm n$ denotes the order, with n = 0, 1, 2, ... The V-number of the doped fibre at the pump wavelength is denoted by V_p, with U_p and W_p representing the core and cladding mode parameters at the pump wavelength, respectively. The fibre V-number (V_p) at the pump wavelength may be calculated from

$$V_p = \frac{2 \cdot 405.\lambda_c}{\lambda_p}$$

Eqn. 6. 4

where λ_c is the cutoff wavelength and λ_p is the pump wavelength. The eigenvalue equation for a step-index fibre [7] may be used to calculate the core parameter (U_p) value of each mode and also, the number of modes. The value for each cladding parameter (W_p) may be calculated from

$$V_p{}^2 = U_p{}^2 + W_p{}^2 \qquad \text{Eqn. 6. 5}$$

The normalised overlap intergral (F_n) between the pump and the signal transverse spatial distributions [1] may be obtained from

$$F_n = A\pi e_n \cdot \int_0^a r_p(r).s_s(r).rdr \qquad \text{Eqn. 6. 6}$$

where $e_n = 2$ for $\ell = 0$ and $e_n = 1$ for $\ell > 0$ (ℓ is the order number of a particular mode), and $r_p(r)$ and $s_s(r)$ refer to the power density of the pump and signal mode, respectively. According to Gloge [8], equation 6.7 may be re-arranged to calculate the mean power density of the pump, or signal beam in the core

$$p(r) = K . \frac{U^2}{V^2} . \frac{P}{\pi a^2} . \frac{J_\ell^2 \left(\dfrac{Ur}{a} \right)}{J_\ell^2(U)} \qquad \text{Eqn. 6. 7}$$

with

$$K = \frac{K_\ell^2(W')}{K_{\ell-1}(W') \cdot K_{\ell+1}(W')} \qquad \text{Eqn. 6. 8}$$

These equations may be manipulated to give a final equation for F_n, where J_ℓ is the Bessel function of the first kind and R is the normalised fibre radius

$$F_n = e_n \cdot \frac{U_p^2}{V_p^2} . \frac{U_s^2}{V_s^2} . \left[\frac{K_\ell^2(U_p)}{K_{\ell-1}(U_p).K_{\ell+1}(U_p)} \right] . \left[\frac{K_\ell^2(U_s)}{K_{\ell-1}(U_s).K_{\ell+1}(U_s)} \right] . \int_0^1 \frac{J_\ell^2(U_p R)}{J_\ell^2(U_p)} . \frac{J_\ell^2(U_s R)}{J_\ell^2(U_s)} . RdR \quad \text{Eqn. 6. 9}$$

The output power for a four-level fibre laser [1] takes the form :

$$P_{out} = \frac{T_2 h\nu_s}{\delta h\nu_p} . (P_{abs} - P_{th}) \qquad \text{Eqn. 6. 10}$$

where ν_s is the frequency of the signal laser, and P_{abs} is the quantity of pump power absorbed by the fibre. This expression only applies for small values of T_2, and shows that above threshold the output power of a fibre laser grows linearly with absorbed power.

The slope efficiency or conversion efficiency s [1], is given by

$$s = \frac{P_{out}}{P_{abs} - P_{th}} = \frac{T_2 h\nu_s}{\delta h\nu_p} \qquad \text{Eqn. 6. 11}$$

The slope efficiency of a fibre laser is proportional to the relative output coupler "loss" T_2 / δ. For a small cavity loss δ_0 and a small output coupler transmission T_2 the conversion efficiency approaches the quantum limit $h\nu_s / h\nu_p$.

6.3 Application of model to Tm^{3+} in a fluoride host

Digonnet's model was applied to the doped fibre and pump laser used in this work. The model was used to assist in selecting the transmission characteristics of the output fibre laser mirror, as the transmission value of this mirror had a major role in determining the operational characteristics of the experimental fibre laser (equations 6.1, 6.10 and 6.11).

In obtaining a value for the threshold of a Tm^{3+}-doped fluoride fibre laser, the stimulated emission value (σ_e), is required and this may be calculated from Judd-Ofelt [9,10] theory, in conjunction with measured absorption and fluorescence spectra. This value was not calculated in this work, as many values have been published for σ_e, for fibres with similar characteristics and dopant concentrations. A value for σ_e of 1.4×10^{-25} m^2 was taken from Percival *et al.* [11] for the 2.31 µm transition. The spontaneous lifetime of the upper laser level ($^3H_4$) was experimentally determined to be 1.56 ms (see chapter 3).

When calculating the cavity round trip loss (Eqn 6.2), the fibre loss (δ_0) was assumed to be negligible, a fibre loss of 1 % was selected for calculations (chapter 7 deals with fibre-mirror interface losses). The fibre had very low losses at 2.3 µm and this model was primarily being used to predict the fibre laser operation and to assist in selecting the fibre laser mirrors. Therefore, the cavity round trip loss was

determined solely by the value for the transmission of the output coupler (T_2) and a negligible background loss of 1 %.

The fibre V-number (V_p) at the pump wavelength was calculated to be 6.3930 by using equation 6.4, with λ_c, the cutoff wavelength was specified by the manufacturer to be to 2.1 μm and λ_p, the pump wavelength equal to 790 nm. The eigenvalue equation for a step-index fibre was solved for the pump wavelength V-number of 6.3930, and a core refractive index of 1.5165. The eigenvalue equation yielded six solutions for the core parameter (U_p). Therefore at 790 nm there are six modes in the doped fibre. Equation 6.5 was used to calculate the corresponding six cladding parameters (W_p).

The values for V_p, U_p and W_p were substituted into equation 6.3 to yield the fraction of power confined in the core of the doped fibre (η_p) for each mode. Equation 6.9 was used to calculate the overlap (F_n) between the pump and signal beams. The values for $V_s = 2.1864$, $U_s = 1.5221$ and $W_s = 1.5690$ were much simpler to calculate as the fibre had only one mode at 2.3 μm ($\lambda_c = 2.1$ μm). Table 6.1 displays the calculated values for V_p, U_p and W_p, together with the fibre mode order numbers (ℓ) and (m) and the calculated values for η_p and F_n.

Mode Number (ℓ,m)	V_p	U_p	W_p	η_p	F_n
0,1	6.3930	2.0686	6.0491	0.9851	0.8145
1,1	6.3930	3.2910	5.4809	0.9594	0.3388
2,1	6.3930	4.3901	4.6473	0.9204	0.2852
0,2	6.3930	4.6939	4.3402	0.8987	0.7008
3,1	6.3930	5.4185	3.3927	0.8612	0.2410
1,2	6.3930	5.8614	2.5523	0.7688	0.2956

TABLE 6.1 DOPED FIBRE PARAMETERS AT THE PUMP WAVELENGTH

Average values for η_p and F_n were calculated for use in equation 6.1.

When calculating P_{out} (Eqn. 6.10) the fibre length was assumed to be long enough so that the power launched equalled the power absorbed by the fibre ($P_{in} = P_{abs}$).

The next section calculates the predicted threshold, output and slope efficiency of the Tm^{3+}-doped fluoride fibre laser, based on a number different values for the transmission of the output coupler or mirror (T_2).

6.4 Results for 2.3 µm oscillators

Equations 6.1, 6.10 and 6.11 were modelled using MATLAB™ to predict the threshold, output power and slope efficiency of the Tm^{3+}-doped fluoride fibre laser, once operational. Four values for the transmittance (0.5 %, 2 %, 4 %, 6 %) of the output mirror at the fibre laser wavelength were used when modelling these equations. An absorbed pump power of 40 mW was selected as an approximate value. By predicting the operation of the fibre laser before lasing occurred, this allowed for the optimum tailoring of the transmission specifications for the output mirror at the fibre laser wavelength (2.3 µm).

Appendix I displays the program listing for the equations used to model the fibre laser. The cavity round trip losses were calculated for four transmission values listed above and with a fibre loss of 1 %. These values were then used to calculate the four threshold values and corresponding slope efficiencies. The output power from each fibre laser model with a given mirror transmittance was calculated over a range of launched powers from $0 \to 40$ mW.

Table 6.2 displays the predicted characteristics of the fibre laser.

O/P Trans (%)	Threshold (mW)	Slope Eff. (%)	Max. O/P Power (mW)
0.5	3.31	11.39	4.16
2	6.66	22.65	7.48
4	11.21	26.93	7.67
6	15.86	28.56	6.85

TABLE 6.2 PREDICTED FIBRE LASER CHARACTERISTICS

Figure 6.1 displays the predicted fibre laser characteristic curves with four different mirrors.
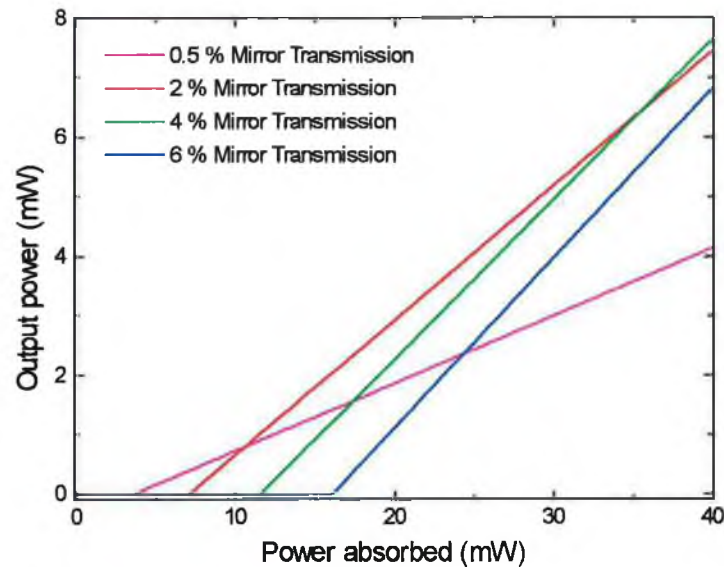
FIGURE 6.1 PREDICTED FIBRE LASER CHARACTERISTICS

These results are not predicting the exact operation and characteristics of the experimental fibre laser. However, they are useful in evaluating the operation of a fibre laser with output mirrors of different transmission values, and therefore, in optimising the selection of appropriate mirrors. The conclusion from this exercise is that an output coupler with a transmission of 2 - 3 % would allow for both a low threshold and high slope efficiency.

6.5 Conclusion

This chapter illustrated the significance of the selection of an output mirror with the correct transmission properties, for a doped fibre with particular parameters. The mirror selected had also to allow for the limited quantity of pump power available. The selected mirror would allow the fibre laser to operate with both a low threshold and a reasonable high output power. If high pump powers were available, as with Ti:Sapphire lasers, a low operating threshold would not be as significant, and this would allow a mirror with a higher transmission value to used.

References :

1. Digonnet M.J. (ed.) : **'Rare earth doped fiber lasers and amplifiers'**, Marcel Dekker, New York, 1993, Chapter 4

2. Digonnet M.J.F., Gaeta C.J. : **'Theoretical analysis of optical fiber laser and amplifiers and oscillators'**, Applied Optics, 1985, Vol. 24, No. 3, pp. 333-342

3. Digonnet M.J.F. : **'Closed-form expressions for the gain in three- and four-level laser fibers'**, IEEE Journal of Quantum Electronics, 1990, Vol. 26, No 10, pp. 1788-1796

4. Koechner W. : **'Solid-State Laser Engineering'**, Vol. 1 in Springer Series in Optical Sciences, Springer-Verlag, New York, 1988 (2nd ed.), Chapter 1

5. Armitage J.R. : **'Three-level fiber laser amplifier : A theoretical model'**, Applied Optics, 1988, Vol. 27, No. 23, pp. 4831-4836

6. Snyder A.W., Love J.D. : **'Optical Waveguide Theory'**, Chapman Hall, New York, 1983, Chapter 14

7. Snyder A.W., Love J.D. : **'Optical Waveguide Theory'**, Chapman Hall, New York, 1983, Chapter 12

8. Gloge D. : **'Weakly guiding fibers'**, Applied Optics, 1971, Vol. 10, pp. 2252-2258

9. Judd B.R. : **'Optical absorption intensities of rare-earth ions'**, Physical Review, 1962, Vol. 127, No. 3, pp. 750-761

10. Ofelt G.S. : **'Intensities of crystal spectra of rare-earth ions'**, The Journal of Chemical Physics, 1962, Vol. 37, No. 3, pp. 511-520

11. Percival R.M., Szebesta D., Davey S.T. : **'Highly efficient and tunable operation of two colour Tm-doped fluoride fibre laser'**, Electronics Letters, 1992, Vol. 28, No. 7, pp. 671-673

Chapter 7

Fibre laser construction and characterisation

7.1 Introduction

A basic fibre laser cavity consists of a length of doped fibre between two mirrors which form a Fabry-Perot cavity. The basic equations governing the operation of a fibre laser were treated in chapter 6. Fibre lasers have been demonstrated in a number of different configurations, shown in figure 7.1. Some have the mirrors butted directly to the fibre end (figure 7.1a) so that the fibre forms a complete laser cavity in itself [1]. As an alternative, it is possible to couple the light out of the fibre end (figure 7.1b) before reflecting it so that an air space is included in the cavity [2]. This allows intra-cavity elements such as tuning gratings to be inserted to intercept the unguided beam. It is also possible to apply optical coatings (figure 7.1c) to the cleaved fibre end [3] instead of using separate mirrors. This serves to reduce losses at the mirror-fibre interface, although it is a technically difficult process and the losses it removes are small. Another common configuration is a ring laser (figure 7.1d) with a dichroic coupler which acts as the input and output mirrors [4].
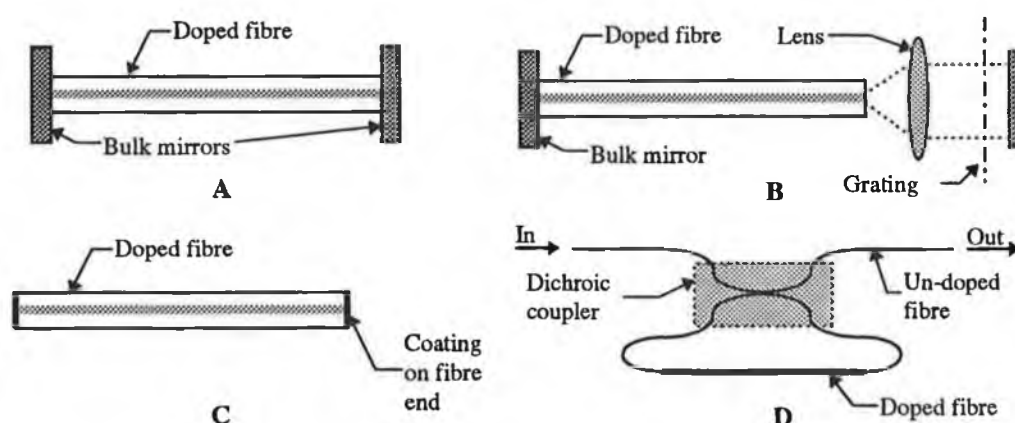

FIGURE 7.1 VARIOUS FIBRE LASER CONFIGURATIONS

A wide range of pump sources has been used for fibre lasers. These include argon and krypton ion lasers and solid state lasers such as neodymium-doped YAG and titanium-sapphire. Perhaps the most important pump source for fibre lasers is the semiconductor diode laser. Although, laser diodes have relatively narrow tuning ranges and are only commercially available at a selection of wavelengths, they have major advantages for use as a pump source in commercial applications of fibre lasers. They are small, efficient and have no moving or sensitive parts which need maintenance or alignment. Their small size and low power requirements makes them ideal for integration into fibre systems in telecommunications and medicine where the main applications of fibre lasers seem to lie. For the reasons outlined above, a diode laser was selected as a pump source with a view to constructing a fibre laser with potential commercial applications. The characteristics of the pump laser diode were discussed in detail in section 4.3 and 4.4.

This chapter deals first with the difficulties involved with the alignment and positioning of the doped-fibre between the laser mirrors, and then the operation of two fibre lasers with high and low power laser diode pump sources, respectively.

7.2 Positioning and alignment

Due to the small dimensions of the doped-fibre very precise control over the movement of the fibre was necessary in order to optimise the launch efficiency. This section explains why careful preparation of the fibre ends and accurate positioning with respect to the mirrors are necessary to reduce intra-cavity losses [5].

7.2.1 Fibre end quality

Fibre ends must be prepared to a high quality, i.e. they must be flat and perpendicular to the fiber axis. The problem of end preparation is important in many applications of optical fibres and as a result, commercial cleaving tools have been developed to provide quality ends.

A fibre cleaver from York Technology, England (Model FK11) was used to achieve high quality fibre ends on the doped fibre. The fibre is enclosed by a plastic outer sleeving which was first stripped by soaking in a mixture of methylene dichloride and methanol (Strypit commercial paint stripper) for approximately a minute and then gently pulling off the swollen and softened coating with lens tissue. The stripped fibre end was then cleaned with a clean lens tissue soaked in methanol. Figure 7.2 displays the York fibre cleaver.
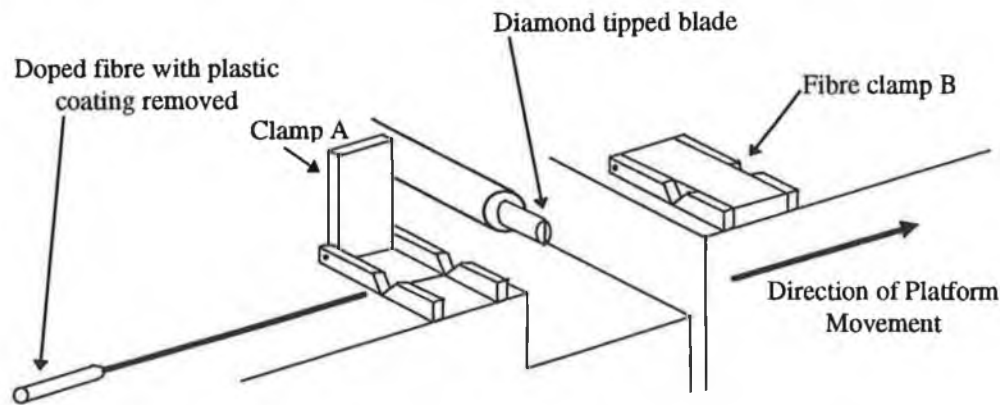
FIGURE 7.2 YORK FIBRE CLEAVER

The doped fibre with the plastic coating removed is placed in the fibre groove in clamps A and B. The fibre clamps are gently lowered to hold the fibre. Clamps A and B are clamped down and locked in position. Clamp B is located on a movable platform to which a variable tension may be applied. After numerous attempts at cleaving with various tensions applied, 0.784 N was determined to be the optimum tension. The tension lever is moved to apply the preset tension axially along the fibre. Once the fibre has been clamped at both ends and the tension applied, the diamond tipped blade Is released. The vibrating blade nicks the side of the fibre and the axial tension causes the fibre to cleave.

The quality of the cleave was inspected under a high power microscope (magnification x 40). An interference lens was also employed to check the cleave quality.

Fluoride fibres are particularly brittle and require extreme care when handling. Cleaving the fibre was a very unreliable operation with a less than 50 % success rate. In order to increase the possibility of a good quality cleave it was found necessary to ensure that the fibre section with the plastic coating removed was thoroughly cleaned with IPA (isopropyl alcohol) or methanol. It was also found necessary to clamp the fibre with the plastic coating intact in clamp A in order to ensure the fibre was tightly gripped during the tensioning stage.

7.2.2 Fibre End-Mirror Interface

The fibre end and the mirror surface should meet at an angle that is as close as possible to 90°. This criterion necessitates the use of micropositioners or the

design of a custom mount to ensure the appropriate location of the fibre with respect to the mirror surface. The three main loss mechanisms associated with the fibre-mirror interface are fibre-mirror separation, tilt and bending. Separation and tilt are micropositioning errors, while bending is due to excessive force being applied to the fibre in order to counteract separation. Figure 7.3 illustrates these three errors.
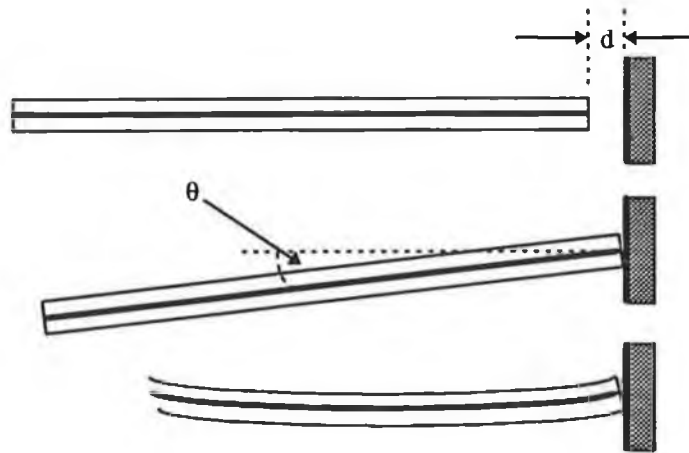
FIGURE 7.3 FIBRE END-MIRROR INTERFACE; SEPARATION, TILT AND BENDING

In 1986, Marcuse proposed a model [6] which treats the fibre end-mirror interface coupling problem. This model assumes that a single-mode fibre brought into contact with a mirror interface will exhibit a combination of separation and tilt. It is also assumed that index matching fluid is present between the fibre and mirror and that the refractive index of the fluid is the same as the fibre core. Marcuse's model uses results discussed in references [7] and [8].

The model requires that the transverse intensity distribution be approximated as a Gaussian beam with a full width (w), which is measured at ^{1}/e of the maximum intensity. The fibre radial coordinate is r and core-cladding boundary is at $r = a$. The Gaussian distribution is given by :

$$\varphi(r) = \exp\left[\frac{-r^2}{w^2}\right]$$

Eqn. 7. 1

The mode spot size is given in terms of the radius (a) and the fibre V-parameter by [7,8] :

$$w = \left(\frac{a}{\sqrt{2}}\right)\left(0.65 + \frac{1.619}{V^{3/2}} + \frac{2.879}{V^6}\right) \qquad \textit{Eqn. 7. 2}$$

where a step refractive index profile is assumed. The V value is given by [9] :

$$V = \frac{2\pi a}{\lambda}.(n_1^2 - n_2^2)^{1/2} \qquad \textit{Eqn. 7. 3}$$

where n_1 and n_2 are the core and cladding refractive indices, respectively. The following equation represents the ratio of recaptured power to exiting power where it is assumed that the fibre end is of high quality and is at normal incidence to the mirror :

$$\rho = \frac{R(4Z^2+1)}{(2Z^2+1)^2 + Z^2} \qquad \textit{Eqn. 7. 4}$$

In this equation R is the reflectivity of the mirror and Z is a normalised length given by

$$Z = \frac{2d}{\beta w^2} \qquad \textit{Eqn. 7. 5}$$

where *d* is the separation distance between the fibre end and the mirror, and β is the plane wave propagation constant given by

$$\beta = \frac{1}{a}\left\{\frac{V^2}{2\Delta} - U^2\right\}^{1/2} \qquad \textit{Eqn. 7. 6}$$

In this equation U is the core mode parameter ([9], see also section 6.3) and Δ is the refractive index parameter given by

$$\Delta = \frac{n_1^2 - n_2^2}{2n_1^2} \qquad \textit{Eqn. 7. 7}$$

Figure 7.4 is a plot of equation 7.4 with R = 1. As expected, the power returned to the fibre decreases as *d* increases. Equation 7.4 was modeled using 'MATLAB'™, and the program is listed in Appendix J.1.
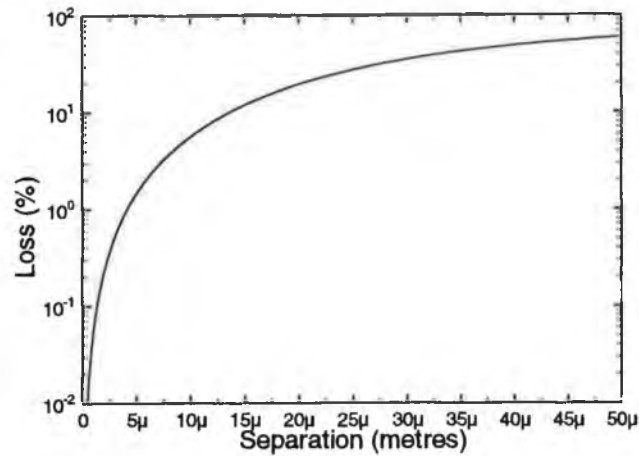
FIGURE 7.4 FIBRE END-MIRROR INTERFACE; PERCENTAGE LOSS AS A FUNCTION OF d

The influence of the tilt can also be examined by considering a high quality fibre end mounted at an angle of θ radians to a perfect front surface mirror of reflectivity R. The ratio of the power of the recaptured light to the power of the light exiting the fibre can be shown [6] to be :

$$\rho = R\exp(-\beta^2 w^2 \theta^2)$$

Eqn. 7. 8

When a tilted end is mounted against a mirror a small amount of separation is present. This separation distance is determined by the fibre cladding diameter (ℓ).
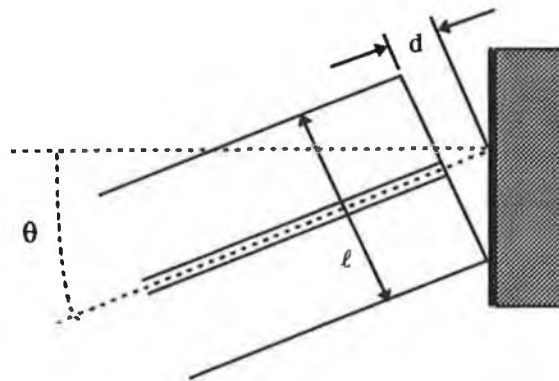
FIGURE 7.5 FIBRE END-MIRROR INTERFACE; SEPARATION DUE TO TILT

The separation due to tilt may be related to the tilt angle (θ) by :

$$\tan\theta = \frac{2d}{\ell} \cong \theta \, (radians) \qquad \{for \; small \; angles\}$$

Eqn. 7. 9

Equation 7.9 may be re-arranged to find the value for *d*. The value for *d* may then be substituted into equation 7.4. It has also been shown by Marcuse that the losses as a result of tilt and separation are approximately additive [6]. Figure 7.6 shows a plot of the loss due to tilt and the loss due to the separation distance (negligible) associated with this tilt angle (equation 7.8 was modeled using 'MATLAB'™, the program is listed in Appendix J.2).
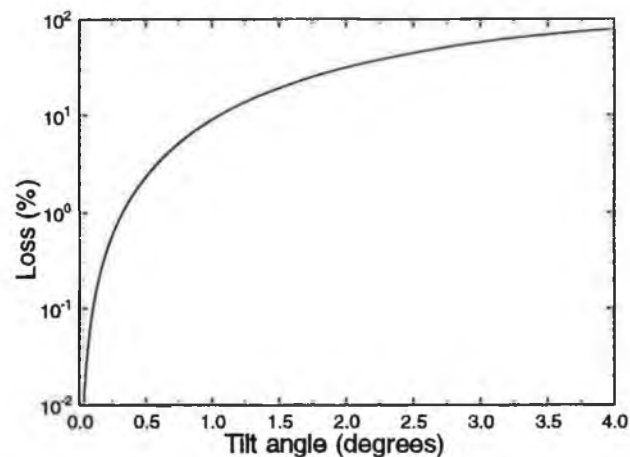
FIGURE 7.6 FIBRE END-MIRROR INTERFACE; PERCENTAGE LOSS AS A FUNCTION OF θ

Clearly, losses due to angular displacement are much more serious than losses due to separation, as the loss associated with a separation of 4-5 μm is one order of magnitude less than that due to a tilt angle of 1°. When the Gaussian laser beam returns to a separated end at normal incidence it has merely diverged, but the peak intensity still coincides with the fibre axis, and therefore the overlap with the guided mode is quite good. In contrast, when the Gaussian beam returns to a tilted end, the intensity peak is off-axis and has a poor spatial overlap. The significance of figures 7.4 and 7.6 for the construction of a fibre laser is that a separation of a few microns is acceptable, but a tilt of a one degree can introduce a serious intracavity loss.

All values used in the equations above have been taken from sections 4.2 and 6.3.

7.2.3 Fibre positioning

The mirrors were mounted in simple mirror holders at a fixed position, but some degree of angular adjustment was incorporated into the mirror holders by adjusting three screws on the holder. Figure 7.7 displays the mirror holder and the screws used to manipulate the mirror angle.
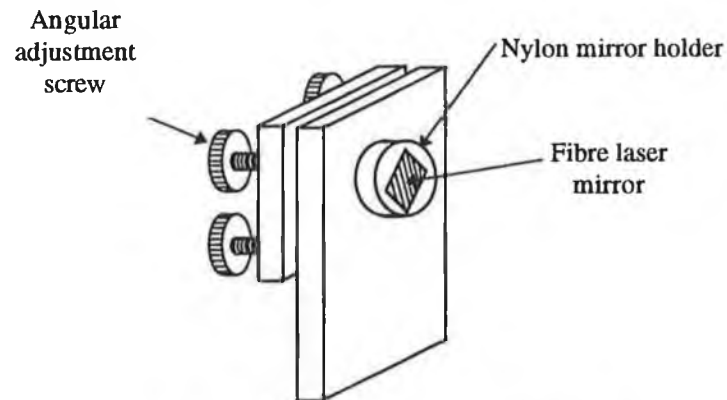
FIGURE 7.7 LASER MIRROR HOLDER

After obtaining a good quality fibre end face, the doped-fibre was held in a vee groove with a spring-loaded clamp arm. The fibre holder was mounted on a three axis XYZ flexure stage (Martock MDE 102). This micropositioner stage had a 0.05 μm resolution in each of the three axes. The following figure (fig. 7.8) displays the fibre-mirror butt coupling scheme employed.
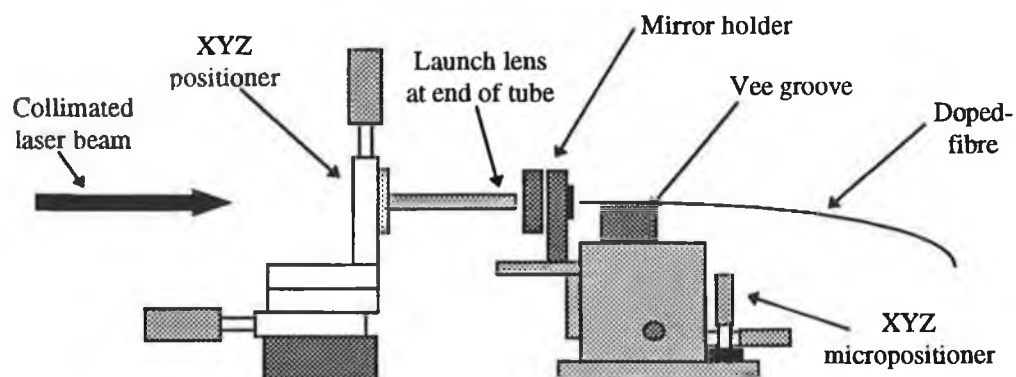
FIGURE 7.8 FIBRE-MIRROR BUTT COUPLING SCHEME

The collimated pump laser beam (launch optics discussed in section 4.3.3) was aligned axially with the fibre end. This was accomplished by removing the launch

lens and positioning the entire fibre and mirror mount assembly in the pump beam, to maximise the pump signal emerging from the fibre output. This signal is mainly due to pump light in the cladding, since without the launch lens the pump beam diameter is far larger than the fibre, and optimising this signal simply centralises the fibre. The launch lens was replaced and positioned approximately to focus the pump beam on the front face (fibre side) of the input mirror. The aluminum tube containing the launch lens (figure 7.8) is located on a XYZ positioner (Photon Control PTS-75-XYZ), which affords a greater degree of movement in the launch system. Index matching fluid was smeared over the area of the mirror to be used and a drop was placed on the end of the cleaved fibre. The fibre end was then brought up to the mirror using the micropositioner, but not wound up all the way to the mirror. An infrared viewer was used to optimise this positioning. As the fibre position was changed pump light could be seen in the fibre using the IR viewer. Once a fluorescence signal was detected, optimisation was continued using that signal. The degree of brightness of the yellow fluorescence (due to upconversion) from the thulium in the fibre core was useful as an indication of how much pump radiation was being guided in the core. Once the point where the pump beam was focused on the mirror was reached, the fluorescence signal varied rapidly as the fibre position was carefully varied in the X and Y directions while the Z position was varied more rapidly. The XYZ positioner which housed the launch lens was also carefully moved continuously in order to maximise the fluorescence signal. During this optimisation process the position of the fibre end was observed continuously using a long focal length microscope, checking to ensure it never came in contact with the mirror face.

Once the fluorescence signal was maximised, the fibre and mirror mount assembly on the output end of the fibre was positioned so that the fibre touched the mirror. The fibre vee groove was not secured on the micropositioner platform. This prevented the fibre from being wound too far and breaking the fibre against the mirror, as the vee groove was simply allowed to slide in the micropositioner platform slot. After this process, the input end of the fibre was moved very gently towards the mirror surface. The fluorescence signal was continually monitored and optimised during this movement of the fibre. Once laser action has been initiated the detected signal increases rapidly possibly by two or three orders of magnitude. The micropositioner is then manipulated very carefully to further increase the signal.

7.3 High power pumping

Pumping a fibre laser with a high power source is the obvious choice when initially testing a fibre laser cavity, due to the high power levels available. A 1 W semiconductor laser diode (detailed in section 4.3.1) was used as the pump source, for testing and characterisation of the laser cavity. The launch optics used for collimation and focusing of the pump laser diode beam have been discussed in detail in section 4.3.3. The following two sections discuss the experimental data recorded for the Tm^{3+}-doped fibre laser with a high power pumping scheme.

7.3.1 Fibre laser oscillation

Laser oscillation was first observed from the doped fibre, using the high power SONY laser as a pump source with the collimation and focusing lenses described earlier (section 4.3.3). A maximum of 29 mW was launched into the fibre with this lens arrangement. The laser cavity was optically aligned, as outlined in the previous section. The experimental laser cavity was setup as shown in figure 7.9.
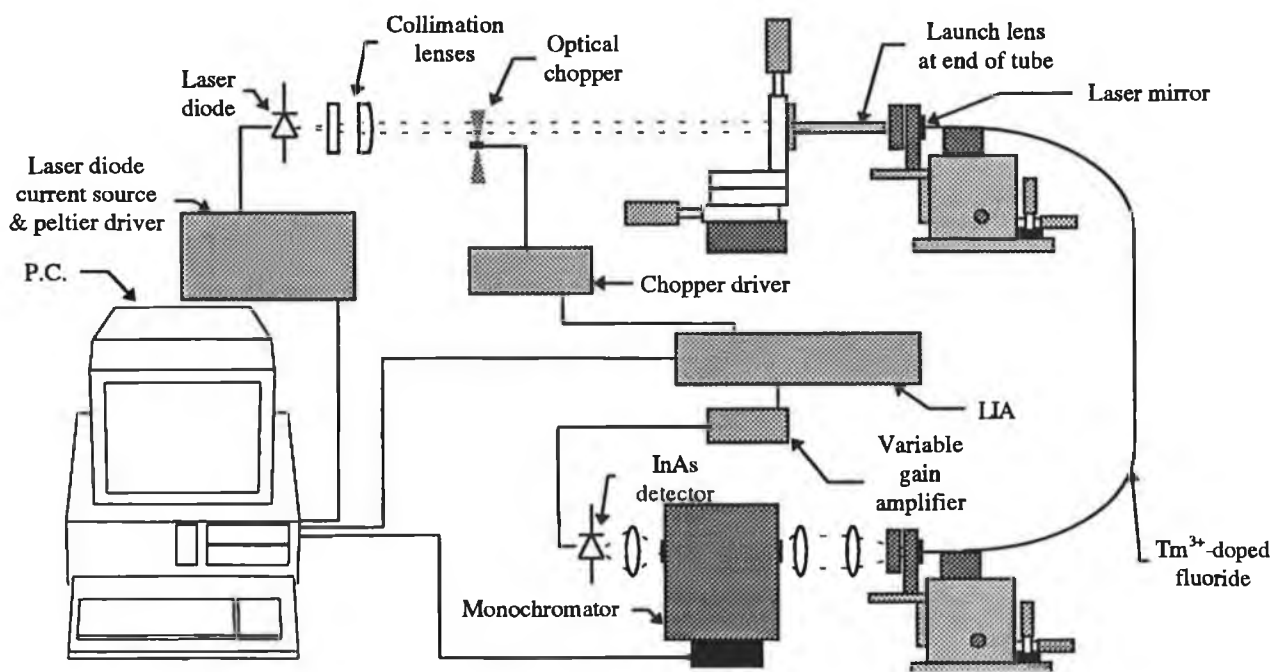
FIGURE 7.9 EXPERIMENTAL LASER CAVITY SETUP

Figure 7.10 displays the first recorded spectral evidence of laser oscillation with this doped fibre.
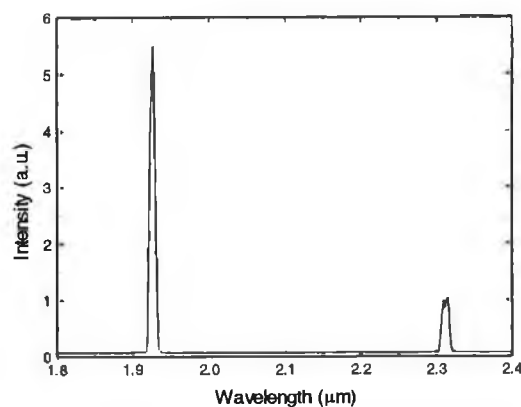
FIGURE 7.10 INITIAL LASER SPECTRUM FROM UN-OPTIMISED SETUP

Dual-laser emission was observed due to a combination of the radiative decay routes for the Tm^{3+} ion (Fig. 7.11) and the characteristics of the laser mirrors.
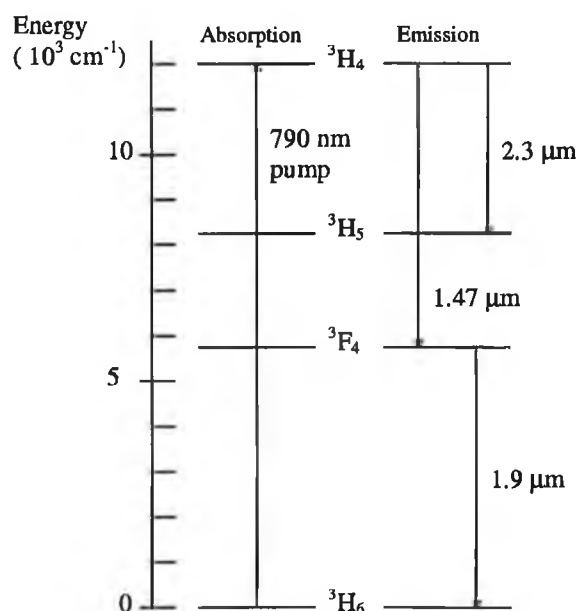
FIGURE 7.11 ENERGY LEVELS FOR Tm^{3+} IN A ZIRCONIUM FLUORIDE HOST

After the Tm^{3+} ion has emitted a laser photon at 2.31 μm ($^3H_4 \rightarrow {}^3H_5$), the excited electrons then relaxed non-radiatively from $^3H_5$ to $^3F_4$. The level $^3F_4$ corresponds to the upper laser level of the 1.92 μm emission line. Therefore, an electron raised to the upper level $^3H_4$ may emit a photon at 2.31 μm, then relax to the next level and subsequently emit a photon at 1.92 μm.

The characteristics of the laser mirrors selected in section 4.5, promote the gain of photons at 1.92 μm and 2.31 μm in the fibre laser cavity, thereby enabling laser action at both 1.92 μm and 2.31 μm. The photons at 1.92 μm and 2.31μm experienced gain due to the high reflectivities of the laser mirrors at both the these wavelengths.

The laser cavity was optimised by setting the monochromator to 2.31 μm, and then adjusting the optical alignment of the various components, while continually monitoring the signal from the lock-in amplifier.

Having optimised the laser cavity, a number of spectra were recorded for increasing optical pump powers. Table 7.1 displays the pump power launched into the doped-fibre, together with the measured signal of the laser emission at 1.92 μm and 2.31 μm, respectively (the graph labels refer to the graph on the following page).

GRAPH LABEL FIGURE 7.12	LAUNCHED PUMP POWER (mW)	LASER INTENSITY @ 1.92 μm (a.u.)	LASER INTENSITY @ 2.31 μm (a.u.)
A	0	0	0
B	3.4	0	0.023
C	5.4	0	0.065
D	8.1	0	0.217
E	11.6	0	0.486
F	14.5	0	0.615
G	17.4	0.2	0.801
H	19.8	1.138	0.908
I	20.9	3.917	1.040
J	23.7	5.841	1.084
K	25.6	7.565	1.343
L	29.8	9.313	1.357

TABLE 7.1 PUMP POWER AND RELATIVE OUTPUT POWERS FROM BOTH LASER EMISSIONS

Figure 7.12 displays the laser output spectra as the pump power was increased. The graph labels refer to table 7.1.
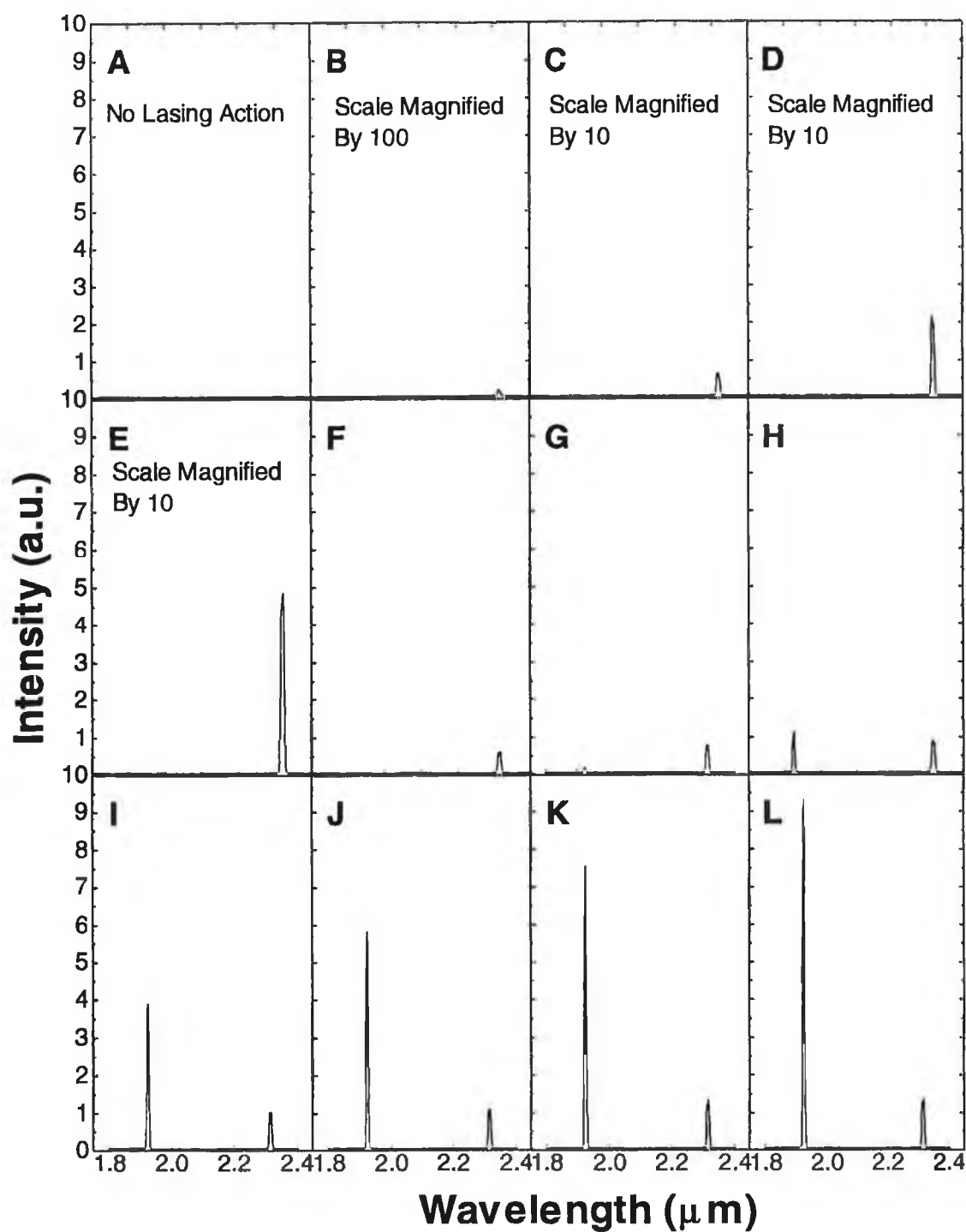
FIGURE 7.12 PUMP POWER VS LASER SPECTRAL OUTPUT FROM OPTIMISED SETUP

7.3.2 Fibre laser characterisation

A number of criteria are used to determine the characteristics of a fibre laser. These include the threshold power, the output power and the slope efficiency of the fibre laser. The threshold value is the launched pump power value at which the fibre laser begins to lase. The slope efficiency of a fibre laser is the efficiency with which the pump power above threshold is converted into laser output power (i.e. if the launched optical power is 10 mW, threshold occurs for a launched power of 4 mW and the output power is 2 mW, then the slope efficiency is 33.3 %).

As no optical power meter was available to measure the optical output power from the fibre laser at either 1.92 μm or 2.31 μm, the power was calculated from the detected signal from the InAs detector and amplifier. As outlined in section 4.6, EG&G supplied the responsivity values for the InAs detector at 1.92 μm and 2.31 μm. The EG&G variable gain amplifier had 10^3, 10^4 and 10^5 gain settings and was calibrated to give exact current to voltage conversion matching the gain settings. Figure 7.13 displays the output power from the fibre laser at both 1.92 μm and 2.31 μm versus the launched pump power, where the output power from the fibre laser was calculated from the detector as outlined above. The monochromator was used to select either the 1.92 μm or the 2.31 μm laser line.
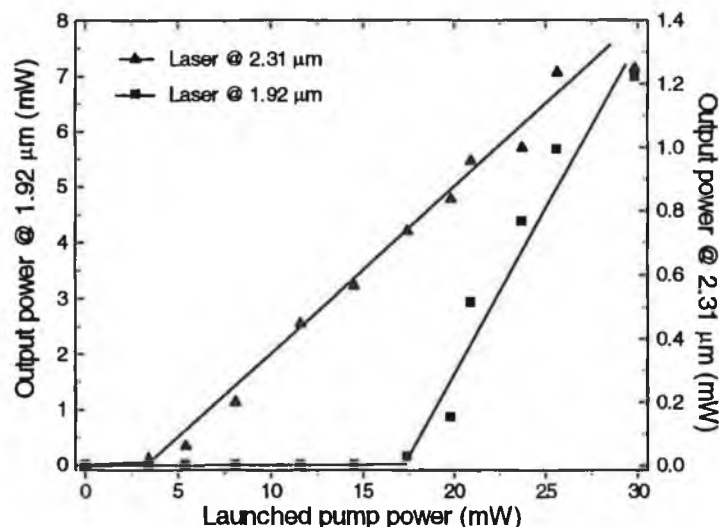
FIGURE 7.13 OUTPUT POWER FROM FIBRE LASER @ 1.92 μm AND 2.31 μm

The irregularity of the data points in figure 7.13, was not a characteristic of the fibre laser, but was due to the irregular coupling (see figure 4.15) of the pump laser into the doped-fibre as the pump power was increased. Table 7.2 displays the calculated optical output power from the fibre laser at both 1.92 μm and 2.31 μm.

LAUNCHED PUMP POWER (mW)	LASER OUTPUT POWER (mW) @ 1.92 μm	LASER OUTPUT POWER (mW) @ 2.31 μm
0	0	0
3.4	0	0.0212
5.4	0	0.060
8.1	0	0.200
11.6	0	0.447
14.5	0	0.566
17.4	0.15	0.737
19.8	0.8535	0.835
20.9	2.93775	0.957
23.7	4.38075	0.997
25.6	5.67375	1.236
29.8	6.98475	1.248

TABLE 7.2 CALCULATED OUTPUT POWERS FROM BOTH LASERS

The threshold for the laser emission at 1.92 μm and 2.31 μm was measured to be 15.8 mW and 3.3 mW, respectively. With a maximum launched pump power of 29.8 mW, a maximum output power of 6.98 mW (see table 7.2) from the 1.92 μm laser emission and 1.25 mW from the 2.31 μm laser emission was measured. Slope efficiencies of 58.7 % for the 1.92 μm laser and 5.1 % for the 2.31 μm laser were calculated from the data above.

The photon conversion efficiency is also used to characterise a fibre laser. The photon conversion efficiency is defined as :

$$Photon\ conversion\ efficiency = \frac{slope\ efficiency\ of\ transition}{maximum\ efficiency\ for\ transition} \qquad Eqn.\ 7.\ 10$$

where the maximum efficiency for a transition is the ratio of energies of the output and input lasing photons. The maximum efficiency is 41.15 % for the $^3F_4 \rightarrow {}^3H_6$ transition (1.92 μm) and 34.2 %. for the $^3H_4 \rightarrow {}^3H_5$ transition (2.31 μm). Therefore, the photon conversion efficiency for the $^3F_4 \rightarrow {}^3H_6$ transition (1.92 μm) is 142.7 % and for the $^3H_4 \rightarrow {}^3H_5$ transition (2.31 μm) is 14.9 %. The possibility of laser operation with a quantum efficiency >1 arises by virtue of a cross-relaxation process. Cross-relaxation is a process in which an ion in an excited state transfers

part of its excitation energy to a neighbouring ion. This process is a well known quenching mechanism for Nd^{3+} ions. Figure 7.14 illustrates how this process may be used to explain a photon conversion efficiency of > 1 for the $^3F_4 \rightarrow {}^3H_6$ transition (1.92 µm).

$^3H_4$

$^3H_5$

$^3F_4$

$^3H_6$

A   B   C
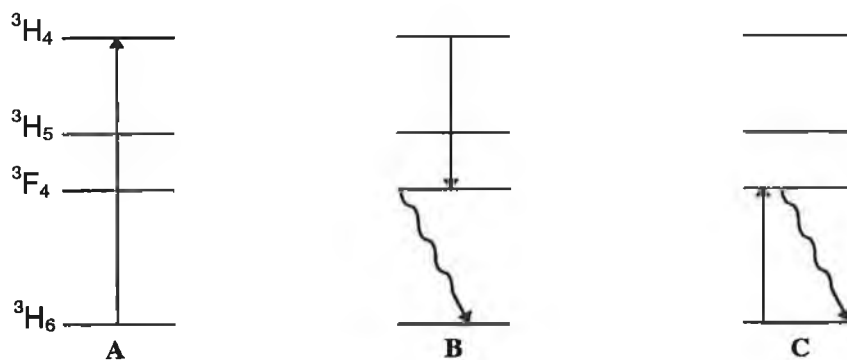
FIGURE 7.14 CROSS-RELAXATION PROCESS

If an ion from the ground state ($^3H_6$) is excited to the $^3H_4$, this excited ion may interact with a nearby ion in the ground state (figure 7.14A). The excited ion in the $^3H_4$ state may transfer part of its energy, in the form of non-radiative decay, to the ion in the ground state (figure 7.14B). The ion in the ground state may absorb this non-radiative energy and become excited to the $^3F_4$ level (figure 7.14C). In this way, one pump photon may excite two photons to a higher energy level ($^3F_4$). This cross-relaxation process in Tm^{3+} has been previously observed by Tropper *et al.* [10], whose work yielded a photon conversion efficiency of ≅120 % at 1.9 µm.

Table 7.3 displays reported characteristics of Tm^{3+}-doped fibre lasers from recent literature. Most of the fibre lasers are made from fluoride glass. The lasers constructed from silica are indicated by an asterix. The results from this work are shown in the highlighted section.

The data reported in this work compare very favorably with other reported Tm^{3+}-doped fibre lasers. Only one paper [11] reports a fibre laser with lower thresholds than achieved in this work, but, the output power and slope efficiency are not reported in this paper.

Laser Output (μm)	Tm Conc. (ppmw)	Core/Clad Diameter (μm)	Length (cm)	N.A.	Pump (nm)	Output Coupler (%R)	Laser Threshold (mW)	Laser Efficiency (%)	Output Power (mW)	Launch Pump (mW)	Ref
1.92, 2.31	2000	11/125	60	0.156	791	45, 97.5	15.8, 3.3	59, 5	7, 1.2	30	*
2.3	1000	15/150	50	0.122	786	50	16	na	na	na	[1]
2.3	1000	15/150	35	0.122	790	98	4	10.0	0.95	17	[12]
2.35	1250	7.2/na	150	0.186	676.4	na	31	3.8	2.2	na	[13]
2.305	740	40/80	86	0.16	791	97	115	18.8	27.0	275	[14]
1.88	1250	7.2/na	150	0.186	676.4	na	50	3.3	1.3	na	[13]
1.942	740	40/80	86	0.16	791	97	115	8.3	13.0	275	[14]
2.0, 1.96	740	40/88	86	0.16	791	99	75	5.3	8.0	225	[14]
1.972	740	40/80	30	0.16	795	99	40	0.3	0.2	100	[15,14]
1.51	1250	7.2/na	177	0.186	647.1	na	6	na	6.0	na	[16]
1.48	1250	7.2/na	150	0.186	676.4	na	40	Poor	0.01	na	[13]
0.82	1250	7.2/na	150	0.186	676.4	na	45	1.6	0.5	na	[13]
0.480	1250	7.2/na	177	0.186	647.1	na	170	na	0.4	500	[16]
0.455	1250	7.2/na	177	0.186	647.1	na	na	na	na	na	[16]
1.9	3000	12/na	na	0.166	790	20	50	32	na	na	[10]
0.480	1000	na	200	0.21	1120	90	46	18	57	200	[17]
2.31	500	na	1000	na	790	50	na	na	0.1	51	[18]
1.97	740	40/80	100	na	791	99	60	<1	2.5	230	[19]
1.90	3000	12/na	22	0.166	810	80	na	36	44	167	[20]
2.038	840	8.6/na	na	0.15	1064	99	60	30	51	230	[21]
1.94	200	na	45	0.2	786	90	4.4	17	1	12	[22]
1.96	830	9/na	27	0.15	797	97	30	13	2.7	na	[23]
1.94, 2.30	1000	7.5/na	150	na	790	99.5, 99.5	3.2, 1.9	na	na	na	[11]
1.475,1.88	1000	7.5/na	270	na	790	43	21.6	43,38	130,115	325	[24]
1.46,1.86	1000	15/na	na	na	790	96,90	na	16,25	49	145	[25]

* silica - not fluoride

TABLE 7.3 SELECTED CHARACTERISTICS OF OTHER PUBLISHED FIBRE LASERS

The dependence of the output power of the fibre laser on the pump wavelength was investigated by temperature tuning the pump wavelength. As stated before, the laser diode current driver controls the temperature of the laser diode peltier cooler. By varying the temperature of the laser diode it is possible to impart a small degree of wavelength tunability to the pump laser diode. Figure 7.15 displays the fibre laser output power dependence on pump wavelength.
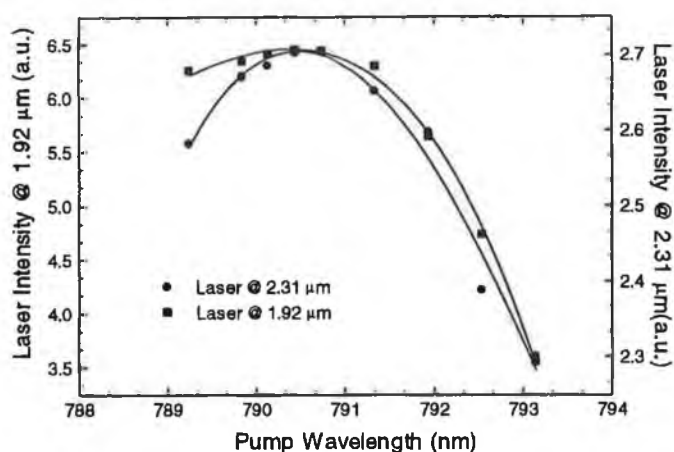

FIGURE 7.15 FIBRE LASER OUTPUT POWER VS PUMP WAVELENGTH

The graph above illustrates that the output power from the fibre laser is highly dependent on the pump wavelength, and that the optimum pump wavelength is 790.5 nm. If the temperature of the laser diode is not controlled, this may cause the output power from the fibre laser to fluctuate considerably (a temperature change of 9 ^{0}C, will change the pump wavelength by 2.7 nm, which will cause the output power of the laser emission at 1.92 μm to vary by up to 50 %).

7.4 Low power pumping

Having observed laser oscillation in the doped fibre with the high power pump laser source, the possibility of achieving laser oscillation with a lower power pump source was investigated. Laser oscillation was achieved at 2.31 μm and 1.92 μm, for a threshold of 3.3 mW and 15.8 mW, respectively with the previous configuration. These results demonstrated that lasing should be possible with a much lower power pump source. Therefore, a doped fibre laser with a low power

pump source would be ideal for sensing applications in areas not covered by commercial laser diodes.

7.4.1 Fibre laser oscillation

The experimental arrangement of the fibre laser with the low power PHILIPS laser diode (output wavelength 785 nm) as the source is as shown in figure 7.9. The SONY laser diode and collimation optics were replaced by the PHILIPS laser diode and MELLES GRIOT lens (as described in section 4.4.3).

Figure 7.16 displays the recorded laser oscillation in the Tm^{3+}-doped fibre with the pump PHILIPS laser diode.
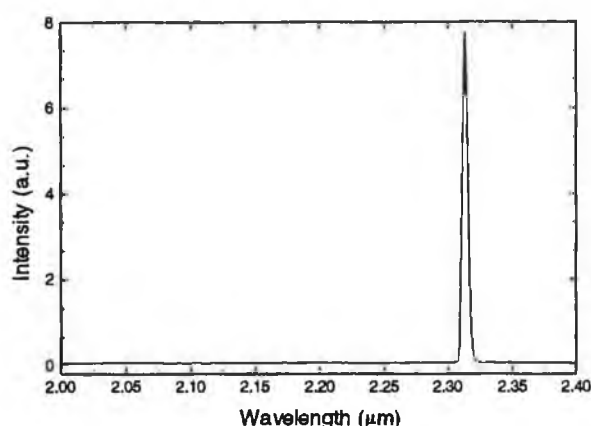

FIGURE 7.16 FIBRE LASER OUTPUT SPECTRUM WITH PHILIPS LASER DIODE

When pumping with the lower power laser no laser oscillation was observed in the 1.9 µm region. This may have been related to the change in wavelength, as the doped-fibre was pumped at 785 nm and not at 790 nm as in the previous configuration. By comparing the pump power necessary to achieve laser oscillation at 1.9 µm with the last configuration, and the power launched with this configuration, enough power was launched into the fibre to achieve oscillation.

7.4.2 Fibre laser characterisation

Having achieved laser oscillation with the lower power pump source, the fibre laser was once again characterised, in terms of output power, threshold and slope efficiency. The threshold for lasing at 2.31 µm was measured to be 6.5 mW. A maximum output power of 1.8 mW was achieved for a launched pump power of

22.5 mW. The laser efficiency curve displayed an unusual dual slope feature, as displayed in figure 7.17.
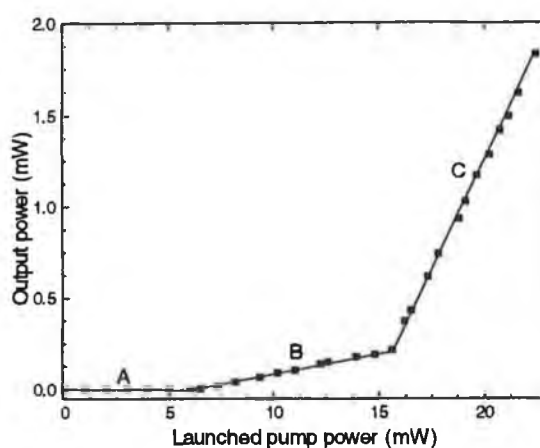
FIGURE 7.17 OUTPUT POWER FROM FIBRE LASER @ 2.31 μm

In region A the fibre laser has not reached threshold. In region B having reached threshold, the slope efficiency was 2.4 % from 6.5 mW to 15.6 mW. Region C displayed an increased slope efficiency of 23.1 % from 15.6 mW to 22.5 mW. The higher slope efficiency corresponded to a photon conversion efficiency of 67.5 %. The reason for the change in slope efficiency from region B to region C is unknown, but, the results were not due to experimental error as they were reproduced a number of times.

LAUNCHED PUMP POWER (mW)	LASER OUTPUT POWER (mW) @ 2.31 μm	LAUNCHED PUMP POWER (mW)	LASER OUTPUT POWER (mW) @ 2.31 μm
0	0	13.91	0.177
1	0	14.8	0.192
2	0	15.6	0.218
3	0	16.2	0.371
4	0	165	0.433
5	0	17.32	0.615
6	0	17.8	0.741
6.5	0.005	18.8	0.934
7.32	0.019	19.1	1.027
8.16	0.041	19.64	1.171
9.34	0.068	20.21	1.283
10.18	0.091	20.71	1.420
11.01	0.105	21.14	1.498
12.21	0.139	21.61	1.621
12.58	0.151	22.45	1.831

TABLE 7.4 CALCULATED OUTPUT POWER FROM FIBRE LASER

7.5 Conclusion

The difficulties involved with the alignment and positioning of a fibre laser are dealt with in detail in this chapter. Results from two fibre lasers are presented. The first laser is optically pumped with a high power laser source. With the high power pumping scheme a dual laser emission was observed (1.92 μm and 2.31 μm) from the Tm^{3+}-doped fibre. Both laser emissions were found to have a high conversion efficiencies, and therefore, would be very useful where dual wavelength high output power laser sources are required.

The second laser was pumped by a much lower power laser. Only one laser emission was observed. This may have been due to the small difference in pump wavelengths between the pump sources. Again this fibre laser was found to have a very high conversion efficiency, compared with current research in this area. This is the first reported Tm^{3+}-doped fluoride fibre laser operating with a low power semiconductor diode laser as a pump source.

The integration of the fibre laser with a low power pump source, into an optical sensor for detection of hydrocarbon gases is discussed in the following chapter.

References :

1. Esterowitz L., Allen R., Aggarwal I. : **'Pulsed laser emission at 2.3 µm in a thulium-doped fluorozirconate fibre'**, Electronics Letters, 1988, Vol. 24, No. 17, pp. 1104

2. Reekie L., Mears R.J., Poole S.B., Payne D.N. : **'Tunable single-mode fiber lasers'**, Journal of Lightwave Technology, 1986, Vol. LT-4, No. 7, pp. 956-960

3. Shimizu M., Suda H., Horiguchi M. : **'High-efficiency Nd-doped fibre lasers using direct-coated dielectric mirrors'**, Electronics Letters, 1987, Vol. 23, No. 15, pp. 768-769

4. Morkel P.R., Cowle G.J., Payne D.N. : **'Travelling-wave erbium fibre ring laser with 60 kHz linewidth'**, Electronics Letters, 1990, Vol. 26, No. 10, pp. 632-634

5. Stone J., Marcuse D. : **'Ultrahigh finesse fiber Fabry-Perot interferometers'**, Journal of Lightwave Technology, 1986, Vol. LT-4, No. 4, pp. 382-385

6. Marcuse D., Stone J. : **'Coupling efficiency of front surface and multilayer mirrors as fiber end reflectors'**, Journal of Lightwave Technology, 1986, Vol. LT-4, No. 4, pp. 377-381

7. Marcuse D. : **'Loss analysis of single mode fiber splices'**, Bell Syst. Tech. J., 1977, Vol. 56, pp. 703-718

8. Geckeler S. : **'Optical Fiber Transmission Systems'**, (Translated from German), Artech House, Norwood, MA, 1987

9. Gloge D. : **'Weakly guiding fibers'**, Applied Optics, 1971, Vol. 10, pp. 2252-2258

10. Tropper A., Smart R., Perry I., Hanna D., Lincoln J., Brocklesby B. : **'Thulium-doped silica fiber lasers'**, Fiber Laser Sources and Amplifiers II Conference, 1990, Vol. 1373, pp. 152-157

11. Percival R.M., Szebesta D., Davey S.T. : **'Highly efficient and tunable operation of two colour Tm-doped fluoride fibre laser'**, Electronics Letters, 1992, Vol. 28, No. 7, pp. 671-673

12. Allen R., Esterowitz L. : **'CW diode pumped 2.3 μm fiber laser'**, Applied Physics Letters, 1989, Vol. 55, No. 8, pp. 721-722

13. Allain J.Y., Monerie M., Poignant H. : **'Tunable CW lasing around 0.82, 1.48, 1.88 and 2.35 μm in thulium-doped fluorozirconate fibre'**, Electronics Letters, 1989, Vol. 25, No. 24, pp. 1660-1662

14. Smart R., Carter J., Tropper A., Hanna D. : **'Fluoride fibre lasers'**, Fiber Laser Sources and Amplifiers II Conference, 1990, Vol. 1373, pp. 158-165

15. Carter J.N., Smart R.G., Hanna D.C., Tropper A.C. : **'CW diode-pumped operation of 1.97 μm thulium-doped fluorozirconate fibre laser'**, Electronics Letters, 1990, Vol. 26, No. 9, pp. 599-601

16. Allain J.Y., Monerie M., Poignant H. : **'Blue upconversion fluorozirconate fibre laser'**, Electronics Letters, 1990, Vol. 26, No. 3, pp. 166-168

17. Grubb S.G., Bennett K.W., Cannon R.S., Humer W.F. : **'CW room-temperature blue upconversion fibre laser'**, Electronics Letters, 1992, Vol. 28, No. 13, pp. 1243-1244

18. Percival R.M., Carter S.F., Szebesta D., Davey S.T., Stallard W.A. : **'Thulium-doped monomode fluoride fibre laser broadly tunable from 2.25 to 2.5 μm'**, Electronics Letters, 1991, Vol. 27, No. 21, pp. 1912-1913

19. Smart R.G., Carter J.N., Tropper A.C., Hanna D.C. : **'Continuous-wave oscillation of Tm^{3+}-doped fluorozirconate fibre lasers at around 1.47 μm, 1.9 μm and 2.3 μm when pumped at 790 nm'**, Optics Communications, 1991, Vol. 82, No. 5,6, pp. 563-570

20. Hanna D.C., Percival R.M., Smart R.G., Tropper A.C. : **'Efficient and tunable operation of a Tm-doped fibre laser'**, Optics Communications, 1990, Vol. 75, No. 3,4, pp. 283-286

21. Hanna D.C., McCarthy M.J., Perry I.R., Suni P.J. : **'Efficient high-power continuous-wave operation of monomode Tm-doped fibre laser at 2 μm**

pumped by Nd:YAG laser at 1.064 μm', Electronics Letters, 1989, Vol. 25, No. 20, pp. 1365-1366

22. Barnes W.L., Townsend J.E. : **'Highly tunable and efficient diode pumped operation of Tm^{3+} doped fibre lasers'**, Electronics Letters, 1990, Vol. 26, No. 11, pp. 746-747

23. Hanna D.C., Jauncey I.M, Percival R.M., Perry I.R., Smart R.G., Suni P.J., Townsend J.E., Tropper A.C. : **'Continuous-wave oscillation of a monomode thulium-doped fibre laser'**, Electronics Letters, 1988, Vol. 24, No. 19, pp. 1222-1223

24. Percival R.M., Szebesta D., Davey S.T. : **'Highly efficient CW cascade operation of 1.47 and 1.82 μm transitions in Tm-doped fluoride fibre laser'**, Electronics Letters, 1992, Vol. 28, No. 20, pp. 1866-1868

25. Allen R., Esterowitz L. Aggarwal I. : **'An efficient 1.46 μm thulium fiber laser via a cascade process'**, IEEE Journal of Quantum Electronics, 1993, Vol. 29, No. 2, pp. 303-306

methane is chosen as a representative species of these gases, as it is perhaps the most frequently encountered species.

8.2.1 Structure of methane

Methane is a highly symmetric, non linear, tetrahedral shaped, polyatomic molecule. It consists of a centre atom of carbon bonded to four atoms of hydrogen. The angle between any two bonds is 109.6° and the bond length between the carbon atom and each of the hydrogen atoms is 1.094 Å [4] as shown in figure 8.1.


H = Hydrogen atom
C = Carbon atom
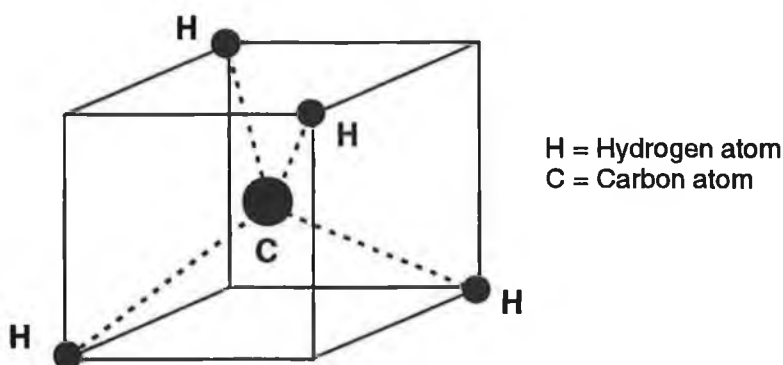
FIGURE 8.1 STRUCTURE OF THE METHANE MOLECULE (CH₄)

The energy of any molecule is quantised. Only certain discrete energy levels are allowed. This energy is not wholly governed by its electronic configuration, as was the case with singular atoms, as discussed in chapter 2 and 3. Nuclear motion of the molecule gives rise to two other forms of energy levels. These are *vibrational* and *rotational* energy levels. Therefore, the total energy of the molecule is the sum of the electronic, vibrational and rotational energies [5]. The energy associated with each transition type varies greatly. The energies associated with electronic, vibrational and rotational transitions correspond to ultra-violet/visible, the infra-red and the far infra-red/micro-wave regions of the electromagnetic spectrum, respectively. Therefore, if infra-red radiation is absorbed there will not be sufficient energy absorbed for electronic transitions and only vibrational and rotational transitions will occur [5].

Molecules vibrate upon collision with other like molecules. The number of ways that each molecule can vibrate is referred to as the number of *modes of vibration*. In any one 'normal' or 'fundamental' mode all the nuclei vibrate in phase

with the same frequency. Each of the N atoms in a non-linear polyatomic molecule has three degrees of freedom corresponding to motion along the three Cartesian co-ordinates. The whole molecule has therefore 3N degrees of freedom. However, three of these correspond to translation of the molecule along the three axes. Three others correspond to an overall rotation of the molecule about that axis. This leaves 3N-6 normal modes of vibration [5].

Methane has five atoms and therefore should have nine normal modes of vibration. However, due to the high symmetry of the molecule some of the modes have the same energy resulting in only four discrete 'normal' or 'fundamental' vibrational modes. These are [6]

v_1 - A symmetric C-H stretch at 3657 cm^{-1} or 2.734 μm

v_2 - A doubly degenerate stretch at 1533 cm^{-1} or 6.523 μm

v_3 - A triply degenerate asymmetric C-H stretch at 3019 cm^{-1} or 3.312 μm

v_4 - A triply degenerate asymmetric H-C-H bend at 1311 cm^{-1} or 7.628 μm

For non-linear, polyatomic molecules the selection rule governing transitions between levels is

$$\Delta v = \pm 1, \pm 2, \pm 3 \ etc.$$

<div align="right">*Eqn. 8. 1*</div>

The transition from the ground vibrational state ($v = 0$) to the first vibrational energy level ($v = 1$) is called the *fundamental transition*. Transitions from the ground vibrational state to higher vibrational energy levels ($v = 2, 3, ...$) are called *overtones*. *Combinations* occur when the quantum numbers of two vibrations change simultaneously. In this case, coupling between particular modes of vibration occurs, resulting in a transition at a well defined frequency. The combinations that can occur are strictly governed by the symmetry of the molecule.

Figure 8.2 displays the transmission spectrum of methane at the v_2+v_3 , v_3+v_4 and v_1+v_4 [6] overtones in the 2.203 μm, 2.304 μm and 2.368 μm spectral regions, respectively. This spectrum was recorded using a Bomem DA8 fourier transform, infra-red spectrometer (FTIR), with a liquid nitrogen cooled Indium Antimonide (InSb) detector. The spectrum was recorded at 1 cm^{-1} resolution, with a 100 % methane concentration, over a 0.1 metre pathlength and at atmospheric pressure. The wavelength of the fibre laser (2.311 μm) pumped by the low-power PHILIPS laser

diode is shown together with the methane transmission spectrum, for reasons of clarity.
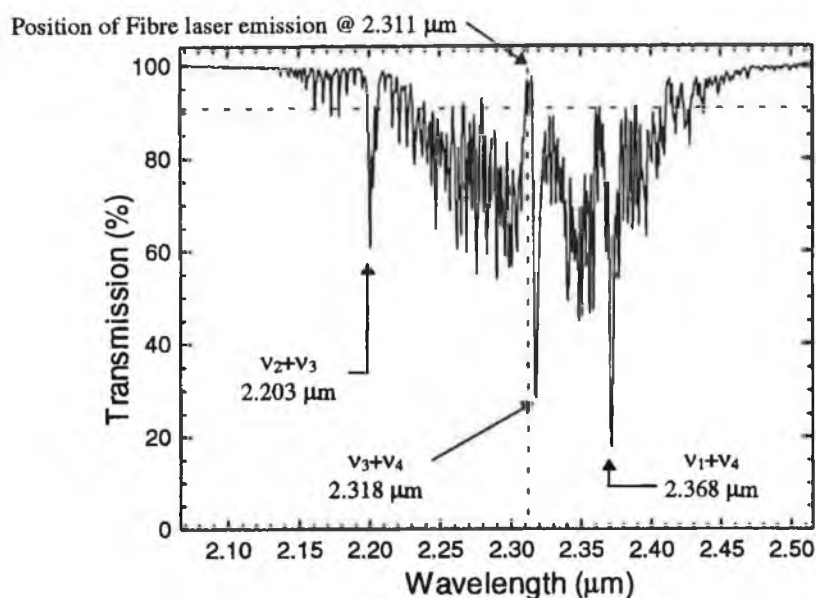
FIGURE 8.2 TRANSMISSION SPECTRUM OF THE METHANE MOLECULE (CH_4)

Table 8.1 displays selected absorption characteristics of the methane molecule. These data are taken from Ref. 6. Table 8.1 displays the wavelengths of the strongest absorption lines of methane, and the wavelengths of interest in this work.

MODE	WAVENUMBER (cm^{-1})	WAVELENGTH (μm)	NO. OF LINES	TOTAL LINE INTENSITY ($cm^{-2} atm^{-1}$) @ 296K
v_1	3657	2.734	-	-
v_2	1533	6.523	810	1.5
v_3	3019	3.312	1903	291
v_4	1311	7.628	1420	135.7
v_1+v_4	4223	2.368	151	5.7
v_3+v_4	4340	2.304	958	11.0
v_2+v_3	4540	2.203	388	1.7

TABLE 8.1 SELECTED METHANE OVERTONES AND THEIR CORRESPONDING INTENSITIES

8.3 Detection of methane

Reports of detection methods for gases, in particular methane gas, using fibre optic configurations have increased rapidly in recent years [7,8,9]. The motivation for this has been the obvious need for sensors that can remotely detect

methane safely and accurately, especially in hazardous or explosive environments such as coal mines or landfill sites. Methane (CH_4) is highly flammable gas if its concentration is between 5 % and 15 % by volume in air. These two percentage limits are defined as the *Lower Explosion Limit* (*LEL*) and the *Upper Explosion Limit* (*UEL*), respectively. Above the *UEL*, there is not enough oxygen to support combustion. Industrial standards require sensors to be capable of sensing 25 % *LEL* (i.e. 1.25 % CH_4 in air) accurately [10].

A number of fibre optic methane sensors has been developed since Chan *et al.* first published a paper which described a system with a detection limit of 2000 ppm, based on absorption at 1.33 μm (v_2+2v_3), over a 2 km fibre length [11].

The work reported here is based on the detection of methane in the 2.3 μm region, where the absorption at 2.31 μm is approximately three times stronger than the methane absorption band at 1.66 μm, were the majority of methane optical sensors operate.

The transmission spectrum of methane displayed in figure 8.2, also illustrates the three main absorption lines in the 2.2 - 2.4 μm region. The emission wavelength of the fibre laser at 2.311 μm is also displayed. Due to the sharpness of the absorption bands of methane, the wavelength of the laser will have to be matched exactly to a particular absorption band. This requirement of exactly matching the laser emission wavelength to the peak absorption band poses a problem, as will be discussed later.

8.4 Experimental system

The use of a fibre laser as a source for an optical methane sensor was experimentally investigated using the system shown in figure 8.3. By passing the collimated fibre laser beam through a cell containing methane gas, the intensity of the laser beam will be reduced, due to absorption by the methane gas present. Therefore, the system may be calibrated by detecting the change in intensity of the laser beam when the concentration of methane gas in the cell is known.
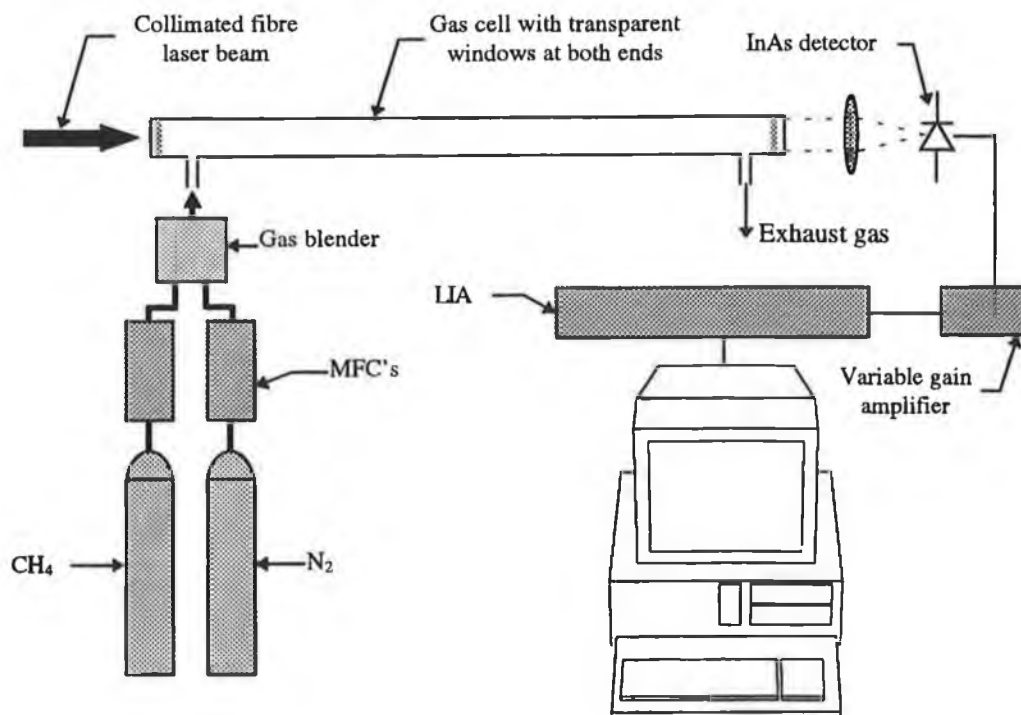
FIGURE 8.3 EXPERIMENTAL CALIBRATION SYSTEM FOR DETECTION OF METHANE GAS

The collimated laser output was passed through a 0.7 metre gas cell and focused on to a InAs detector, as shown above. Absorption was measured for selected mixtures of methane and nitrogen which were flowed through the gas cell using mass flow controllers (MFC's). Nitrogen was used as a reference gas as it is non-absorbing in the near-IR. The signal from the LIA was digitised with an A/D card (Bytronics) and passed to the computer for display and storage. Software was written in Turbo C to store the data and plot the data versus time. The program is given in Appendix H.

8.5 Results

The transmitted signal I was recorded for each gas concentration and an effective absorbance

$$Effective\ Absorbance\ =\ \log_{10}\frac{I_0}{I}$$

Eqn. 8. 2

was calculated, where I_0 was the signal detected for 0 % methane (i.e. 100 % nitrogen). The effective absorbance values are plotted for 20 % LEL increments in figure 8.4.
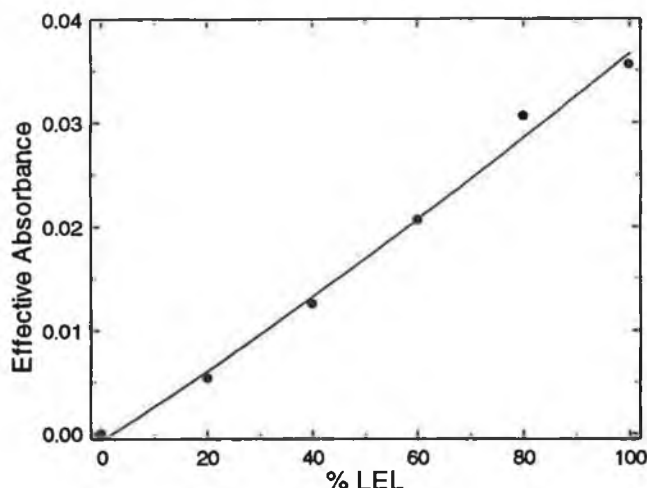

FIGURE 8.4 SENSOR RESPONSE CURVE FOR METHANE GAS

From the data displayed in figure 8.4, the minimum detectable methane gas concentration is $\cong$ 3 % LEL or alternatively 0.15 % (1500 ppm) methane in air. The detection limit is often expressed as the product of the minimum detectable gas concentration and the distance over which the measurement was made (units of ppm metres). This unoptimised sensor configuration was capable of detecting a methane (CH_4) concentration of 1050 ppm metres. This performance can be improved considerably by reference compensation which would serve to remove the laser output power instability and, more importantly, by tuning the laser to a wavelength of stronger absorption. The laser output wavelength in the present set-up does not correspond to a strong methane absorption peak (see figure 8.2), but, by increasing the wavelength by 6-7 nm, the absorption can be increased by a factor of 12. Thulium has broad fluorescence bands and has been shown to be easily tuned by a number of groups [3,12].

This un-optimised optical sensor with a detection limit of 0.15 % methane in air, exhibits a detection limit 8.3 times better than the detection limit (1.25 % methane in air) required by industry.

Figure 8.5 shows the repeatable real-time response when alternate concentrations of 100 % nitrogen and 100 % LEL methane were passed through the gas cell.
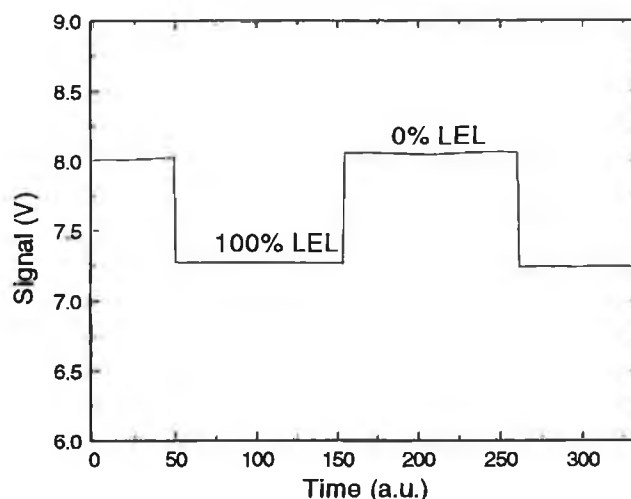
FIGURE 8.5 REAL-TIME REPEATABILITY OF METHANE GAS SENSOR

A slight drift is obvious in the graph displayed above. This may be due to the location of the emission wavelength in a spectral region of rapidly changing absorption (refer to Fig. 8.2). Consequently, a small variation in the fibre laser wavelength caused a large change in the detected signal.

8.6 Conclusion

A hydrocarbon gas sensor using a 2.31 µm CW thulium-doped fibre laser pumped by a low power laser diode, has been demonstrated for the first time. This device has been shown to have important potential for hydrocarbon gas sensing. A limit of detection of approximately 1000 ppm metres has also been demonstrated. Improvements in this sensor configuration, by incorporating tuning and referencing, will lead to a significant reduction in the detection limits. Other configurations have been identified (chapter 9) which are of a simpler design and lend themselves to miniaturisation.

References :

1. McCabe S., MacCraith B.D. : **'Novel mid-infrared LED as a source for optical fibre gas sensing'**, Electronics Letters, 1993, Vol. 29, No. 19, pp. 1719-1721

2. Barnes W.L., Dakin J.P., Edwards H.O., Reekie L., Townsend J.E., Murray S., Pinchbeck D. : **'Tunable fibre laser source for methane detection at 1.68 μm'**, Proc. SPIE, 1992, Vol. 1796, pp. 110-114

3. Percival R.M., Szebesta D., Davey S.T. : **'Highly efficient and tunable operation of two colour Tm-doped fluoride fibre laser'**, Electronics Letters, 1992, Vol. 28, No. 7, pp. 671-673

4. Bransden B.H., Joachain C.J. : **'Physics of Atoms and Molecules'**, Longman Scientific & Technical, England, 1990, Chapter 9

5. Wheatley P.J. : **'The Determination of Molecular Structure'**, Dover Publications, New York, 1981

6. Crossley S.D., Norris J.O.W. : **'OSCA : Review of Principles and Devices for Absorption-Based Optical Gas Sensing'**, OSCA Contract 95, 1992, Section 5.3.11

7. Dubaniewicz Jnr. T.H., Chilton J.E. : **'Remote fiber-optic methane monitor'**, United States Department of the Interior & Bureau of Mines, 1991, Report of Investigations 9407

8. Zientkiewicz J.K. : **'Self referenced fiber optic methane detection system'**, Proc. SPIE, 1988, Vol. 992, pp. 182-187

9. Alarcon M.C., Ito H., Inaba H. : **'All-optical remote sensing of city gas through CH_4 gas absorption employing a low-loss optical fiber link and an InGaAsP light-emitting diode in the near-infrared region'**, Applied Physics B, 1987, Vol. 43, pp. 79-83

10. European Standard, EN 50055, **'Electrical Apparatus for the Detection and Measurement of Combustible Gases'**, 1991

11. Chan K., Ito H., Inaba H. : **'Optical remote monitoring of CH₄ gas using low-loss optical fiber link and InGaAsP light-emitting diode in 1.33 μm region'**, Applied Physics Letters, 1983, Vol. 43, No. 7, pp. 634-636

12. Hanna D.C., Percival R.M., Smart R.G., Tropper A.C. : **'Efficient and tunable operation of Tm-doped fibre laser'**, Optics Communications, 1990, Vol. 75, No. 3,4, pp. 283-286

Chapter 9

Conclusions and future work

The work presented in this thesis described the development of a thulium-doped fluoride optical fibre laser, together with its application as a novel source for optical sensing of hydrocarbon gases, specifically methane.

The concept of fibre lasers for optical sensing was introduced, together with the advantages offered by this type of optical source over conventional incandescent sources and LED's.

The structure and spectroscopy of rare-earth doped fibres was reviewed, including the energy levels, absorption, fluorescence and fluorescence lifetimes of the rare-earths. Specifically, thulium in a fluoride glass host was treated in some detail, including an experimental spectroscopic characterisation of the element.

A number of criteria determine the operational characteristics of a fibre laser; these include the transmission properties of the doped fibre, the amount of optical power launched into the fibre and the transmission properties of both the input and output laser mirrors, each of these criteria was fully evaluated. Mathematical models were used to assist in determining the optimum properties, of the optical launch lens arrangement and the transmission of the laser mirrors.

Two fibre laser arrangements were demonstrated. The first laser pumped by a high power laser exhibited two laser emissions. Each of these emissions had high slope efficiencies and consequently a high output power. This dual emission laser had among the lowest thresholds and highest slope efficiencies reported to date for this type of fibre laser. This type of dual emission laser would be beneficial where two high power laser emission lines are required for optical sensors which operate by using differential absorption techniques. The second fibre laser was optically pumped by an inexpensive low power (40 mW) laser diode. This laser had one laser emission line, which displayed and a low lasing threshold of 6.5 mW, a high slope efficiency of 23.1 %, and an fibre laser output power of 1.8 mW. The sensing

of hydrocarbon gas with a 2.31 µm CW thulium-doped fibre laser pumped by a low power, low-cost laser diode was demonstrated for the first time. This optical gas sensor was shown to be capable of detecting 1000 ppm metres of methane, with an unoptimised system.

This type of fibre laser is ideal for optical sensors as it is compact, requires very little electronic control circuitry and may be incorporated easily into a portable sensor. Other advantages include a laser emission at 2.3 µm which is of interest for industrial and environmental sensing, where fibre compatible sources are not available.

A number of possible improvements would help improve the sensors performance. These include reference compensation of any laser instability and more importantly, imparting tunability to the fibre laser. Tunability, would allow selective tuning of the fibre laser output wavelength to the strongest absorption line of a particular hydrocarbon gas. Furthermore, the cavity design shown in figure 9.1, would allow for a more flexible alignment of the fibre laser cavity components, while also reducing the number of expensive components.
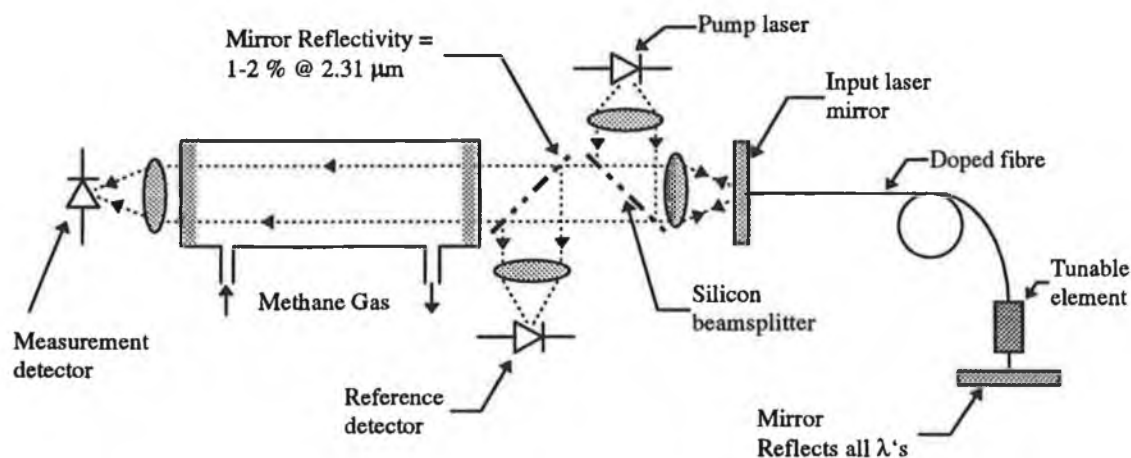

FIGURE 9.1 PROPOSED IMPROVEMENT IN THE FIBRE LASER CAVITY AND SENSOR DESIGN

The arrangement shown above would allow for miniaturisation, tunability, a reduction in the number of expensive components and reference compensation.

The fluorescence emission from a Tm^{3+}-doped fluoride fibre pumped with a low-power, low-cost laser diode was also shown to function as a useful source for water sensing. This type of source for optical sensing purposes offers a number of

advantages over conventional incandescent and LED sources, including a stable output spectrum, reasonable output power and an intrinsic reference signal. This approach could be extended to other relevant analytes by tailoring glass structures and incorporating appropriate dopant ions.

List of Publications & Conference Presentations

ORAL PRESENTATIONS

i)   **'Water detection using fluorescent thulium-doped fibre pumped by low-cost semiconductor laser'.** 10th Optical Fibre Sensors Conference, Glasgow, 11th -13th October, 1994

REFEREED PUBLICATIONS

i)   McAleavey F.J., MacCraith B.D. : **'Efficient diode pumped Tm^{3+}-doped fluoride fibre laser for hydrocarbon gas sensing'.** Electronics Letters, 1995, Vol. 31, No. 10, pp. 800-802

ii)   McAleavey F.J., MacCraith B.D. : **'Diode-pumped thulium-doped zirconium fluoride fibre as a fluorescent source for water sensing'.** Electronics Letters, 1995, Vol. 31, No. 16, pp. 1379-1380

CONFERENCE PUBLICATIONS

i)   MacCraith B.D., McAleavey F.J. : **'Water detection using fluorescent thulium-doped fibre pumped by low-cost semiconductor laser'.** SPIE Proceedings, Glasgow, Vol. 2360, Tenth International Conference on Optical Fibre Sensors, 1994, pp. 90-93.

APPENDIX A

## ABSORPTION SPECTRA FOR RARE-EARTH IONS IN A ZBLANP GLASS

A.1
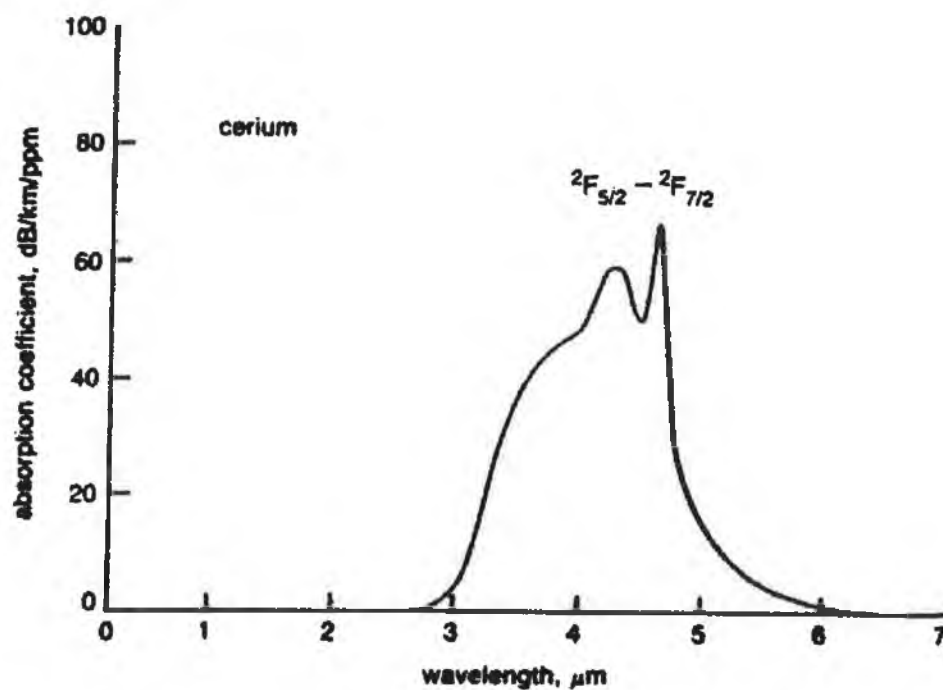
FIGURE A.1 THE ABSORPTION SPECTRUM OF Ce^{3+} IN A ZBLANP GLASS

A.2
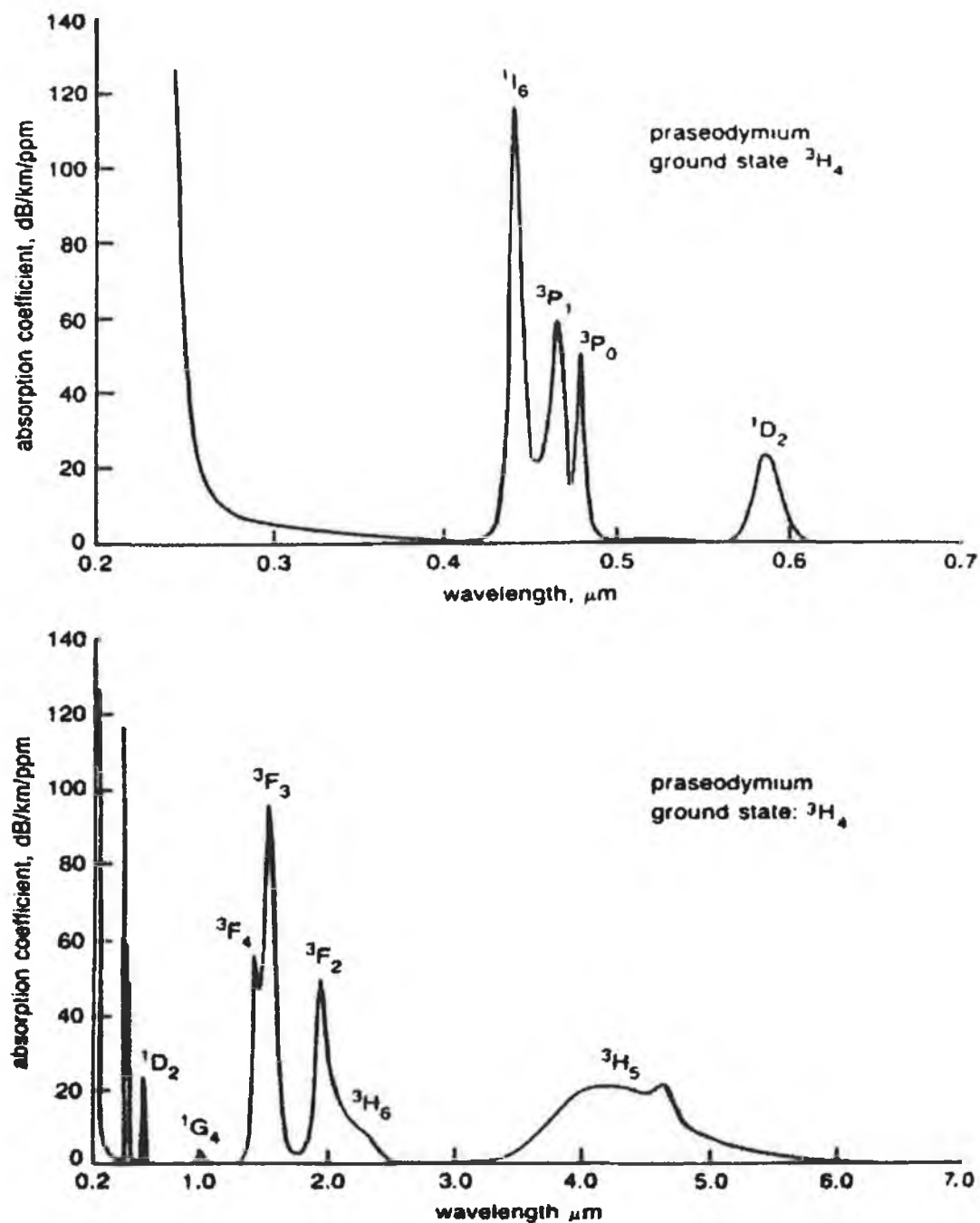
FIGURE A.2 THE ABSORPTION SPECTRUM OF Pr^{3+} IN A ZBLANP GLASS

A.3
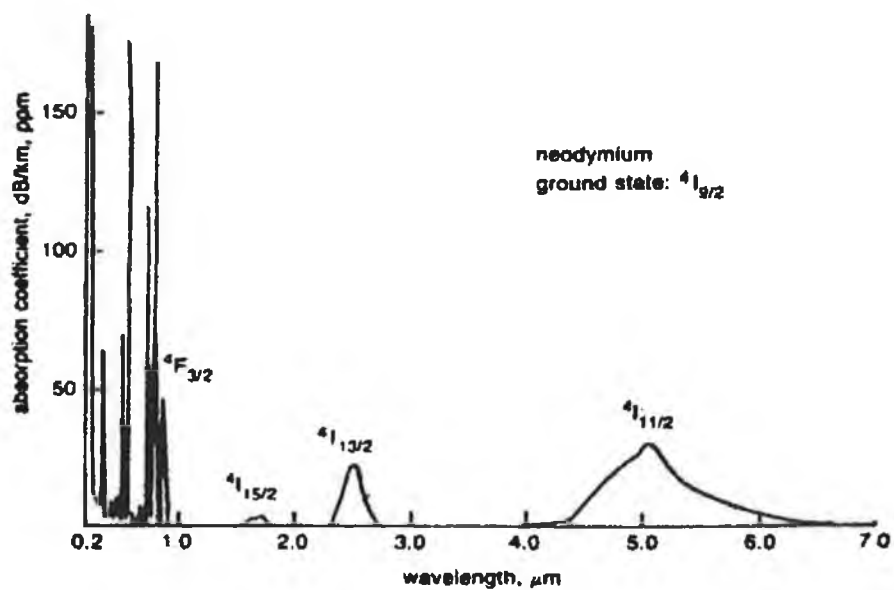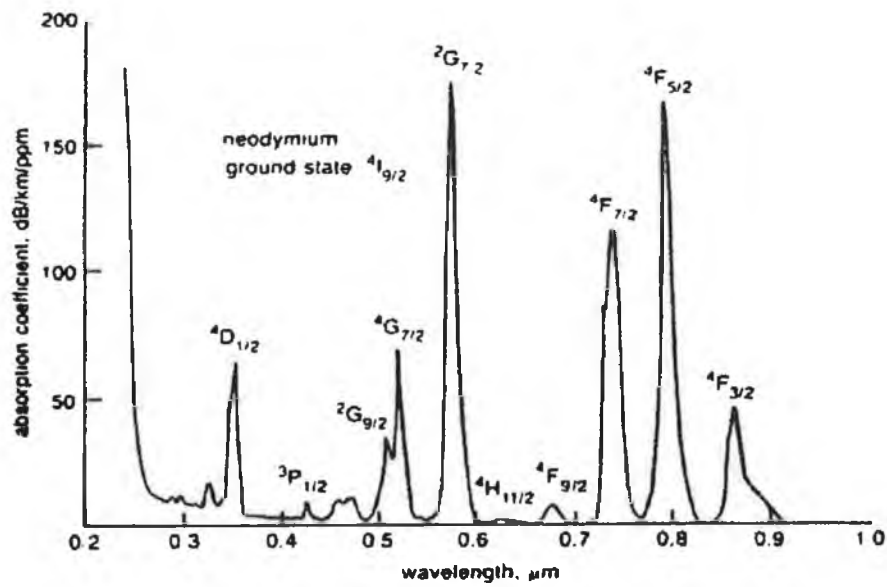
FIGURE A.3 THE ABSORPTION SPECTRUM OF Nd^{3+} IN A ZBLANP GLASS

A.4
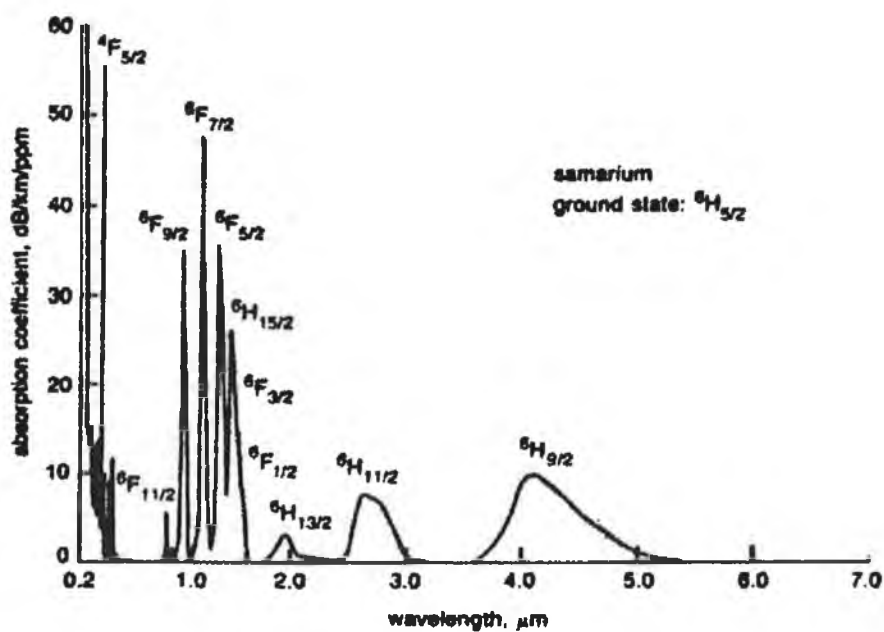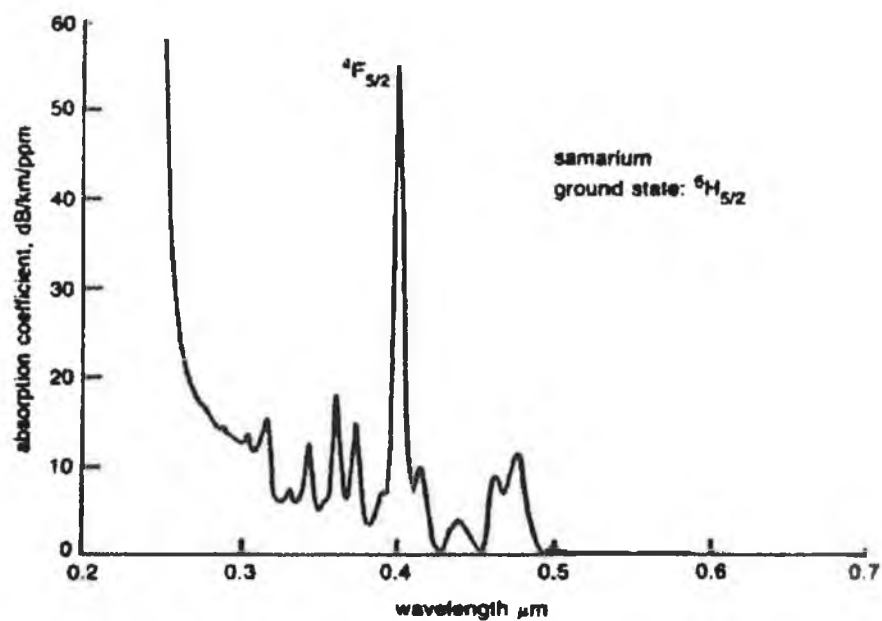
**FIGURE A.4** THE ABSORPTION SPECTRUM OF Sm³⁺ IN A ZBLANP GLASS

A.5
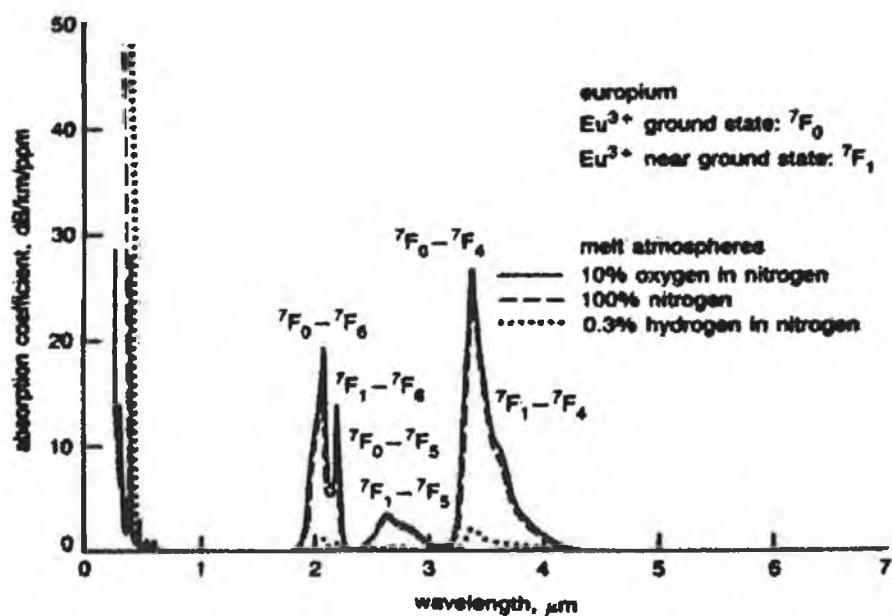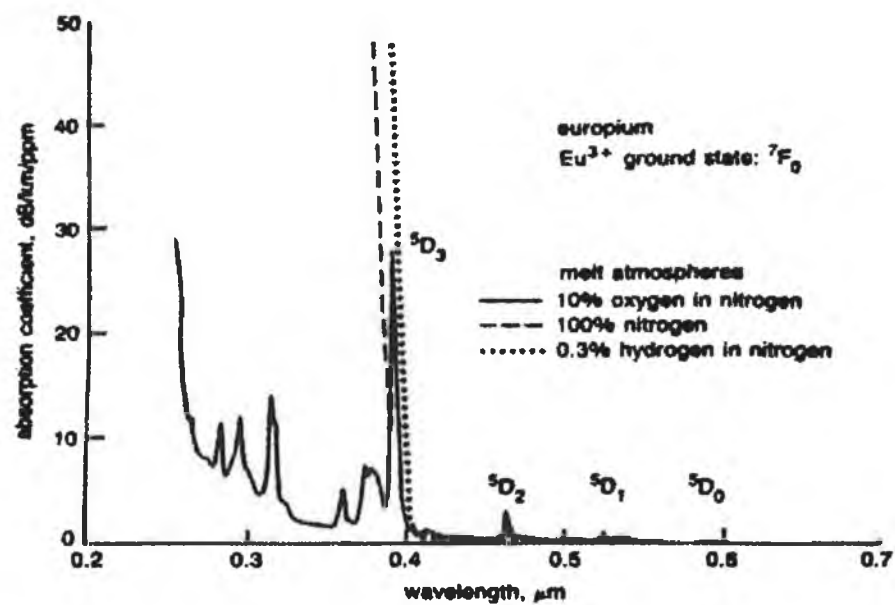
FIGURE A.5 THE ABSORPTION SPECTRUM OF Eu³⁺ IN A ZBLANP GLASS

A.6
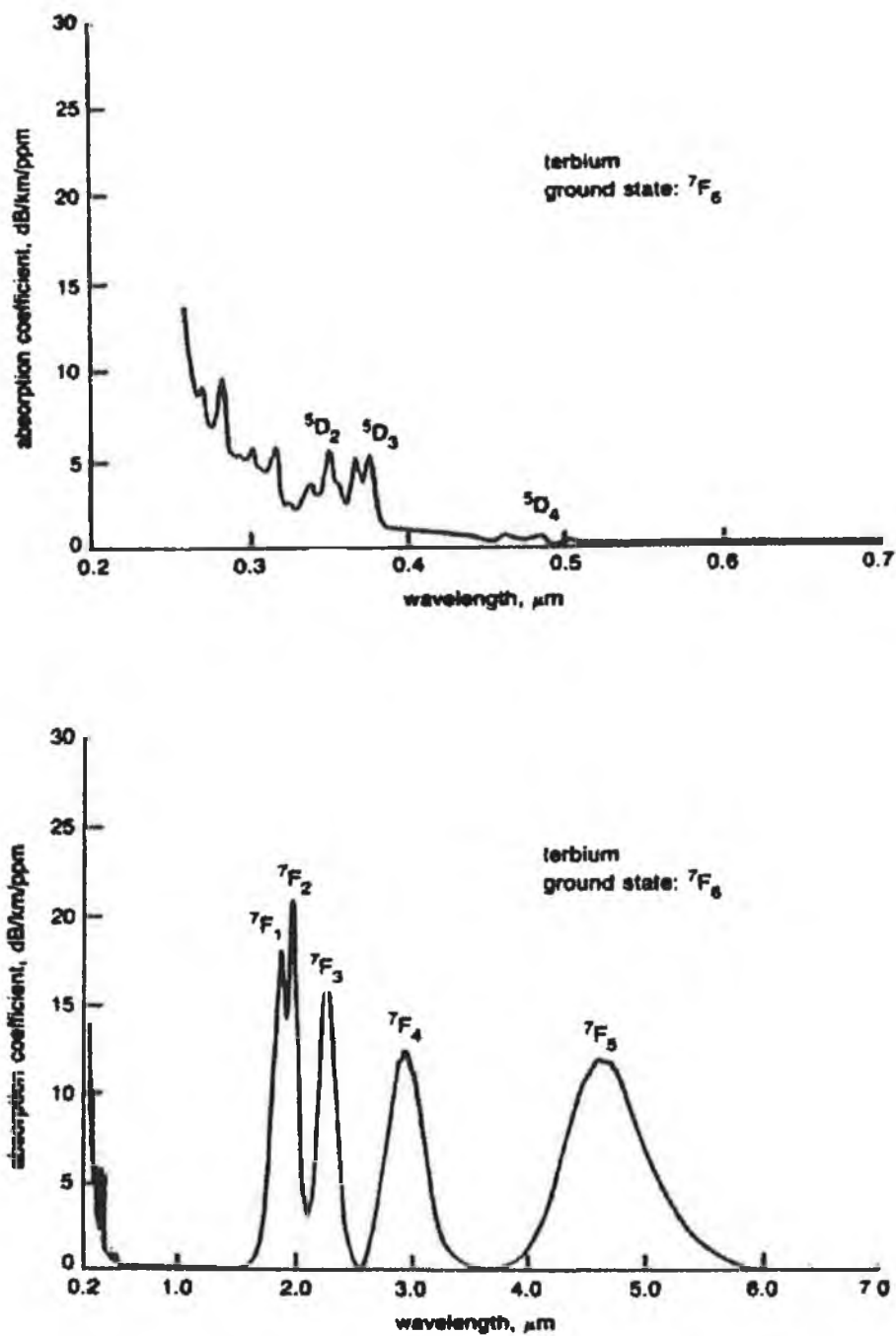
**FIGURE A.6** THE ABSORPTION SPECTRUM OF Tb^{3+} IN A ZBLANP GLASS

A.7
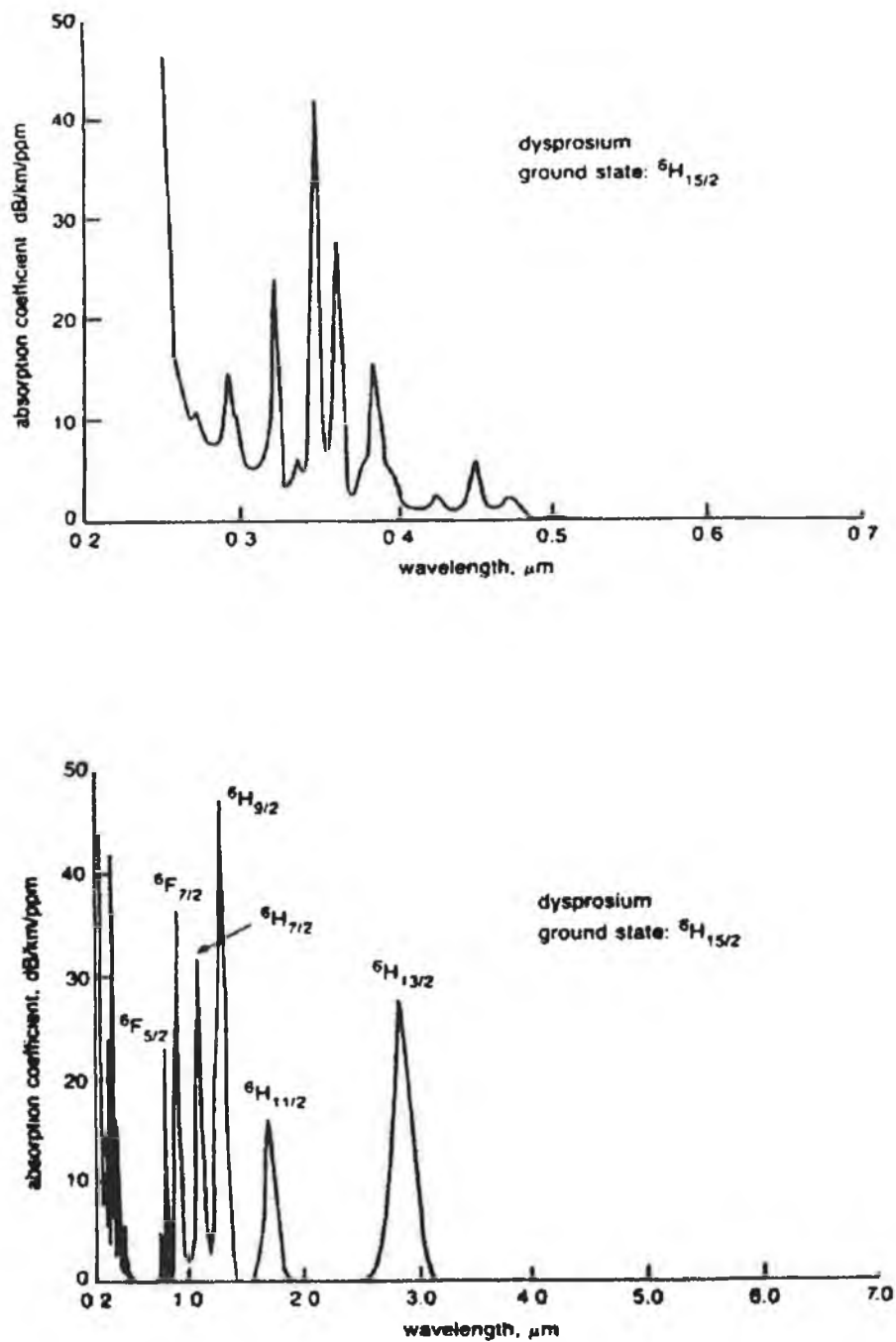
FIGURE A.7 THE ABSORPTION SPECTRUM OF Dy^{3+} IN A ZBLANP GLASS

A.8
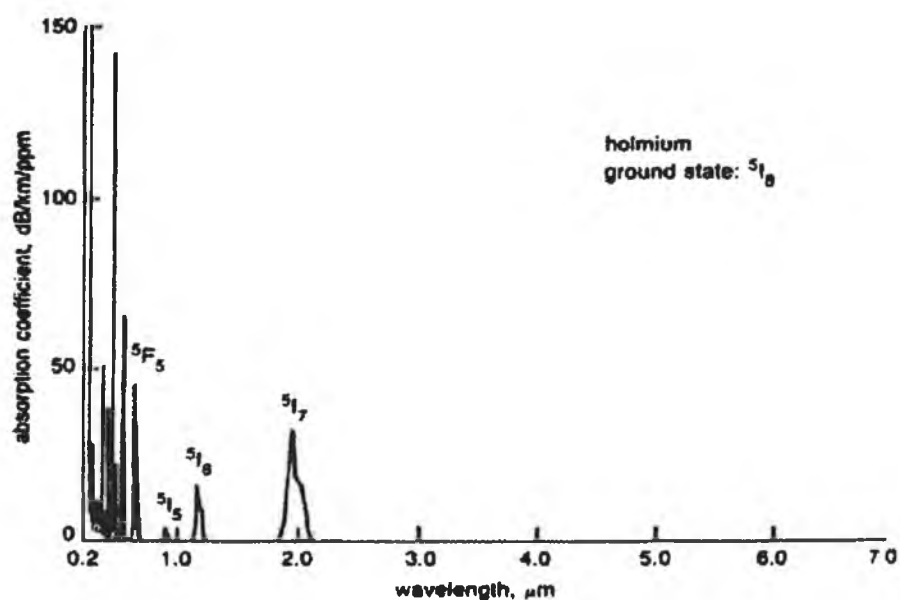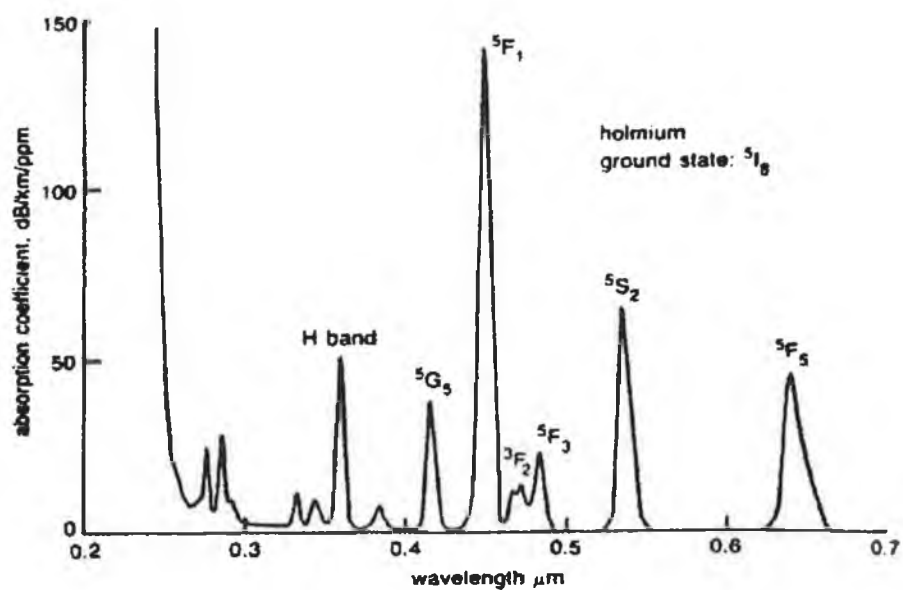
FIGURE A.8 THE ABSORPTION SPECTRUM OF Ho^{3+} IN A ZBLANP GLASS

A.9
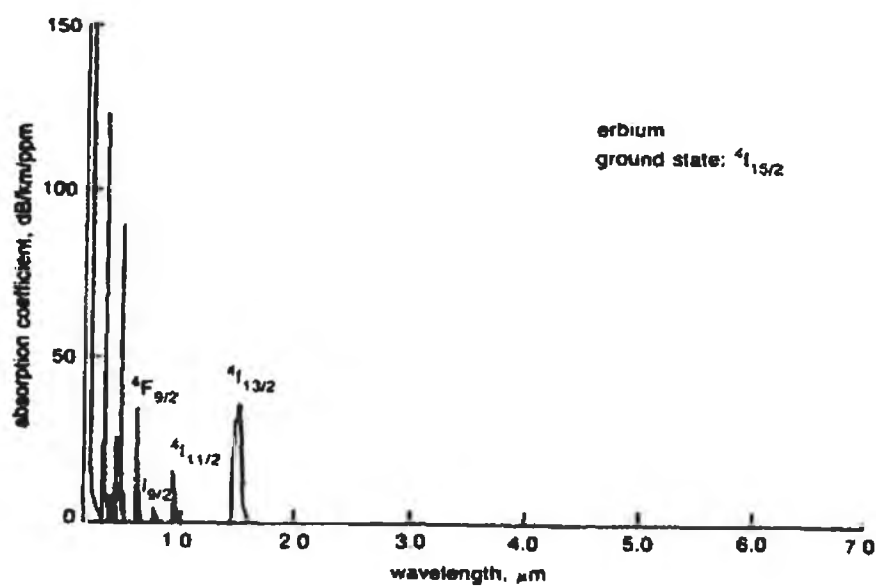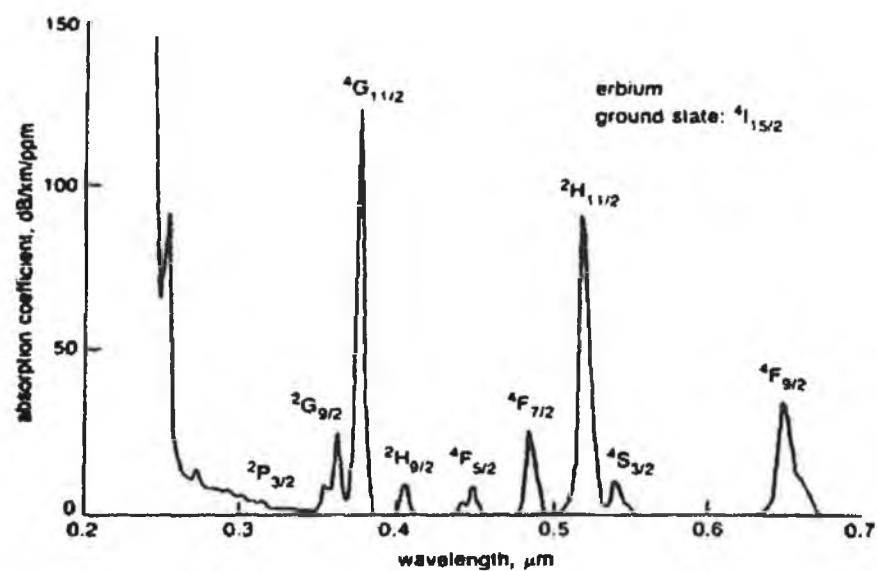
FIGURE A.9 THE ABSORPTION SPECTRUM OF Er^{3+} IN A ZBLANP GLASS

A.10
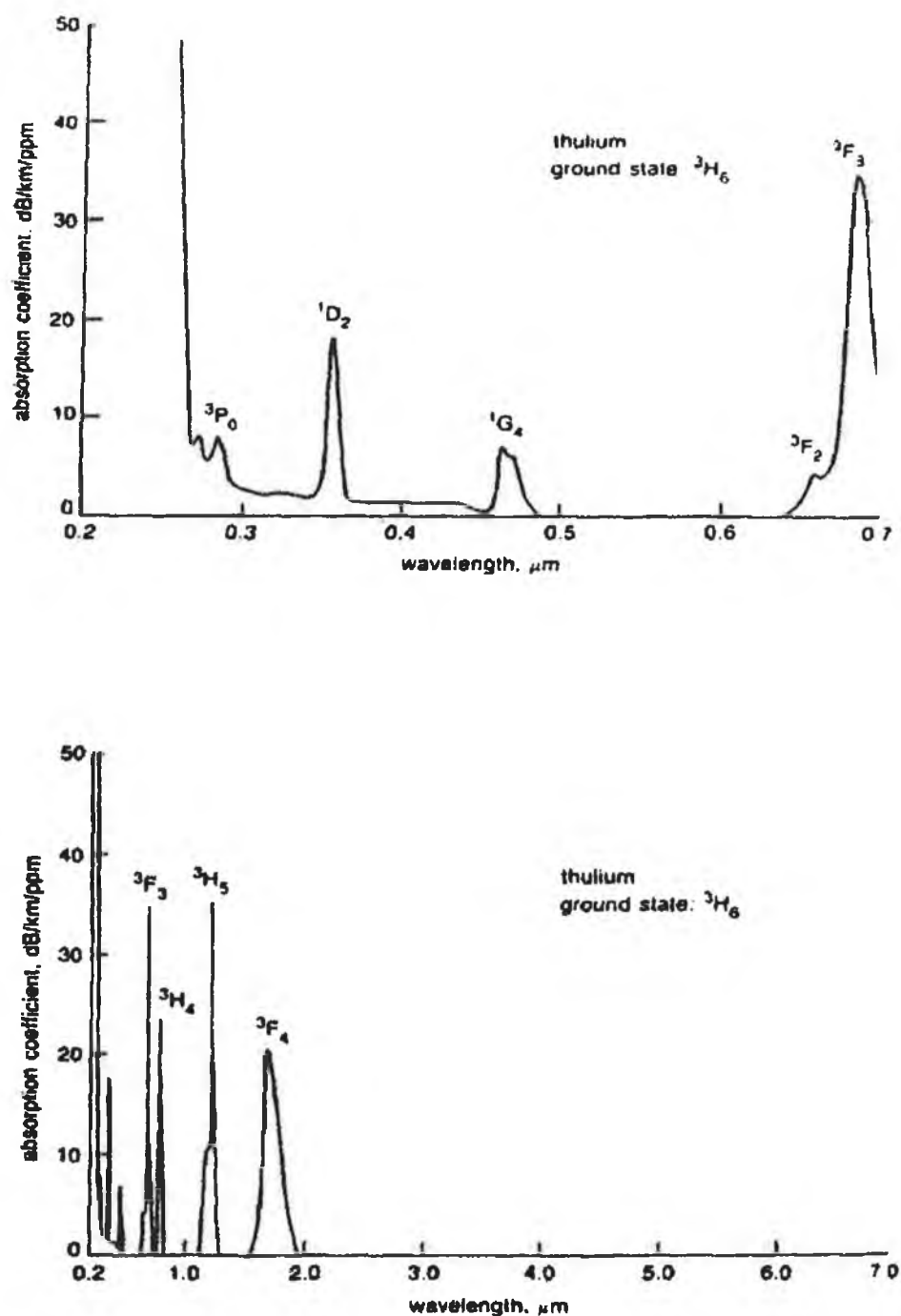
FIGURE A.10 THE ABSORPTION SPECTRUM OF Tm^{3+} IN A ZBLANP GLASS

A.11
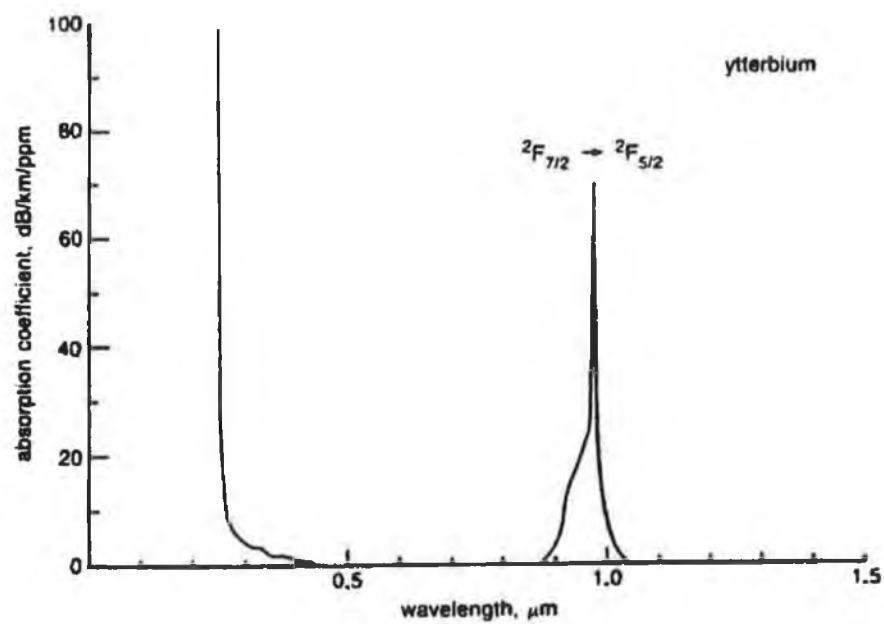
**FIGURE A.11** THE ABSORPTION SPECTRUM OF Yb^{3+} IN A ZBLANP GLASS

APPENDIX B

SONY LASER DIODE SPECIFICATIONS FOR SLD 323 XT

B.1

SONY. **SLD323XT**

High Optical Density 1W Near Infrared Laser Diode | Advance Information

Features
- High power
  Recommended optical power output   Po=0.8W
- High optical density
  Optical power output 1.0W/Emitting aperture 100 μm
- Low power consumption
- Flat package
  With built-in photo diode, TE cooler, thermistor

Applications
- Solid state laser excitation
- Medical use
- Material processing
- Measurement

Package Outline   Unit : mm

Absolute Maximum Ratings (Tth=25℃)

Radiant power output	Po		1.0	W
Reverse voltage	V_R LD		2	V
	PD		15	V
Operating temperature (Tth) Topr			−10 to +30	℃
Storage temperature	Tstg		−40 to +85	℃
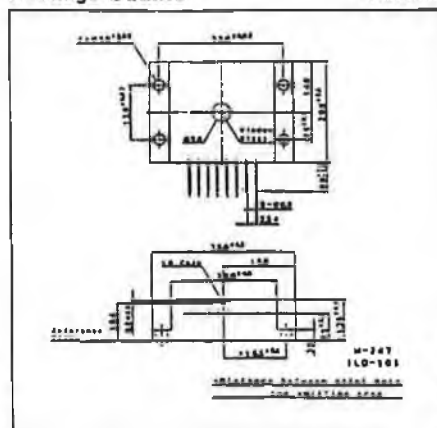
Structure
  GaAlAs double-hetero laser diode

Electrical and Optical Characteristics   (Tth=25℃)

Item		Symbol	Condition	Min.	Typ.	Max.	Unit
Threshold current		Ith			0.3		A
Operating current		Iop	Po=0.8W		1.3		A
Operating voltage		Vop	Po=0.8W			3.0	V
Oscillation wavelength		λp	Po=0.8W	790		830	nm
Monitor current		Imon	Po=0.8W, V_R=15V		1.3		mA
Radiation angle (F. W. H. M.)	Perpendicular	$\theta_\perp$	Po=0.8W		30		degree
	Parallel	$\theta_{\scriptstyle \parallel}$	Po=0.8W		10		degree
Positional accuracy	Position	$\Delta X, \Delta Y$	Po=0.8W			±100	μm
	Angle	$\Delta \phi_\perp$	Po=0.8W			±3	℃
Slope efficiency		η	Po=0.8W		0.8		mW/mA

FINAL TEST SHEET DATA FOR SLD 323 XT -1 SERIAL No. 4B003-013

B.2

LIGHT-CURRENT CHARACTERISTICS
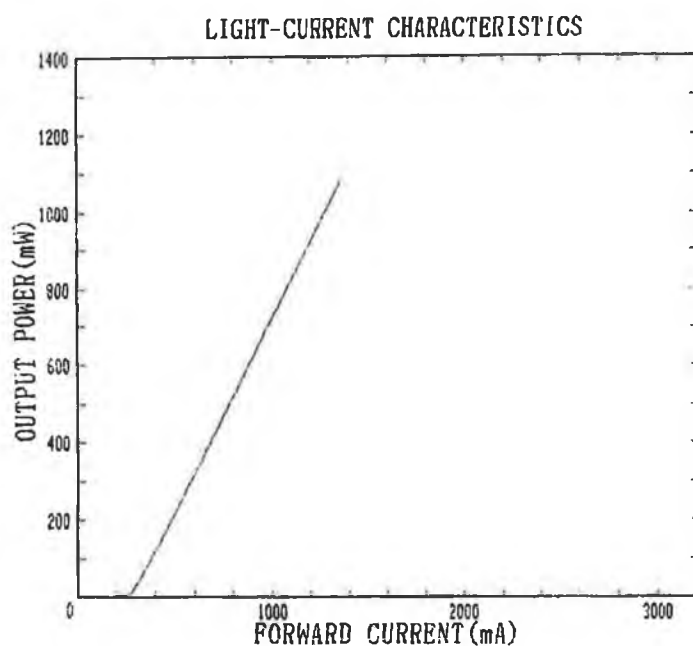
CHECKED BY	MEASURED BY

TYPE	SLD-323XT-I
SER No.	4B003 -013
DATE	94/02/09

λ [nm]	794.7
Iop [mA]	1279.3
Imon [mA]	1.070
$\theta_{\parallel}$ [deg]	9.6
$\theta_{\perp}$ [deg]	32.5

at 25°C 1000mW

SONY LD DATA

Note : Where -1 is used by SONY to specify the operating wavelength range

APPENDIX C

SPECIFICATIONS FOR IE OPTOMECH 'AK SERIES' LASER DRIVER

C.1

AK SERIES SPECIFICATION

AK-10A/1

No. of Channels	One
CURRENT CONTROL MODE	
Average/Peak	
Current Range	0.05 – 10A
Average/Peak Current Resolution	0.003A
Current Accuracy	±0.01A
Analogue Input Scale Factor	2V/A
Input Impedance	20KΩ
Bandwidth	30Khz
POWER CONTROL MODE	
Average/Peak	
Power Range	0.01 – 5W
Average/Peak Power Resolution	0.002W
Power Accuracy	+0.002W
Analogue Input Scale Factor	1V/W
Input Impedance	20KΩ
Bandwidth	20Khz
MONITOR PHOTODIODE	
Control Range	0.1-20μA/mW(mA/W)
Current Limit Range	0.25-10A
Accuracy	0.01A
THERMOELECTRIC COOLERS	
Setpoint Range	-10 – 40°C
Accuracy¹	0.1°C
Max. Current Drive	8A
Drive Limit Range	0 – 8A
MONITOR OUTPUTS	
Output Impedance	< 1KΩ
Current Scale Factor	2V/A
Accuracy	±0.03A
Power Scale Factor	1V/W
Accuracy	±0.005W
REMOTE INTERLOCK	
Open Circuit Voltage	5V ± 10%
Short Circuit Current	<2mA
Threshold	< 1V enables
ENVIRONMENTAL AND UTILITIES	
Operating Temperature	10°C – 40°C
Storage Temperature	-40°C 75°C
Supply Voltage	110/115/220/240/VAC+5% -10% 50/60Hz
Power Consumption	<350W
Size	530mm × 420mm × 160mm (21" × 16.5" × 6.25")

¹ Depending upon thermister accuracy

SAFETY REQUIREMENTS

The AK series laser diode devices have been designed to incorporate all necessary safety features specified for operation of lasers up to class IV level as defined by the Centre for Devices and Radiological Health (C.D.R.H. – U.S.A.) and by BS EN 60825: 1992 as defined by the European Committee for Electrotechnical Standardisation (CENELEC).

IE Optomech Ltd
The Cottage
Crabtree Farm
Newnham
Northants NN11 6ET
United Kingdom
Tel: (0327) 704916
Fax: (0327) 300052

As our policy is constantly to improve the design and specification of IE Optomech products the details given in this brochure are not to be regarded as binding

APPENDIX D

PHILIPS LASER DIODE SPECIFICATIONS FOR CQL 784 OD

D.1

Laser diode Serial Number 4A00556

**PHILIPS**

Philips Optoelectronics Centre

Quick reference data
May 1993

CQL7840/D   780 nm laser diode

FEATURES:
- wavelength typ. 780 nm
- high power 40 mW
- low threshold current
- operating temperature -10/+60°C
- built-in monitor-diode
- ø 9.0 mm encapsulation

Mechanical data
Dimensions in mm

Top view
Pin configuration

Pin	Description
1	laser anode
2	common case
3	monitor diode anode
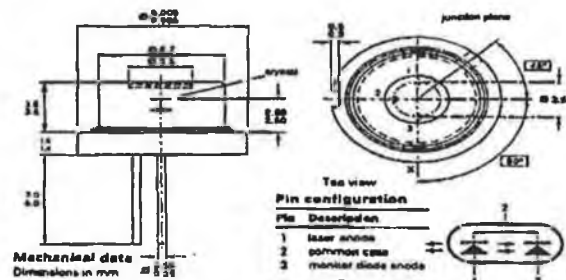
MAXIMUM RATINGS (T_{case}=25°C)

Symbol	Parameter	Min.	Max.	Unit
P_o	CW optical output power	-	50	mW
V_{rl}	laser diode reverse voltage	-	10	V
V_{rm}	monitor diode reverse voltage	-	30	V
I_{fm}	monitor diode forward current	-	10	mA
T_{op}	operating temperature range (T_{case})	-10	+60	°C
T_{stg}	storage temperature range	-40	+85	°C

CHARACTERISTICS (T_{case}=25°C; P_o=40 mW; V_{rm}=15 V)

| Symbol	Parameter	Min.	Typ.	Max.	Unit
I_{th}	threshold current	-	35	-	mA
I_{op}	operating current	-	90	110	mA
V_{op}	operating voltage	-	1.9	2.5	V
λ_p	wavelength at peak emission	-	785	805	nm
$\theta_\parallel$	farfield angle parallel	8	10	12	deg
$\theta_\perp$	farfield angle perpendicular	19	22	25	deg
I_M	monitor current	-	12	-	µA
I_D	monitor dark current	-	-	20	nA

The information presented in this document does not form part of any quotation or contract, is believed to be accurate and reliable and may be changed without notice. No liability will be accepted by the publisher for any consequence of its use. Publication thereof does not convey nor imply any license under patent- or other industrial or intellectual property rights.

**Philips Optoelectronics Centre**

APPENDIX E

SHARP LASER DIODE DRIVER IC - IR3C02

E.1
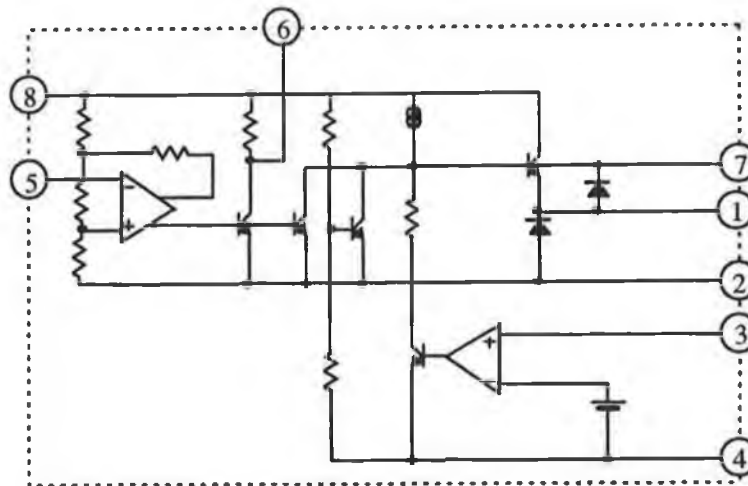
LASER DIODE DRIVER CIRCUIT USING IC - IR3C02

E.2
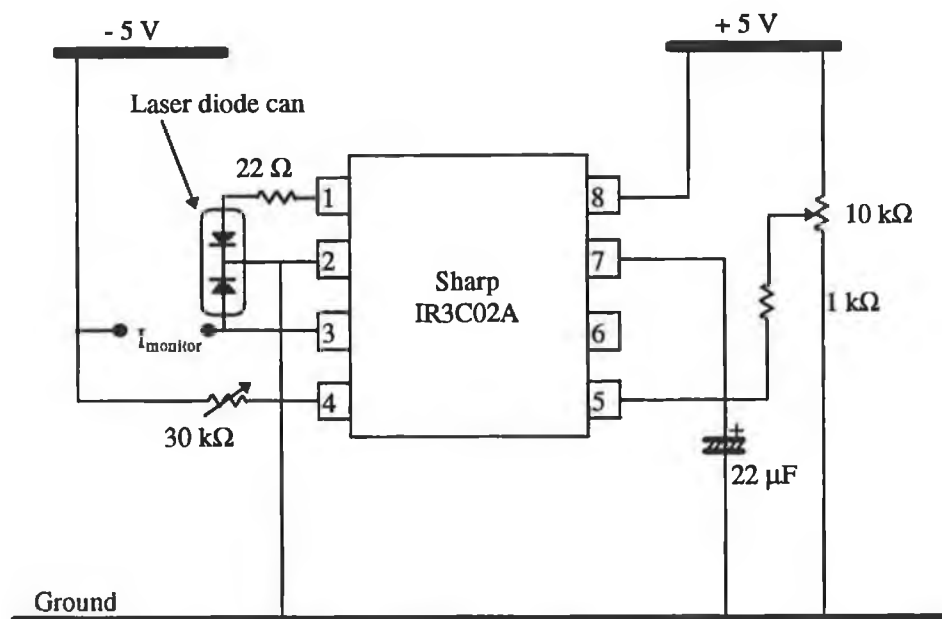
APPENDIX F

TEMPERATURE CONTROL CIRCUIT FOR THERMO-ELECTRIC COOLER

F.1
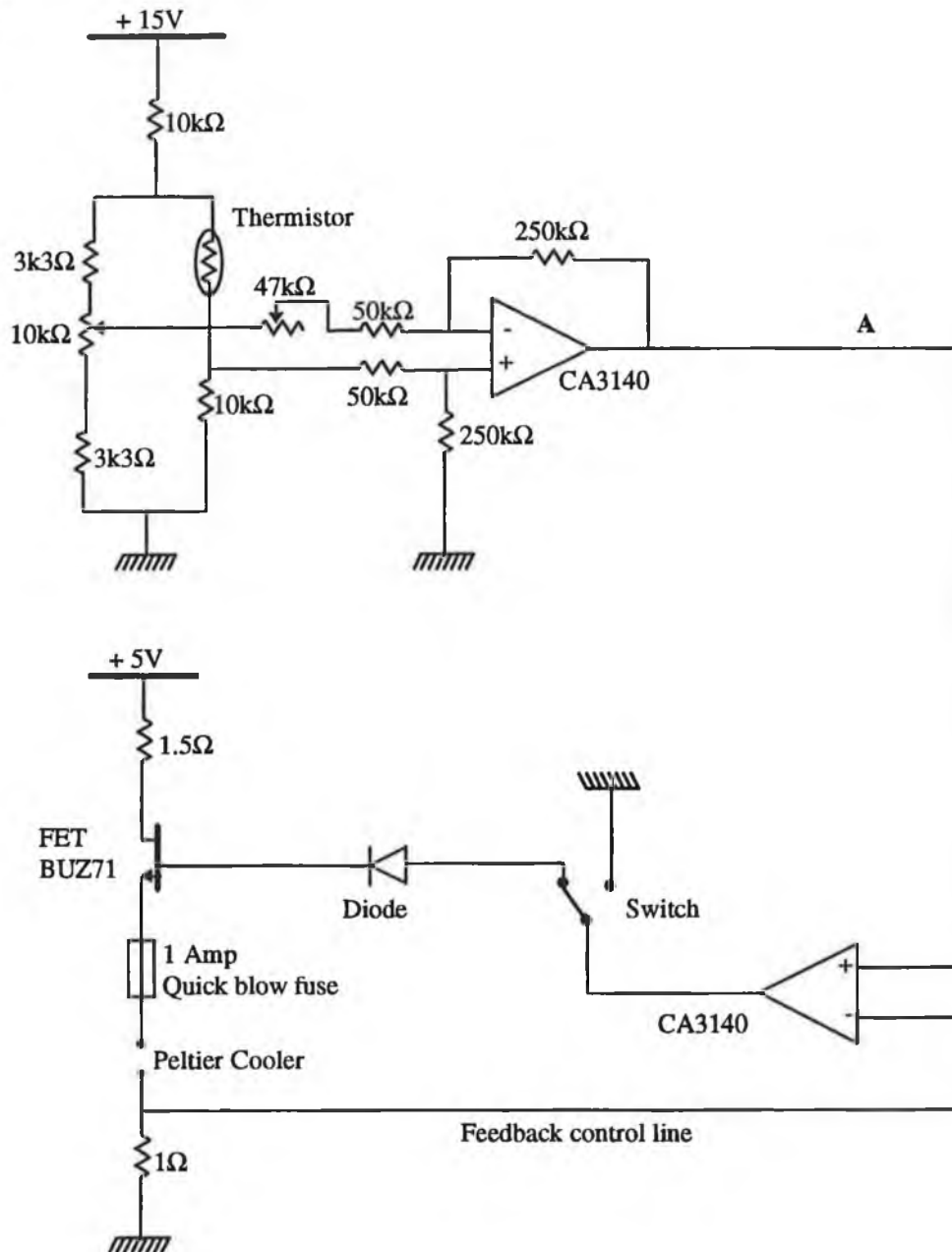
To set the thermo-electric cooler to - 30°C, the thermistor must be replaced by a variable resistor set to 11k6Ω, the bridge is then balanced by varying the 10kΩ resistor. Once the bridge is balanced, the thermistor is then replaced into the circuit. The resistor bridge is out of balance when the circuit is turned on, (due to the thermistor and the thermo-electric cooler being at ambient temperature). As a

result, the output at A is greater than zero, thereby turning on the FET and the thermo-electric cooler begins to draw current, thereby cooling the device. The feedback control line ensures that the circuit has a fast response to temperature change. An equilibrium thermo-electric current is reached when the circuit stabilises, once the bridge is in balance. To maintain a temperature of - 30°C at a room temperature of 22°C, a current of approximately 0.6-1 A is drawn by the thermo-electric cooler.

APPENDIX G

PROGRAM LISTING FOR MONOCHROMATOR CONTROLLING SOFTWARE

G.1

```
#include <stdio.h>
#include <dos.h>
#include <math.h>
#include <conio.h>
#include <float.h>
#include <graphics.h>
#include <string.h>
#include <stdlib.h>
#include <stdarg.h>
#include <dir.h>
#include <alloc.h>
#include "\graph\smouse.h"                                /*mouse handling routines*/
#define BASE 640

float ad(void);
void motor(int,int,int);                                 /*declaring function type*/
void graph(void);
void pointer(void);
void testchoice(int);
void openscr(void);
int menu(void);
char ch;
int choice;
float rightofgraph,ewave,swave;

int gprintf( int *xloc, int *yloc, char *fmt, ... );

void main(void)                                          /*beginning of main*/
        {
                int choice;

                openscr();
                graph();

                do
                {
                        choice = menu();
                        if (choice == 0)
                        {
                                cleardevice();
                                textmode(3);
                                window(1,1,80,25);
                                textbackground(BLACK);
                                textcolor(LIGHTGRAY);
                                clrscr();
                                chdir("c:\\graph");
                                exit(0);
                        }
                        else testchoice(choice);
                }
                while ( choice != 0 );

        }


        void testchoice(int choice)                      /*testing for choice*/
        {
                switch (choice)
                {
                        case 1 : graph();
                                break;
                        case 2 : pointer();
```

```
                                    break;
                          }
                 }
int menu(void)                                                          /*menu listing*/
          {
     settextstyle(0,HORIZ_DIR,1);
          setcolor(GREEN);
          outtextxy(130,460, " (0) .. Exit    (1) .. Scan Again   (2) .. Pointer");

     ch = getch();
          while ((ch < '0' ) II (ch > '2'))
                     ch = getch();
          return(ch-'0');
          }

void openscr(void)                                                      /*opening screen*/
          {
          int driver,mode;

          driver=DETECT;
          mode=VGAHI;
          detectgraph( &driver, &mode);
          initgraph( &driver, &mode, "c:\\tc\\bgi");

          settextstyle(TRIPLEX_FONT, HORIZ_DIR, 4);
          setbkcolor(BLUE);

          setcolor(YELLOW);
          moveto (90,70);
          setusercharsize(3, 1, 3, 1);
          outtext("Spectrum");
          rectangle(10,10,630,470);
          rectangle(20,20,620,460);
          setcolor(GREEN);

          moveto(120,400);
          setusercharsize(1,1,1,1);
          outtext("Press any key to continue");
          getch();
          }

void graph(void)                                                        /*realtime graphing routine*/

          {
          int x,n,d,steps,scansteps,incr;
          int dlay,dirn,loop,max,pos,horstep;                           /*initialising variables*/
          int xmax,ymax,count,verstep;
          int xco,yco,xcora,ycora,y_plot,abc,cba,x_pos,j;
          float z,wave,realinc,realstw,y,p,sum1;
          float yoffset,xoffset,xstep,ystep,volt,xgra,ygra,signal;
          float leftofgraph,topofgraph,bottomofgraph;
          float *x_cords,*y_cords,*a,*sig1;
          float wavel;
          int true=1;
          char name[30],swa[4],ewa[4],z_z[7],vol_t[4];
          FILE *data = NULL;

          yoffset = 90;
          xoffset = 18;
          outportb(BASE+7,130);
          outportb(BASE+4,1);

          xmax = getmaxx();
          ymax = getmaxy();

          setviewport(0,0,xmax,ymax,true);

          clearviewport();
          setbkcolor(BLUE);
          setcolor(YELLOW);
          rectangle(10,10,630,470);
          rectangle(20,20,620,460);
          settextstyle(0,HORIZ_DIR,1);
```

```
setcolor(LIGHTGREEN);
outtextxy(70,80,"Monochromator is moving to the zero order position");    /*going to low stop*/

dirn=0;dlay=5;loop=10000;                                                 /*neg dirn,fast */
motor(dirn,dlay,loop);                                                     /*finding 0 order*/

pos=0;max=0;
for(x=0;x<100;x++)
  {
  dirn=1;dlay=100;loop=1;                                                  /*pos dirn,slow*/
  motor(dirn,dlay,loop);
  signal = ad();                                                          /*reading in signal from A/D*/
  signal = signal/409.5*2;
  signal = signal-10.12;

  if (signal > max) {max=signal;pos=x;}
  delay(200);                                                            /*delay for LIA*/
  }
dirn=0;dlay=100;loop= (x-pos)+2;                                          /*stepper moves back to*/
motor(dirn,dlay,loop);                                                    /*zero order position    */

                                                                          /*scan set up procedure*/

setcolor(YELLOW);
outtextxy(70,132,"Start wavelength (Microns)...........................?");   /*requesting information*/
do{                                                                       /*from user*/
gotoxy(66,9);
printf("       ");
gotoxy(66,9);
gets(swa);
swave = atof(swa);
}
while ((swave < 0.5) || (swave > 10));

outtextxy(70,181,"End wavelength (Microns)..............................?");
do{
gotoxy(66,12);
printf("       ");
gotoxy(66,12);
gets(ewa);
ewave = atof(ewa);
}
while ((ewave < 1) || (ewave > 10));

outtextxy(70,229,"Input the spacing between data points (Microns).......?");
do{
gotoxy(66,15);
printf("       ");
gotoxy(66,15);
gets(z_z);
z = atof(z_z);
}
while ((z < 0.00149) || ( z > 0.1));

outtextxy(70,277,"Max signal (Volts)....................................?");
do{
gotoxy(66,18);
printf("       ");
gotoxy(66,18);
gets(vol_t);
volt = atof(vol_t);
}
while ((volt < 0.1) || (volt > 10));

outtextxy(70,325,"Name of file for data................................?");
chdir("c:\\graph\\spectrum");
do{
        gotoxy(66,21);
        printf("       ");
        gotoxy(66,21);
        gets(name);
  }
while ((data = fopen(name,"wt")) == NULL);
```

```
setcolor(LIGHTGREEN);
outtextxy(70,390,"Moving to starting wavelength");


n = z/(1.5/1000);
realinc = n * (1.5/1000);
steps= swave/(1.5/1000);
realstw=steps*(1.5/1000);
                                                    /* required start wave */
scansteps=(ewave-realstw)/ (1.5/1000);              /*and end wave*/
p=scansteps/n;
a=(float *)malloc((p+1)*sizeof(float));             /*setting up arrays*/
x_cords=(float *)malloc((p+1)*sizeof(float));
y_cords=(float *)malloc((p+1)*sizeof(float));
sig1=(float *)malloc((p+1)*sizeof(float));

dirn=1;dlay=10;loop=steps;
motor(dirn,dlay,loop);                              /*moving stepper to*/
                                                    /* start wave*/

clearviewport();

topofgraph = 20;                                    /*screen co-ordinates*/
leftofgraph = 100;
rightofgraph = xmax - 20;
bottomofgraph = ymax - yoffset;

verstep = (bottomofgraph - topofgraph)/10+1;
horstep = (rightofgraph - leftofgraph)/10+1;

ystep = volt/10;
xstep = (ewave-swave)/10;

setbkcolor(BLACK);
setcolor(CYAN);

setlinestyle(0,0,3);
line(100,20,100,ymax-yoffset);
line(100,ymax-yoffset+1,xmax-xoffset+1,ymax-yoffset+1);
line(100,20,xmax-xoffset+1,20);
line(xmax-xoffset+1,20,xmax-xoffset+1,ymax-yoffset+1);

gotoxy(15,1);
printf("File Name = %s\n",name);

settextstyle(1,HORIZ_DIR,2);
setcolor(CYAN);
outtextxy(240,425,"Wavelength (microns)");

settextstyle(1,VERT_DIR,2);
setcolor(CYAN);
outtextxy(6,130,"Intensity (a.u.)");

setlinestyle(0,0,1);
setcolor(DARKGRAY);
for (count=1; count < 10; count ++)
        {
        line(leftofgraph+2,bottomofgraph - verstep * count+2,
            rightofgraph+2,bottomofgraph - verstep * count+2);
        line(leftofgraph + horstep * count+2,bottomofgraph,
            leftofgraph + horstep * count+2,topofgraph+1);
        }

settextstyle(1,HORIZ_DIR,1);
setcolor(LIGHTGRAY);
abc = 87;
cba = 392;
gprintf(&abc,&cba,"%3.2f",swave);
outtextxy(73,375,"0");

for (incr=1; incr <11; incr++)
        {
        ygra = ystep*incr;
        xgra = swave+xstep*incr;
```

```
                xco = leftofgraph-55;
                yco = bottomofgraph - verstep * incr - 9;
                xcora = leftofgraph + horstep * incr - 17;
                ycora = bottomofgraph + 3;
                gprintf(&xco,&yco,"%4.2f",ygra);
                gprintf(&xcora,&ycora,"%3.2f",xgra);
                }
x_pos = 100;
y_plot = 200;
moveto(leftofgraph,bottomofgraph);
getch ();


a[0]=ad();                                              /*beginning the scan*/

                                                        /*scan at start wave*/
dirn=1;dlay=30;loop=n;
for (y=1; y<(p+1); y++)                                 /*scan to end wave in*/
        {                                               /*intervals of z*/
        motor(dirn,dlay,loop);
        a[y] = ad();
        a[y] = a[y]/409.5*2;
        a[y] = a[y]-10.12;

        sum1=0;                                         /*averging signal from A/D*/
        for ( j=0; j<10; j++ )
                {
                delay(3);
                sum1 = sum1 + a[y];
                }
        sig1[y] = sum1/j;
        delay(300);

        x_pos = (leftofgraph + (( y / p ) * (rightofgraph - leftofgraph)));
        x_cords[y] = x_pos;                             /*x co-ordinates for screen*/

        y_plot = (bottomofgraph-((sig1[y]/volt)*(bottomofgraph - topofgraph)));
        if ( y_plot > bottomofgraph)
        {
                y_plot = bottomofgraph-2;
        }
        else if ( y_plot < topofgraph )
        {
                y_plot = topofgraph;
        }
        y_cords[y] = y_plot;                            /*y co-ordinates for screen*/

        setcolor(GREEN);
        lineto(x_cords[y],y_cords[y]);
        setcolor(YELLOW);
        circle(x_cords[y],y_cords[y],1);                /*plotting data points on screen*/

        wavel = swave + (y*z);
        gotoxy(39,1);
        printf("Wavelength = %5.4f\r",wavel);
        gotoxy(62,1);
        if ( sig1[y] < 0 )
                {
                sig1[y] = 0;
                }
        printf("Voltage = %4.2f\r",sig1[y]);            /*printing voltage on screen*/

    }

wave = realstw;                                         /*writing signal & wavelength to file*/
 for(d=0;d<p+1;d++)
 {
        fprintf(data,"%5.3f\t",sig1[d]);
        wave = wave + realinc;
        fprintf(data,"%6.4f\n",(wave));
 }

 fclose(data);
```

```
        }

        void pointer(void)                                      /*screen pointer routine*/
        {
                int button,xpos,ypos;
                float x,ans,wavel,wavell,cp,cpp;

                mouseinit();
                display_mouse();
                do
                {
                do
                        {
                                mousebuttoninfo(&button,&xpos,&ypos);
                        }
                while (!button);

                x = rightofgraph-100;
                cp = xpos - 100;
                cpp = cp/x;
                wavel = ewave-swave;
                wavell = wavel*cpp;
                ans = wavell+swave;
                hide_mouse();
                line(xpos-3,ypos,xpos+3,ypos);
                line(xpos,ypos-3,xpos,ypos+3);
                xpos = xpos-15;
                ypos = ypos-12;
                gprintf(&xpos,&ypos,"%4.3f",ans);               /*mouse/data position on screen*/
                display_mouse();
                delay(300);
                }
                while (button != 2);
        }

        void motor(int dirn,int dlay,int loop)                  /*routine for stepper motor control*/
         {
         int i;
         outportb(BASE+7,130);
         outportb(BASE+6,dirn);
          for(i=0; ((i<loop) && ((inportb(BASE+5) & 1) == 1)); i++)
           {
            outportb(BASE+4,0);
            delay(dlay);
            outportb(BASE+4,1);
            delay(dlay);
           }
         }

        float ad(void)
         {
         float signal;
         int l,m;
         outportb(BASE+16,0);
         while (!(inportb(BASE+20)&1));
         m= inportb(BASE+18);
         l= inportb(BASE+19);
         signal = (m*16)+(l/16);
         return (signal);
         }


                /*GPRINTF: Used like PRINTF except the output is sent to the */
         /*screen in graphics mode at the specified co-ordinate. (taken from bgidemo program)*/


int gprintf( int *xloc, int *yloc, char *fmt, ... )
{
 va_list  argptr;                                       /* Argument list pointer       */
 char str[140];                                         /* Buffer to build sting into  */
 int cnt;                                               /* Result of SPRINTF for return */

 va_start( argptr, fmt );                               /* Initialize va_ functions    */
```

```
cnt = vsprintf( str, fmt, argptr );                    /* prints string to buffer*/
outtextxy( *xloc, *yloc, str );                        /* Send string in graphics mode*/
*yloc += textheight( "H" ) + 2;                        /*Advance to next line*/

va_end( argptr );                                      /*Close va_ functions*/

return( cnt );                                         /* Return the conversion count  */

}
```

PROGRAM LISTING FOR MOUSE HANDLING ROUTINES

G.2   (mouse routine written by Dr. S. McCabe)

```
/*Mouse handling routines....using interrupt 33h        (note must install mouse to use)

        pass value in ax as below

        ax      0               :get mouse status and initialise
                                :status returned in ax  0 => not installed
                                                        0ffffh=> otherwise
                                :number of buttons returned in bx

                1               :show mouse cursor

                2               :hide mouse cursor

                3               :get mouse position and button status
                                :xpos in cx
                                :ypos in dx
                                :buttons pressed returned in bx as follows
                                                left - 01b
                                                right- 10b
                                                both - 11b

                4               :put mouse at defined pos
                                :xpos - cx
                                :ypos - dx

                8               :set limits to mouse movements (vertical)
                                :min  - cx
                                :max  - dx

                9               :assign a shape to the mouse
                                :es - contains array data segment
                                :dx - segment offset to data
                                :bx - xpos hot spot
                                :cx - ypos hot spot
*/

#include <dos.h>
#include <math.h>
#include <bios.h>
#include "fluor.h"

void mousebuttoninfo(int *button, int *xpos, int *ypos) {
        _AX = 3;
        asm int 33h;
        asm mov ax,bx;
        *button=_AX;    /*1 = left  2 = right 3 = both  */
        *xpos =_CX;
        *ypos =_DX;
}

int mousebutton(int button) {
        _AX = 6;
        _BX = button;
        asm int 33h;
        return(_AX);
}
```

```c
void display_mouse(void) {
        _AX = 1 ;
        asm int 33h;
}

int mouseinit(void) {
        _AX = 0;
        asm int 33h;
        return (_AX);
}

void hide_mouse(void) {
        _AX = 2 ;
        asm int 33h;
}

void mousemaxmin(dsply *display) {
        _AX = 7;
        _CX = 0;
        _DX = MAXX;
        asm int 33h;

        _AX = 8;
        _CX = 0;
        _DX = MAXY;
        asm int 33h;
}

void mouseshape(int type) {
        static unsigned hand[32]={0xF9ff,0xE1FF,0xE9FF,0xE9FF,
                                  0xE9FF,0xE849,0xE800,0x8924,
                                  0x0924,0x0986,0x0DFC,0x2FFC,
                                  0x3FFC,0x3FFC,0x0000,0x8001,
                                  0x0C00,0x1200,0x1200,0x1200,
                                  0x1200,0x13B6,0x1249,0x7249,
                                  0x9249,0x9001,0x9001,0x8001,
                                  0x8001,0x8001,0x8001,0x7FFE
                                  };

        static unsigned check[32]={0xFFF0,0xFFE0,0xFFC1,0xFF83,
                                   0xFF07,0x060F,0x001F,0x8037,
                                   0xC07F,0xE0FF,0xF1FF,0xFBFF,
                                   0xFFFF,0xFFFF,0xFFFF,0xFFFF,
                                   0x0003,0x0006,0x000C,0x0018,
                                   0x0030,0x0060,0x70C0,0x3980,
                                   0x1F00,0x0E00,0x0400,0x0000,
                                   0x0000,0x0000,0x0000,0x0000
                                   };

        static unsigned larrow[32]={0xFE3F,0xFC7F,0xF87F,0xF0FF,
                                    0xE0FF,0xC000,0x8000,0x0000,
                                    0x8000,0xC000,0xE0FF,0xF0FF,
                                    0xF87F,0xFC7F,0xFF3F,0xFFFF,
                                    0x0080,0x0100,0x0300,0x0600,
                                    0x0E00,0x1C00,0x3FFF,0x7FFF,
                                    0x3FFF,0x1C00,0x0E00,0x0600,
                                    0x0300,0x0100,0x0080,0x0000
                                    };

        unsigned far *ptr;
        hide_mouse();
        _AX = 9;
        _BX = 1;
        _CX = 1;
        if(type==1) ptr=hand;
        if(type==2) ptr=check;
        if(type==3) ptr=larrow;

        if(type==4) mouseinit();
        else {
        _ES = (unsigned)FP_SEG(ptr);
        _DX = (unsigned)FP_OFF(ptr);
         asm int 33h;
        }
```

```
            display_mouse();
            display_mouse();
}

void mousesetpos(int x, int y) {
            _AX = 4;
            _CX = x;
            _DX = y;
            asm int 33h;
}
```

APPENDIX H

PROGRAM LISTING FOR DATA ACQUISITION AND REAL-TIME PLOTTING OF DATA VERSUS TIME

H.1

```
#include <stdio.h>
#include <math.h>
#include <float.h>
#include <conio.h>
#include <graphics.h>
#include <string.h>
#include <stdlib.h>
#include <dos.h>
#include <stdarg.h>
#include <dir.h>
#include <alloc.h>

void opening_scr(void);                                              /* declaring function type */
int  menu(void);
void graph(void);
void testchoice(int);

char ch;
int choice;
int gprintf( int *xloc, int *yloc, char *fmt, ... );

void main(void)                                                      /* beginning of main */
        {
                int choice;

                opening_scr();
                graph();

                do
                {
                        choice = menu();
                        if (choice == 0)
                        {
                                cleardevice();
                                textmode(3);
                                window(1,1,80,25);
                                textbackground(BLACK);
                                textcolor(LIGHTGRAY);
                                clrscr();
                                chdir("c:\\graph");
                                exit(0);
                        }
                        else testchoice(choice);
                }
                while ( choice != 0 );
        }

int menu(void)                                                       /* menu listing */
{
        settextstyle(0,HORIZ_DIR,1);
        setcolor(BLACK);
        outtextxy(180,460, "Press 'p' to pause : Press 'p' to continue");
        setcolor(GREEN);
        outtextxy(200,460, " (0) .. Exit    (1) .. Scan Again");

        ch = getch();
        while ((ch < '0') || (ch > '1'))
                ch = getch();
        return(ch-'0');
```

```
}

void testchoice(int choice)                                          /* testing for choice */
{
        switch (choice)
        {
                case 1 : graph();
                            break;
        }
}

void opening_scr(void)                                               /* opening screen */
        {
        int driver,mode;

        driver=DETECT;
        mode=VGAHI;
        detectgraph( &driver, &mode);
        initgraph( &driver, &mode, "c:\\tc\\bgi");

        settextstyle( TRIPLEX_FONT, HORIZ_DIR, 4 );
        setbkcolor(BLUE);

        setcolor(YELLOW);
        moveto ( 150, 70 );
        setusercharsize( 3, 1, 3, 1 );
        outtext ("GRAPH");
        rectangle(10,10,630,470);
        rectangle(20,20,620,460);
        setcolor (GREEN);

        moveto(90,400);
        setusercharsize( 1, 1, 1, 1 );
        outtext(" Press any key to continue");
        getch();
        }

void graph(void)                                                     /* realtime graphing routine */
{
        float yoffset,xoffset,ystep,ygra,xgra,xstep;                 /* initialising variables */
        float leftofgraph,rightofgraph,topofgraph,bottomofgraph,del;
        char tim[4],vol[4],name[30],chan1[4],chan2[4],gg[4],timd[4];
        float volt,x_pos,a,b,c,aa,bb,cc,time,sum1,sum2,y_pos,yy_pos,test_vol;
        int true=1;
        int xmax, ymax, limit, z, y_plot,x_plot,yy_plot,test_tim,d,p,channel1,channel2,numavg,g,timdel;
        int count, verstep, horstep, incr, xco, yco, xcora, ycora,ss,s;
        float *x_cords,*y_cords,*yy_cords,*sig1,*sig2;
        FILE *data = NULL;

        yoffset = 90;
        xoffset = 18;
        limit = 519;

        xmax = getmaxx();
        ymax = getmaxy();

        setviewport( 0, 0, xmax, ymax, true );
        clearviewport();

        setbkcolor(BLUE);
        setcolor(YELLOW);
        rectangle(10,10,630,470);
        rectangle(20,20,620,460);
        settextstyle(0,HORIZ_DIR,1);

        outtextxy(70,132, "Length of time to scan (Seconds) ? ");   /* requesting information from user */
        outtextxy(70,145, "Minimum scan time is 15 seconds");
        do{
        gotoxy(66,9);
        printf("            ");
        gotoxy(66,9);
        gets(tim);
        test_tim = atoi(tim);
        }
```

```
while ((test_tim < 15) || (test_tim > 1800));

outtextxy(70,164, "Max signal (Volts) ? ");
do{
gotoxy(66,11);
printf("            ");
gotoxy(66,11);
gets(vol);
test_vol = atof(vol);
}
while ((test_vol < .01) || (test_vol > 10));

outtextxy(70,196, "Name of file for data ?");
chdir("c:\\graph\\data");
do{
gotoxy(66,13);
printf("        ");
gotoxy(66,13);
gets(name);
}
while((data = fopen(name,"wt")) == NULL);

outtextxy(70,228, "Input channel for signal ?");
do{
gotoxy(66,15);
printf("        ");
gotoxy(66,15);
gets(chan1);
channel1 = atoi(chan1);
}
while ((channel1 < 0) || (channel1 > 6));

outtextxy(70,260, "Input channel for reference signal ?");
do{
gotoxy(66,17);
printf("        ");
gotoxy(66,17);
gets(chan2);
channel2 = atoi(chan2);
}
while ((channel2 < 0) || (channel2 > 6));

outtextxy(70,292, "Number of points to average ?");
do{
gotoxy(66,19);
printf("        ");
gotoxy(66,19);
gets(gg);
numavg = atoi(gg);
}
while ((numavg < 1) || (numavg > 10000));

outtextxy(70,324, "Time delay for gas to reach equilibrium (seconds) ?");
do{
gotoxy(66,21);
printf("        ");
gotoxy(66,21);
gets(timd);
timdel = atoi(timd);
}
while ((timdel < 1) || (timdel > 300));

clearviewport();

x_cords=(float *)malloc((limit+1)*sizeof(float));          /* allocating memory */
y_cords=(float *)malloc((limit+1)*sizeof(float));
sig1=(float *)malloc((limit+1)*sizeof(float));
sig2=(float *)malloc((limit+1)*sizeof(float));
yy_cords=(float *)malloc((limit+1)*sizeof(float));

topofgraph = 20;                                           /* screen coordinates */
leftofgraph = 100;
rightofgraph = xmax - 20;
bottomofgraph = ymax - yoffset;
```

```
verstep = (bottomofgraph - topofgraph ) / 10+1;
horstep = (rightofgraph - leftofgraph) / 10+1;

volt = atof(vol);
time = atof(tim);
xstep = time/10;
ystep = volt/10;

setbkcolor(BLACK);
setcolor(CYAN);
gotoxy(40,1);
printf("File Name = %s No. of averages = %d",name,numavg);

setlinestyle(0,0,3);
line(100,20,100,ymax-yoffset);
line(100,ymax-yoffset+1,xmax-xoffset+1,ymax-yoffset+1);
line(100,20,xmax-xoffset+1,20);
line(xmax-xoffset+1,20,xmax-xoffset+1,ymax-yoffset+1);

settextstyle(1, HORIZ_DIR, 2);
setcolor(CYAN);
outtextxy(300,425, "Time (secs)");

settextstyle(1, VERT_DIR, 2);
setcolor(CYAN);
outtextxy(6,130, "Intensity (a.u.) ");

settextstyle(0, HORIZ_DIR, 1);
setcolor(GREEN);
outtextxy(180,460, "Press 'p' to pause : Press 'p' to continue");

setlinestyle(0,0,1);
setcolor(DARKGRAY);
for (count=1; count < 10; count ++)
        {
        line(leftofgraph+2, bottomofgraph - verstep * count+2,
            rightofgraph+2, bottomofgraph - verstep * count+2);
        line(leftofgraph + horstep * count+2, bottomofgraph,
            leftofgraph + horstep * count+2, topofgraph+1);
        }
settextstyle(1, HORIZ_DIR, 1);
setcolor(LIGHTGRAY);
outtextxy(95,392, "0");
outtextxy(73,375, "0");

for (incr=1; incr < 11; incr++)
        {
        ygra = ystep*incr;
        xgra = xstep*incr;
        xco = leftofgraph-55;
        yco = bottomofgraph - verstep * incr - 9;
        xcora = leftofgraph + horstep * incr - 17;
        ycora = bottomofgraph + 3;
        gprintf(&xco,&yco,"%4.2f",ygra);
        gprintf(&xcora,&ycora,"%3.0f",xgra);
        }

del = time - 30;
x_plot = ((del*1000)/(limit));
x_pos = 100;
moveto(leftofgraph,bottomofgraph);

getch();
for ( z=1; z < (limit+1); z++)
{
        while(kbhit())
        {
                p = getch();
                if ((p == 80) || (p == 112))
                {
                getch();
                        for ( s=timdel; s > 9; s--)
                        {
                                gotoxy(1,1);
```

```
                                    printf("Restart (Seconds) %d\r",s);
                                    sleep(1);
                            }
                    gotoxy(19,1);
                    printf("  ");
                    for ( ss=9; ss > 0; ss--)
                    {
                            gotoxy(20,1);
                            printf("%d\r",ss);
                            sleep(1);
                    }
                    printf("                        ");
            }
};

delay(x_plot);
sum1 = 0;
sum2 = 0;

for(g=0;g<numavg;g++)
        {                                       /* averaging */
            delay(1);

            outportb(640+24, channel1);
            outportb(640+16, channel2);
            while((inportb(640+20) & 1) != 1);

            a = inportb(640+18);
            b = inportb(640+19);

            outportb(640+16, channel1);
            while((inportb(640+20) & 1) != 1);

            aa = inportb(640+18);
            bb = inportb(640+19);
            c = (a*16 + b/16);
            y_pos = c/409.5*2;
            y_pos = y_pos-10.12;

            if ( y_pos < 0 )
            {
                    y_pos = 0.001;
            }
            else if ( y_pos > 10 )
            {
                    y_pos = 10;
            }
            cc = (aa*16 + bb/16);
            yy_pos = cc/409.5*2;
            yy_pos = yy_pos-10.12;

            if ( yy_pos < 0 )
            {
                    yy_pos = 0.001;
            }
            else if ( yy_pos > 10 )
            {
                    yy_pos = 10;
            }
            sum1=sum1+y_pos;
            sum2=sum2+yy_pos;
}

sig1[z] = sum1/g;
sig2[z] = sum2/g;
gotoxy(1,1);
printf("Signal(Ch.%d) = %5.3f Ref(Ch.%d) =%5.3f ",channel1,sig1[z],channel2,sig2[z]);

y_plot = (bottomofgraph-((sig1[z]/volt)*(bottomofgraph - topofgraph)));
y_cords[z]=y_plot;
yy_plot = (bottomofgraph-((sig2[z]/volt)*(bottomofgraph - topofgraph)));
yy_cords[z]=yy_plot;
x_cords[z]=x_pos+z;
```

```
                              if ( y_cords[z] > bottomofgraph )
                              {
                                      y_cords[z] = bottomofgraph;
                              }

                              else if ( y_cords[z] < topofgraph )
                              {
                                      y_cords[z] = topofgraph;
                              }

                              if ( yy_cords[z] > bottomofgraph )
                              {
                                      yy_cords[z] = bottomofgraph;
                              }

                              else if ( yy_cords[z] < topofgraph )
                              {
                                      yy_cords[z] = topofgraph;
                              }

                              putpixel(x_cords[z],y_cords[z],GREEN);
                              putpixel(x_cords[z],yy_cords[z],YELLOW);
                      }

              fprintf(data,"Meas\tRef\n");

              for (d=1; d<limit+1; d++)
              {
              fprintf(data,"%6.4f\t",sig1[d]);
              fprintf(data,"%6.4f\n",sig2[d]);
              }

              free(x_cords);
              free(y_cords);
              free(sig1);
              free(sig2);

      }




                      /*GPRINTF: Used like PRINTF except the output is sent to the */
                      /*screen in graphics mode at the specified co-ordinate.*/

int gprintf( int *xloc, int *yloc, char *fmt, ... )
{
 va_list  argptr;                                        /* Argument list pointer*/
 char str[140];                                          /* Buffer to build sting into*/
 int cnt;                                                /* Result of SPRINTF for return */

 va_start( argptr, fmt );                                /* Initialize va_ functions*/

 cnt = vsprintf( str, fmt, argptr );                     /* prints string to buffer*/
 outtextxy( *xloc, *yloc, str );                         /*Send string in graphics mode */
 *yloc += textheight( "H" ) + 2;                         /* Advance to next line */

 va_end( argptr );                                       /* Close va_ functions*/

 return( cnt );                                          /* Return the conversion count  */

}
```

APPENDIX I

MATLAB PROGRAM LISTING FOR EQUATION 6.1, 6.10 AND 6.11

I.1

```
h = 6.626e-34;                                    % Planck's constant
vs = 1.299e+14;                                   % Freq. of signal
vp = 3.797e+14;                                   % Freq. of pump
lifetime2 = 1.56e-3;                              % Lifetime of upper laser level
Area = 9.503e-11;                                 % Area of fibre core
np = [0.9851 0.9594 0.9204 0.8987 0.8612 0.7688]; % Fraction of power in
                                                  core at pump
np_avg = 0.8989;                                  % Average fraction of
                                                  power in core at pump
l = [0 1 2 0 3 1];                                % l value for modes
ns = 0.8087;                                      % Fraction of power in
                                                  core at signal
Fn = [0.8145 0.3388 0.2852 0.7008 0.2410 0.2956]; % Normalised overlap
                                                  between pump and signal
Fn_avg = 0.4460;                                  % Average normalised
                                                  overlap between pump and signal
sigma_e = 1.4e-25;                                % Stimulated emission
                                                  cross section


delta = 0;
Trans2 = [0.005 0.02 0.04 0.06];                  % Selected O/P transmission
delta_0 = 0.01;                                   % Fibre loss
                                                  (scattering,coupling losses)


fid = fopen('c:\matlab\data\output','wb');
fib = fopen('c:\matlab\data\outputa','wb');

fprintf(fib,'Trans2\t threshold\t slope_eff\n');

for x = 1:4;

        % Cavity round trip loss
        delta = (delta_0 - log(1-Trans2(x)) );

        % Threshold power
        threshold(x) = (( h * vp * Area * np_avg * delta ) / ( lifetime2 * Fn_avg *
sigma_e )) * 1e+3;

        % Slope efficiency
        slope_eff(x) = ((Trans2(x) * h * vs) / (delta * h * vp)) * 100;

        fprintf(fib,'%f\t %f\t %f\n',Trans2(x),threshold(x),slope_eff(x));
```

```
for p_abs = threshold(x):0.5:40,

        % Output power
        pin(p_abs) = p_abs;
        b = (Trans2(x) * h * vs) / (delta * h * vp);
        a = pin(p_abs) - threshold(x);
        p_out(p_abs,x) = b * a;

        fprintf(fid,'%f\n',p_out(p_abs,x));

    end;
end;

fclose(fid);
fclose(fib);
```

APPENDIX J

MATLAB PROGRAM LISTING FOR EQUATION 7.4

J.1

```
a = 5.5e-6;              % fibre radius
vp = 6.3930;             % fibre V number at pump wavelength
vs = 2.1864;             % fibre V number at signal wavelength
Trans1 = 0.0;            % Transmission of output mirror
R = 1-Trans1;            % Reflectivity of output mirror
t = 1;
Us = 1.5221;             % core parameter (U) value at signal wavelength
Ws = 1.5690;             % cladding parameter (W) value at signal wavelength
nco = 1.5165;            % core refractive index
ncl = 1.5085;            % cladding refractive index

delta = (((nco^2) - (ncl^2)) / (2 * (nco^2)));
beta = ( (1/a) * ( ((vs^2)/(2*delta)) - (Us^2) )^0.5);
w = (a / sqrt(2)) * ( 0.65 + ( 1.619 / (vs^1.5)) + (2.879 / (vs^6)) );
q = (2 / ( (w^2) * beta ));

        fid = fopen('c:\matlab\loss_ad1','wb');

            for d = 1:5000;
                    rhooo(t) = 0;
                    real_d = d * 1e-8;

                    z = q * real_d;
                    a = ( (4 * (z^2)) + 1);
                    b = ( (2 * (z^2)) + 1);
                    c = b^2;
                    rho = (R * a) / (c + (z^2) );

                    rhoo = rho * 100;
                    rhooo(t) = 100 - rhoo;

                    fprintf(fid,'%g\t%g\n',real_d,rhooo(t));
                    t = t + 1;
            end;

        fclose(fid);
```

MATLAB PROGRAM LISTING FOR EQUATION 7.8

J.2

```
a = 5.5e-6;              % fibre radius
vp = 6.3930;            % fibre V number at pump wavelength
vs = 2.1864;            % fibre V number at signal wavelength
Trans1 = 0.0;           % Transmission of output mirror
R = 1-Trans1;           % Reflectivity of output mirror
t = 1;
dia = 125e-6;           % Fibre outer diameter
Us = 1.5221;            % core paramter (U) value at signal wavelength
Ws = 1.5690;            % cladding paramter (W) value at signal wavelength
nco = 1.5165;           % core refractive index
ncl = 1.5085;           % cladding refractive index

delta = (((nco^2) - (ncl^2)) / (2 * (nco^2)));
beta = ( (1/a) * ( ((vs^2)/(2*delta)) - (Us^2) )^0.5);
w = (a / sqrt(2)) * ( 0.65 + ( 1.619 / (vs^1.5)) + (2.879 / (vs^6)) );
q = (2 / ( (w^2) * beta ));

        fid = fopen('c:\matlab\loss_tot','wb');

                for theta = 1:5000;
                        rho_total(t) = 0;
                        rhooo(t) = 0;
                        rhooo_d(t) = 0;
                        real_theta = theta * 8e-4;      % 0-4 degrees
                        real_d = (dia * ((pi/180) * real_theta) * 0.5);

                        z = q * real_d;
                        aa = ( (4 * (z^2)) + 1);
                        bb = ( (2 * (z^2)) + 1);
                        cc = bb^2;
                        rho_d = (R * aa) / (cc + (z^2) );
                        rhoo_d = rho_d * 100;
                        rhooo_d(t) = 100 - rhoo_d;

                        a = (-1 * (beta^2) * (w^2) * (((pi/180) * real_theta)^2) );
                        b = exp(a);
                        rho = R * b;
                        rhoo = rho * 100;
                        rhooo(t) = 100 - rhoo;

                        rho_total(t) = rhooo_d(t) + rhooo(t);

                fprintf(fid,'%g\t%g\t%g\n',real_d,real_theta,rho_total(t));
                        t = t + 1;
        end;

fclose(fid);
```